2017

Self-lubricating non-cyanide silver-polytetrafluoroethylene composite coating for threaded compression fittings

Sieh, Raymond

http://hdl.handle.net/10026.1/9703

http://dx.doi.org/10.24382/1079
University of Plymouth

RESEARCH DEGREES WITH PLYMOUTH UNIVERSITY

SELF-LUBRICATING NON-CYANIDE SILVER-POLYTETRAFLUOROETHYLENE COMPOSITE COATING FOR THREADED COMPRESSION FITTINGS

by

RAYMOND SIEH

A thesis submitted to Plymouth University
in partial fulfilment for the degree of

DOCTOR OF PHILOSOPHY

Marine Science and Engineering Doctoral Training Centre

September 2016

Acknowledgements

I would like to take this opportunity to express my sincerest gratitude to my supervisor, Dr. Huirong Le, for his assistance, expertise and academic input throughout the project. His knowledge of tribology, as well as dedication and commitment towards the advancement of knowledge in the field, is in my opinion, second to none. Furthermore, he had also provided numerous personal development opportunities throughout my PhD journey, without which it would not be the same.

I am also sincerely grateful to my second supervisor, Dr. Alistair Cree for his support and guidance throughout my dissertation writing and for being a valuable sounding board in my PhD journey.

I would also like to thank Professor Janet Richardson and Dr. Jane Grose for their expertise, advice, support and understanding during the first year of my PhD.

This dissertation would not have been possible without the support of my family who has provided unconditional support and understanding throughout this journey.

Thanks are also due to the various technical departments and staff at Plymouth University for their assistance and input throughout the project. I am grateful and blessed in having received the assistance and support of Terry Richards, Dr. Zoltan Gombos, Gregory Nash from the Engineering technical team and also Roy Moate, Pete Bond and Glenn Harper from the Electron Microscopy Centre. Also not forgetting the assistance provided by Ian Doidge, Andy Arnold and Andrew Tonkin from the Chemistry Department.

<u>AUTHOR'S DECLARATION</u>

At no time during the registration for the degree of Doctor of Philosophy has the author been registered for any other University award without prior agreement of the Graduate Sub-Committee.

Work submitted for this research degree at Plymouth University has not formed part of any other degree either at Plymouth University or at another establishment.

Relevant scientific seminars and conferences were regularly attended at which work was often presented;

Publications:

R. Sieh, H. R. Le, and A. M. Cree, "Process optimisation of non-cyanide Ag–PTFE metal matrix composite electroplating for threaded connections," Trans. IMF, vol. 93, no. 5, pp. 232–240, Sep. 2015.

R. Sieh and H. Le, "Non-Cyanide Electrodeposited Ag–PTFE Composite Coating Using Direct or Pulsed Current Deposition," Coatings, vol. 6, no. 3, p. 31, Jul. 2016.

Conference Presentation:

Nanosmat Dublin 2014; NANO-285: "Advanced Nanocomposite Coating for Offshore Threaded Connections"

Word count of main body of thesis: 36228

Signed :

Date: 29th September 2016

Abstract

Silver is a precious metal that has traditionally been used for jewellery and money. It also possesses desirable properties such as being corrosion resistant and having good electrical conductivity, resulting in its use for industrial applications. Furthermore, it is also recognised for its tribological properties in non-cost prohibitive applications.

Silver can be used as a surface coating and can be deposited using an electroplating process. The utilisation of silver as a surface coating is advantageous and sustainable, as the substrate material properties are enhanced while usage of silver is kept to a minimum. On the other hand, electroplating has been used for over a century. It is a process which is able to produce a layer of uniform and dense coating that adheres well to the substrate metal, thus modifying the properties of the substrate. It benefits from being relatively low cost and is scalable. Silver is electroplated onto stainless steel threaded compression fittings to prevent galling. Traditional silver electroplating, which contains the use of cyanide as a complexing agent in the electroplating bath, is still in use within industry, even to this day. Cyanide, in its various forms can be poisonous, toxic and even lethal, which presents a risk during the silver electroplating process. Furthermore, the toxic wastes created during the cyanide silver electroplating process are detrimental to the environment.

The aim of this work is to develop a self-lubricating non-cyanide silver PTFE composite coating suitable for use in threaded compression fittings of the ferruled type. The composite can be considered self-lubricating when a concentration of 8% or more by volume of the self-lubricating PTFE substance is incorporated. My original contribution to knowledge is firstly the successful development and

characterisation of a self-lubricating non-cynanide Ag-PTFE coating on stainless steel without a strike resulting in improved CoF of 0.06 from the CoF of 0.6 based on an unlubricated surface. Secondly is the application of a non-cyanide Ag-PTFE MMC for threaded compression fittings. Thirdly is the characterisation of the make-up process of threaded compression fittings through the proposed use of the torque-angle slope in assessing coating performance for threaded compression fittings during make-up.

Conclusions that can be drawn for the work are that the performance non-cyanide Ag-PTFE coating exceeded the performance of the pure Ag coating made using the same non-cyanide process. Moreover, the performance of the Ag-PTFE coating shows promising results when compared to the performance of the commercial silver cyanide coating. As a viable replacement to the current silver cyanide process, the self-lubricating non-cyanide Ag-PTFE coating, will improve the working conditions and have a positive contribution to the environment. Moreover, a thinner coating with has the potential to reduce raw material usage and electroplating waste disposal costs.

Preface

This dissertation is submitted for the degree of Doctor of Philosophy at Plymouth University. The research described herein was carried out under the supervision of Dr. Huirong Le and Dr. Alistair Cree in the School of Marine Science and Engineering (Faculty of Science and Environment), Plymouth University.

This work is to the best of my knowledge original, with the exception where acknowledgements and references are made to previous work. Neither this, nor any substantially similar dissertation has been or is being submitted for any other degree, diploma or other qualification at any other university.

Part of this work has been presented in the following publications:

R. Sieh, H. Le, and A. M. Cree, "Process optimisation of non-cyanide Ag–PTFE metal matrix composite electroplating for threaded connections," Trans. IMF, vol. 93, no. 5, pp. 232–240, Sep. 2015.

R. Sieh and H. Le, "Non-Cyanide Electrodeposited Ag–PTFE Composite Coating Using Direct or Pulsed Current Deposition," Coatings, vol. 6, no. 3, p. 31, Jul. 2016.

Accepted for publication:

R. Sieh, H. Le, "Evaluation of environmentally friendly Ag-PTFE composite coating for use in threaded compression fittings," IMechE Part J, Accepted 6th June 2017

Table of Contents

List of Figures

List of Tables

List of Symbols

V = Wear volume (mm^3)

s = Sliding distance (mm)

k = Wear constant

F_n = Normal load applied (N)

H = Hardness of the softer material (kg/mm^2)

P_{max} = Maximum contact pressure (N/mm^2)

F = Applied force (N)

a = Contact area (mm^2)

Faraday's law of electrolysis:

Q = charge (Coloumb)

z = Change in oxidation state (g/Coloumb)

I = Current (A)

t = Time (s)

m = Mass (g)

M = Molar mass (g/mol)

F = Faraday's constant (96485 Coloumb/mol)

n = Amount of oxidised or reduced substance (mol)

For Stoke's law:

g = Gravitational acceleration (m/s^2)

r_p = particle size (m)

ρ_p = Particle density (kg/m^3)

ρ_c = Electrolyte density (kg/m^3)

μ = Viscosity (kg/ms)

Chapter 1 Introduction

Surface coatings on metal are typically applied to alter the surface properties of a surface (substrate) to improve its decorative and functional aspects as part of the finishing process. Decorative aspects may include physical aesthetics while functional aspects include improved chemical resistance and mechanical properties. These coatings may have decorative, functional or even dual purposes and often metals such as gold, silver, copper or nickel can be easily deposited on a substrate. These coatings are typically in the form of thin film depositions and range from nanometer thicknesses to micrometre thicknesses. To deposit the thin film onto a metal substrate, chemical or physical deposition processes may be used. Chemical deposition methods typically involve a fluid precursor which deposits a thin film after undergoing a chemical reaction to leave a solid layer. The physical deposition method, on the other hand, uses mechanical, electromagnetic or thermodynamic methods to produce a thin film [1]–[3]. Although the outcome of both methods will result in a thin film being deposited on the substrate layer, physical deposition methods utilise mechanical, electromagnetic or thermodynamic phenomena while chemical deposition typically involves using a fluid or gaseous precursor [1]–[3].

Electroplating is a high-performance, low-cost method of chemical deposition which is commercially viable and can be used in a wide variety of applications, from improving the aesthetics of a substrate to depositing semiconductors for electronics [4]. Silver is a metal which can be electroplated to provide desirable properties such as being a good conductor of electricity, chemically stable in being able to resist corrosion, and even being able to provide tribological improvements [5]–[9].

Background of the problem

One main issue when working with stainless steel as a substrate is galling. Galling is a phenomenon of surface damage as a result of sliding contact between solid surfaces under conditions of inadequate or no lubrication and under high contact pressure which is visible through macroscopic effects of surface roughening or protrusions [10], [11]. Under high compressive forces, the adhesion of the materials can cause slipping and tearing of crystal structures beneath the surface, which often results in material transfer, plastic flow or friction welding between the sliding surfaces.

A silver coating on threaded stainless steel compression fittings is deposited through an electroplating process to prevent galling and is crucial to the successful assembly and sealability of the system as a whole. According to a major compression fitting manufacturer, this silver plating is used on the inner surfaces of the nut including its threads to remove the possibility of galling and reduce assembly torque [12]. The quality of the coating will thus affect the tribology in the assembly process which plays an important role in the integrity and sealability of the product; where tribology can be defined as the 'science and technology of interacting surfaces in relative motion and of related subjects and

practices' [13]. The variation in aspects such as galling resistance, friction, and wear will inevitably affect the make-up torque and interface contact pressure.

The current commercial silver electroplating processes continue to utilise a traditional silver cyanide electroplating bath. Cyanide is both dangerous and noxious so that the wastes of the electroplating process require that cyanide as a poisonous substance to be carefully controlled from storage to use and ultimately disposal. The electroplating bath waste containing cyanide requires treatment through further chemical processing and disposal which typically involves either complete destruction with chlorine gas or conversion into the less poisonous cyanate which are costly and detrimental to the environment [14], [15]. Furthermore, workers are exposed to toxic cyanide gas which threatens their health and safety.

Although traditional cyanide silver plating is typically associated with having detrimental effects on the environment, it can offer a consistent plating deposit quality at the lowest cost [15]. It was only in the 20th century that alternatives to silver cyanide electroplating were able to produce mirror bright and ductile surface finishes while also being able to adhere sufficiently to substrates upon which the silver film is being deposited [16]. Cyanide alternatives to silver electroplating include simple salts, inorganic complexes and organic complexes [15]. Although initial attempts at eliminating cyanide from silver electroplating had failed to meet the quality of surface finish produced by a cyanide bath, later successes were found in the use of inorganic complex thiosulfate and organic complex succinimide which have been successfully adopted for selective commercial uses [17].

Furthermore, research has also shown the potential for improving tribological properties of metal coatings through incorporating particles to form a metal matrix composite (MMC). There are benefits to incorporating dispersed foreign particles in a coating. Several authors have reported successes in obtaining performance enhancements from coatings [18]–[20]. Research into the incorporation of finely dispersed particles into a metallic matrix composite (MMC) has previously been successfully carried out [20]–[32]. Variables that affect particle incorporation include current density, pH and bath composition, hydrodynamics and particle size, type and shape [33]–[38]. Based on reviews of particle incorporation into MMCs, Walsh et. al. [39] believed that it is possible to incorporate chemically inert but hydrophobic PTFE particles with parameters such as particle size, surfactant type, and concentration being critical in obtaining high particle incorporation rates in the metal matrix through a stable plating bath. The authors also pointed out that the difficulty of obtaining PTFE suspension compatibility with the bath due to the anionic surfactants, alcoholic or aqueous liquid used. However, the benefits of PTFE in a MMC could be a reduction in coating thickness and thus material usage from coating performance improvements. Also, a self-lubricating coating would negate the use of liquid lubricants. Based on 2007 values, 37.2 million tons of lubricants were used globally, with industrial lubricants making up 35% of this value (or just over 13 million tons). Lubricants prevent the onset of premature component failure through various mechanisms. However, liquid lubricants cause environmental pollution over its entire lifetime, from manufacture to its use and ultimately disposal due to emissions, spillages, leaks and waste from the manufacturing process. In Europe alone, it is estimated that over 2 million tons pollute the environment every year [40].

Purpose of the study

The aim of the project is to develop a self-lubricating non-cyanide silver PTFE coating suitable for use in threaded compression fittings of the ferruled type. Self-lubrication is defined as having a concentration of 8% or more by volume of the self-lubricating substance in the composite, whereby PTFE is the lubricating substance in this study. As such, studies carried out have been focused on developing a potential replacement for the existing cyanide silver electroplating bath with one that is less toxic to humans and environmentally friendly while still being able to perform under the demanding conditions required of it during the compression fitting make-up process.

On the other hand, the objectives of the study are firstly to develop a non-cyanide silver electroplating bath capable of depositing a coating on a stainless-steel substrate. The second objective is to develop a self-lubricating coating that possesses superior tribological properties over a pure silver coating. The third objective is to investigate the performance of the non-cyanide silver and silver PTFE coating when used on threaded compression fittings.

Significance of the study

This study is significant for several reasons. Firstly, it has the potential to have a direct impact on improving the working conditions under which workers carrying out the electroplating process are subjected to on a daily basis. Secondly, the study also has the potential to provide a positive contribution to the environment from the removal of cyanide through purchase to use and ultimately disposal. Furthermore, potential cost savings can also be realised through less material usage and electroplating waste disposal costs. The benefits arising from this

project will have a positive impact towards social, economic and environmental issues, which are incidentally the three pillars of sustainability as set out by the Brundtland committee.

Unique contribution to knowledge

The unique contribution to knowledge as a result of this study is firstly the successful development and characterisation of a self-lubricating non-cynanide Ag-PTFE coating on stainless steel without a strike resulting in improved CoF of 0.06 from the CoF of 0.6 based on an unlubricated surface. Secondly is the application of a non-cyanide Ag-PTFE MMC for threaded compression fittings. Thirdly is the characterisation of the make-up process of threaded compression fittings through the proposed use of the torque-angle slope in assessing coating performance for threaded compression fittings during make-up.

Thesis structure and research design

This work has been structured to investigate a suitable non-cyanide silver plating process based on using succinimide as a replacement salt to achieve project aims. Following that, characterisation of the coating have been carried out through the investigation into its tribological properties. The composite non-cyanide Ag-PTFE coatings are compared against the performance of pure non-cyanide silver using the same process. Development of the coating also includes testing of its performance characteristics during the make-up process of threaded compression fittings.

The next two chapters of this thesis will present a literature review which is relevant to achieving the research aims and objectives. Considering that the electroplating process is a key part of the development of the coating, this will be

investigated along with the methods of particle incorporation to form a metal matrix composite coating.

Chapter 2 Contact mechanics of threaded compression fittings and Coating Deposition

2.1 Introduction

The previous chapter provided an overall introduction to this thesis and research project in addition to outlining project aims and objectives. The developed coating will ultimately be used on threaded compression fittings as part of the project aim. It is, therefore, important for a review of the current knowledge associated with threaded fittings to be made, with the particular focus on the mechanical and tribological aspects in relation to it, as tribology is impacted by the physical, chemical and mechanical properties of the material surface.

This chapter is therefore organised to introduce concepts relating to tribology and contact mechanics firstly. Following that, the chapter will delve into the realm of threaded connections and threaded compression fittings in particular, drawing from concepts previously introduced. These provide a context and outline the conditions under which the coating will ultimately face during its use.

Furthermore, silver electroplating is carried out as a finishing process on the internal threads of the threaded compression fitting nut. Literature surrounding traditional silver electroplating, the incorporation of particles as part of the electroplating process and present research on silver composite coatings are also critically reviewed in this chapter.

2.2 Contact Mechanics

2.2.1 Tribology

The study of tribology is the study of the science and technology behind interacting surfaces in relative motion that includes wear, friction, and lubrication. It incorporates mechanical engineering, physics, chemistry and even materials science. The word 'tribos' means 'to rub' in Greek, and the term was coined in the 1960s as a conscious attempt at scientifically naming the important applications of these sciences. According to the Jost Report where the term tribology originated, the application and understanding of tribological properties involved potential savings of approximately 1% of the British gross national product at the time [41]. Tribological studies encompass a wide range of applications, from the automotive to aerospace and aeronautics, computing storage technology and even human joints [42].

Economic implications have motivated tribological studies because costs such as wear on equipment or machinery and losses in energy from friction can be quantifiable with relative ease. There are, however, other benefits that can be attributed to tribological improvement that are not as easy to quantify. These benefits can be attributed to environmental sustainability through reduced parts

or equipment waste through a reduction of friction and prolonging of component lifespan. Prolonging of component lifespan through tribological understanding would also lead to avoidance of premature wear which could ultimately result in the failure of critical components and potentially endanger human life. An increased understanding would also reduce the need for over-engineering components to compensate for lack of detailed knowledge such as accurate prediction models for friction and wear.

Friction

Friction has been in use by human beings since the Stone Age with the discovery of flint tools and the use of fire which had been unknowingly created through friction. The earliest studies of the subject can be traced back to 350 BC, where Thermistius discovered the frictional differences between sliding and rolling. Remarkably, it was only in the 1500s that studies into the phenomena of friction were only carried out by Leonardo Da Vinci who noted the first friction laws. Studies relating to friction were then further expanded by Isaac Newton in the 1700s through Newton's third law for the interaction of bodies. The rediscovery of friction laws in the late 1700s was attributed to the French inventor and physicist Guillaume Amontons, who proposed his laws of friction. Throughout the 1800s, Leonhard Euler refined his roughness theory of friction and Coulomb proposed a model for friction between two surfaces of contact that demonstrates friction independence of roughness and sliding velocity. It was only in the late 19th century that Heinrich Hertz conducted the first study on contact of deformable solids. The 20th century saw many advances in theory on friction, with authors such as Holm, Ernst, and Merchant as well as Bowden and Tabor who carried

out studies on differences between the real and apparent contact areas and proposed the adhesion theory.

The phenomenon of friction is a double-edged sword. On one hand, it is welcomed in larger quantities for applications such as car brakes or when traversing a slippery surface. It is also often the limiting factor when it comes to providing traction for trains. On the other hand, friction can cause unwanted and irreversible damage to moving parts in automotive or aeronautic and aerospace applications. Insufficient lubrication resulting in high friction in combustion engines or gearboxes will result in the grinding of parts when they are in motion. The re-entry of a spacecraft into Earth's atmosphere has to be adequately shielded from the large amounts of heat generated as a result of friction.

Friction is a result of complex molecular and mechanical interactions that occur in solids, liquids, and gases in different forms. Fluid friction is the frictional force exerted by liquids or gases thus causing drag as a result of objects moving through them. It is dependent on the velocity and shape of the object as well as the properties of the fluid itself. Solid friction on the other hand, occurs between two solids that are in contact and exists in both static and dynamic forms. It is dependent on the size of the contact zone, surface morphology (roughness and asperities) as well as the load or pressure on these surfaces.

Friction is related to types of motion that the two contacting bodies experience. Two general motions are sliding and rolling. The force required for sliding an object is typically higher than the force required to roll a cylindrical object as discovered by Thermistius. There are of course other variables that will affect the forces required such as the types of material in contact and other parameters. A

dimensionless ratio, μ known as the coefficient of friction (CoF) is used to quantify the ratio of frictional force to normal force that presses the bodies together, given by Eq 2-1.

$$Coefficient\ of\ friction, \mu = \frac{Tangential\ Force}{Normal\ Force}$$ *- Eq 2-1*

Sliding friction is an operation of sticking and slipping, where highest friction occurs during the sticking and lowest during the slipping, which results in contact area and surface temperature changes [43]. Incidentally, this is also the friction type for this work. The mechanism of friction is based on contact occurring at the high points or asperities of the surface. The mating surfaces encounter close contact, promoting adhesion of surfaces due to Van Der Waals forces [44]. It is also a commonly held belief that friction is typically independent of normal load, the area of contact and behaves as a resistive force acting in the opposite direction of an applied force.

Wear

Wear can be defined as the erosion or damage of material through mechanical action. It is typically a slow but steady and continuous process which equates to approximately 6% of Gross National Product for the United States. According to Rabinowicz, wear as an important sub-field in tribology involves not just mechanical engineering, but also fields such as materials science, chemistry (surface and general) and even applied mechanics [45].

Surface roughness highly influences the phenomenon of wear. The asperities or high points of both surfaces which come into contact with each other will result in material being removed [46]. Main types of wear are adhesive, abrasive, corrosive, and surface fatigue wear while other forms of wear include fretting,

erosion (including low and high speed) and cavitation [45]–[47]. With adequate knowledge of wear mechanisms for each main type of wear, this can be prevented or its impact reduced.

Abrasive wear is caused when materials of different hardness interact with each other during motion. It can be reduced or even eliminated by ensuring the smoothness of hard surfaces or non-existence of abrasive particles in the system. Corrosive wear, on the other hand, is the chemical reaction between a material and its environment. It can be arrested by ensuring non-reactivity of the material in question with either the atmosphere or its operating environment. Surface fatigue wear occurs when a surface is cyclically stressed and unstressed. Adhesive wear is the most common, but it is not the most dangerous due to slow rates and gradual onset.

Rabinowicz proposed several laws for adhesive wear based on results from experiments carried out using metal on metal sliding contact with no lubrication [45]. The laws were then formulated based on the results of the experiments which state the amount of wear is directly proportional to load and sliding distance while being inversely proportional to surface hardness. A quantitative method for calculating rate of wear can be obtained through Archard's equation as seen in Eq 2-2 [46]:

$$\frac{V}{s} = \frac{kF_n}{H} \qquad\qquad \textit{- Eq 2-2}$$

Where,

V = Wear volume (mm^3)

s = Sliding distance (mm)

k = Wear constant

F_n = Normal load applied (N)

H = Hardness of the softer material (kg/mm^2)

Stainless steel is a hard and wear resistant material. Galling occurs for dynamic applications involving stainless steel on stainless steel contact. The ideal situation in dynamic applications involving steel as a substrate is to have a coating that is wear resistant while possessing low friction properties. The reality of the situation is that soft, polymeric bearing materials with excellent low friction properties such as HDPE, nylon, polyimide or PTFE have high wear rates. A compromise between low friction properties and wear is made with functional soft coatings. These are required to resist wear while also ideally possessing low friction characteristics. Nuts for threaded compression fittings are made from stainless steel coated in silver, which results in a dynamic silver on stainless steel contact during assembly. This is in line with Rabinowicz's suggestions of using metallurgically incompatible materials such as silver for steel applications, where silver is the hardest material (and thus most resistant to wear) out of all the soft coatings proposed [45].

Kato summarised that the wear of a soft coating is influenced by substrate roughness and transfer effects [48]. In the published paper, Kato pointed out that substrate roughness directly influences the frictional and wear characteristics of a thin film metal coating under friction, however, no explanation was provided to clarify why this has occurred. On the other hand, Kato argued that the transfer effects of a soft coating onto a hard counter-surface effectively reduces its wear

rate. This argument was based on a polymer-metal composite coating which is relevant to the research into a Ag-PTFE coating, however Kato neglected to point out the adverse effects of increased variability in wear rates and friction coefficient observed in the published results.

The studies of wear mechanisms in thin film coatings on the other hand, can be best explained through the work of Holmberg et. al. who have provided an illustrated version of the issues surrounding macro-mechanical contact considered for thin coating wear in Figure 2-1 [49]. The authors provide a comparison of two scenarios where one is a soft coating on a hard substrate and the other a reverse. The former scenario is of best interest as it is fitting for coatings employed on threaded compression fittings. The authors summarised that coating thickness affects friction ploughing for a smooth sphere surface while a rough sphere surface affects substrate asperity penetration in scenarios (a), (b), (e) and (f). Abrasive wear caused by debris is shown in (i) and (j). Based on the work carried out, Holmberg et. al. suggested that thick, soft coatings on a hard surface tend to plough whereas thinner coatings will shear.

Figure 2-1 has been removed due to Copyright restrictions.

Figure 2-1 Mechanisms that affect friction based on a hard sphere sliding on a flat coated surface, from Holmberg et. al. [49]

Lubrication

Lubrication can either be carried out using fluids such as lubricating oils or solids such as thin films. Work carried out by Bowden and Tabor highlighted the role and importance of oxides on providing lubrication [50]. Metals such as stainless steels which are resistant to oxide formation on its surface can be classified to have "clean" surfaces. These metals tend to have no lubricity and tend to weld together under direct contact. A form of lubrication is then required during the use of these metals, with the solid lubrication acting to prevent direct contact between these surfaces through a low shear strength solid film [43]. The lubrication and the lubrication properties of fluids or solids are affected by variables such as surface temperature, speed and load and these are well documented in texts on lubrication [51]. Metal composite coatings can be considered to fall within the

"self-lubricating" category when a concentration of 8% or more by volume of the self-lubricating substance is included within the composite [45].

Tribological coatings are thin coatings which are electroplated onto a substrate material to enhance its properties depending on its required application as shown in Table 2-2. To function as a lubricant, the coating has to either exhibit low friction or lubricity, which based on the summary provided by Holmberg et. al., the coating type should either be soft or liquid. There are benefits of utilising PTFE as a soft coating for these purposes as the lubrication of PTFE does not depend on adsorbed vapours or moisture and has a low surface energy [52]. As a lubricant, the macromolecules of PTFE are able to slip easily along each other during sliding operations, a key consideration for the reduction in friction. As a polymer, PTFE asperities which are softer than metals tend to favour deformation under applied load which results in the draping of metal asperities and improve its performance. There are however several downsides to PTFE. Firstly, although it is more capable of load carrying relative to liquids, as a solid it does not have a great load carrying capacity. Furthermore, it has a low thermal conductivity. The low thermal conductivity results in the inhibition of heat dissipation, which can cause premature failure due to melting. It also restricts its use to low-speed sliding applications. Being a solid lubricant, consideration of its wear and life limits its application to intermittent sliding situations.

The consideration of liquid coatings as a lubricant for threaded applications will be further discussed in Section 2.5.

Table 2-1 Properties of thin coatings; extracted from Holmberg et. al. [53]

Required property of coating	Type of coating	Potential materials	Typical Thicknesses (µm)
Wear resistance	Hard Coatings	TiN, TiC, Al_2O_3, diamond	0.5 – 5
Low friction	Soft/layered coatings	Pb, PTFE, MoS_2, diamond	0.5 – 5
Lubricity	Liquid coatings	Perfluoropolyether	0.001 – 0.05
Corrosion resistance	Dense, inert coatings	Au, Zn, Cd, Al2O3	3 – 20
Adhesion to substrate	Soluble/bonding coatings	Ti, Cr, Si_2N_3	0.01 – 1
Diffusion barrier	Dense, inert coatings	Ni, NiAl, Al_2O_3	1 – 30
Thermal barrier	Insulating coatings	ZrO_2, PSZ	50 – 250
Electrical conductivity	Noble/pure metal coatings	Au, Cu	1 – 10

Holmberg et al. summarised that soft coatings are able to provide low friction. In the context of this research, the soft coating is deposited onto a hard substrate, namely stainless steel. Based on work carried out by Jiang shown in Figure 2-2, soft coatings on a hard substrate will function by firstly increasing the contact area of a wear pin. As it is only the soft coating that will deform, the interfacial shear

strength for hard substrate will be decreased. According to Jiang, no changes will occur to the interface between substrate and coating as there is no significant deformation of the hard surface. Due to this phenomenon, the soft coating manages to not only prevent wear on the substrate but is also able to provide a low CoF through its role in lubricating the contact surfaces.

Figure 2-2 has been removed due to Copyright restrictions.

Figure 2-2 Computer generated model of Von Mises stresses for a soft coating on a hard substrate from Jiang et al. [54]

2.2.2 Contact Mechanics

To achieve the objective of coating development for a potential replacement of the current cyanide silver coating, it is important to have an understanding of contact mechanics which studies the deformation of solid bodies. This will be used for assessment of CoF performance for the coating during development.

Hertzian contact stress (contact stresses within the system)

Any discussion of contact mechanics will not be complete without the mentioning Hertzian contact theory. Heinrich Hertz first expanded on the elastic contact behaviour between two bodies comprised of circular arc geometries. Through his work, he illustrated the relationship between applied normal load within the system and the resulting contact area when the two bodies are subjected to forces as shown in Figure 2-3.
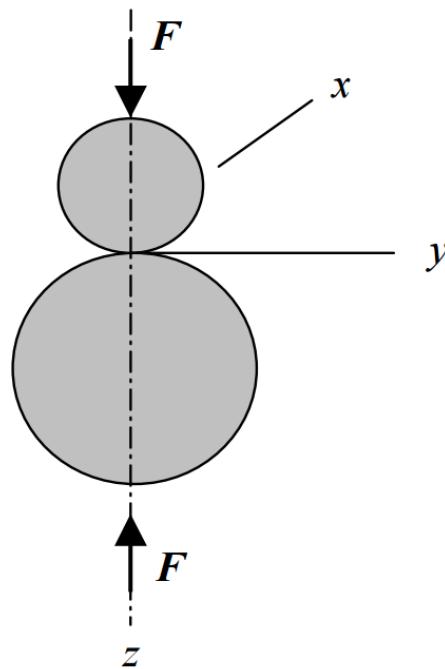
Figure 2-3 Hertz's theory on two spheres in contact

The maximum contact pressure that occurs at the centre point of the contact area can then be calculated using Eq 2-3:

$$P_{max} = \frac{3F}{2\pi a^2}$$ *- Eq 2-3*

Where,

P_{max} = Maximum contact pressure (N/mm^2)

F = Applied force (N)

a = Contact area (mm^2)

The area can be determined based on the following equation, Eq 2-4:

$$a^2 = \frac{4PR'}{\pi E^*}$$

- Eq 2-4

Where,

a = Contact area (mm^2)

P = Normal load applied (N)

R' = Reduced radius

E* = Contact modulus based on Eq 2-5 and Eq 2-6:

$$\frac{1}{R'} = \frac{1}{R_1} + \frac{1}{R_2}$$

- Eq 2-5

$$\frac{1}{E^*} = \frac{1-v_1^2}{E_1} + \frac{1-v_2^2}{E_2}$$

- Eq 2-6

Where,

E* = Contact modulus

E_1 = Elastic modulus for 1st material

E_2 = Elastic moduls for 2nd material

v₁ = Poisson's ratio for 1st material

v_2 = Poisson's ratio for 2nd material

Although the resulting contact pressures are idealised in nature, they can be used for the identification of contact pressures during the determination of CoF through the linear tribometer.

Surface roughness

The frictional interaction between two contacting surfaces in motion can be influenced by surface roughness. One of the ideas in relation to the effects of surface topography towards friction was proposed by Leslie in the 19th century, which believed that fluctuations in surface topography when in contact with each other provided an explanation for the resultant fluctuations in friction [55]. These fluctuations are quantified using the term surface roughness and according to Greenwood and Williamson, roughness exists on varying levels, and surfaces that can typically be considered to be flat will exhibit roughness on some level [56]. Surface roughness in turn directly affects the assumed contact area, where even fully contacting areas will in reality be of smaller magnitudes when considering theories of contact mechanics. Based on this, the authors concluded that pressure does not have a significant enough impact towards separation distance when two surfaces are in contact and that separation distance between surfaces remained constant during load changes.

Fundamental features set out within the Greenwood and Williamson model for predicting the ratio of asperity contact are well established and relevant. Their model is based on rough surface elastic contact mechanics and makes the assumption that surface asperities deform in an elastic manner and deformation

of surrounding features do not affect each asperity. From these assumptions, their model is based on height, and mean plane of surface follows a normal distribution, where asperities are spherical in nature.

Sedlacek et. al. investigated effects of surface fabrication towards roughness, friction and wear of both lubricated and unlubricated steel plates [57]. Using a pin-on-disc tribometer with ball-on-disc contact, the authors found that under dry sliding conditions, an inverse relationship was present between CoF and roughness, in that when surface roughness was high, the CoF was low. The authors also concluded that based on dynamic sliding, the higher sliding speeds resulted in reduced friction regardless of lubrication conditions.

2.2.3 Threaded Fasteners

Screw Threads

Screw threads are manufactured helical structures which are capable of converting a rotational force to a linear movement. One of its main uses is for fastening applications. Primary fastening applications for material to be held together involves the use of nuts and bolts or machine screws. On the other hand, primary fastening application of creating connections in plumbing applications involve the use of pipe connectors such as threaded compression fittings, or alternatively screw threads are embedded into pipes. As a simple machine, the converted force is dependent on the geometry of the thread design, also known as thread profile, with a limited selection shown in Figure 2-4.

Thread Form	Figure
Unified	
Metric	
Square	
ACME	
Buttress	

Figure 2-4 Types of thread profiles

Although there is a wide range of thread profiles available, the selection of an appropriate thread profile is mainly down to application. For instance, unified and metric thread profiles are for general use, square thread profiles for power transmission, ACME thread profiles for heavy duty power transmission due to load carrying capacity of threads and buttress thread profiles for heavy loads or forces in a single direction such as for jacks. The most commonly used thread profiles are ISO metric screw threads for nuts and bolts or threaded compression fittings. Plumbing applications where the threads are directly embedded into the

pipes follow standards such as the National Pipe Thread (NPT) or British Standard Pipe Thread (BSP).

Although unified threads standards (UTS) are commonly used in North America, there are no differences between its profile and that of metric threads. The differences lie instead in the units used for its characterising dimensions, with unified being quoted in inches and metric in millimetres. The UTS system also stipulates threads as being coarse, fine and extra fine depending on the diameter/pitch combination. A tolerance class system denoting the acceptable ranges of pitch diameter is also sometimes used. Fine-thread series of unified thread has less thread depth and large minor diameter compared to coarse threads used where high strength is required. [58]

Comparison between fastener types

Although the application of fasteners varies between either falling into the category of holding the material together or creating plumbing connections, certain similarities exist between these two. From this point onwards, the former application will be referred to as threaded fastener (i.e. bolt and nut) and the latter as threaded compression fitting. Firstly, both types of fasteners are fundamentally bound by the application of screw threads which is to convert torque to linear displacement. Secondly, assuming that both the bolt for threaded fasteners and the body for compression fittings are properly secured during installation, the application of torque to both the nuts which will results in the compression of all the parts in between the nut and bolt or body. The main difference between these two is a number of contact areas which have to be considered for tribological study as illustrated in Figure 2-5.
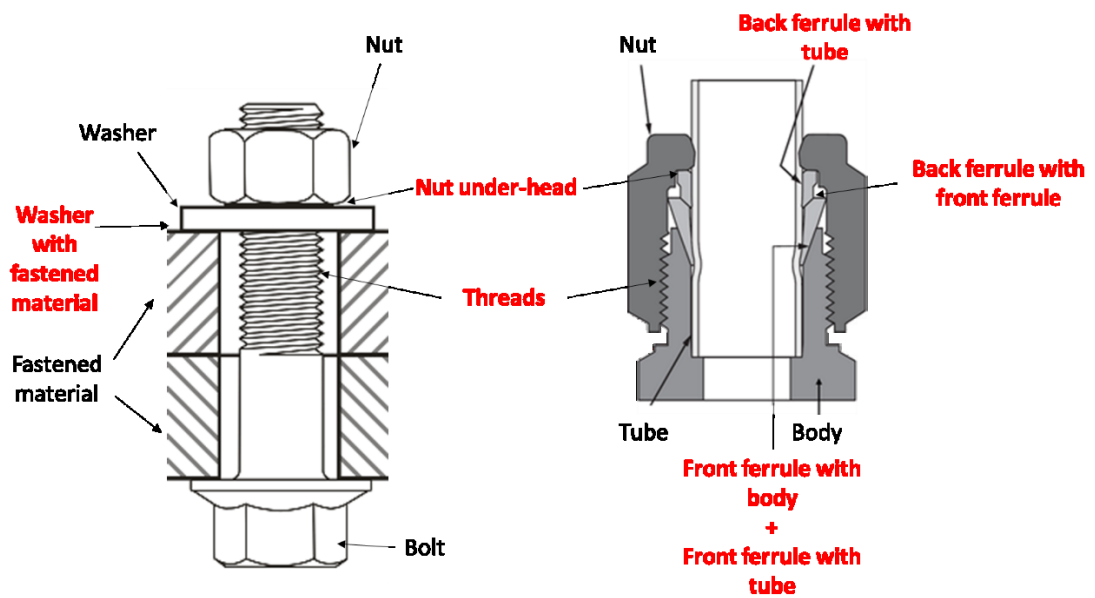
Figure 2-5 Comparison between the two different fastener types, with threaded fasteners (left) and threaded compression fittings (right); Contact areas are indicated with bold red text

Assuming that the conversion of forces required for both applications are within the ranges permissible for metric/unified thread standards to be used, there is a wide range of research that has been carried out for threaded fasteners which have the potential to be applied to the study of threaded compression fittings. One of these areas is the work that has gone into the study of the relationship between input torque and applied force for threaded fasteners which relates to the second similarity assumption. The relationship can be expressed by the short form equation as per Eq 2-7:

$$T = F * C \qquad\qquad - Eq\ 2\text{-}7$$

Where,

T = Input torque (Nm)

F = Applied force (N)

C = Experimentally determined constant

Although the constant "C" is an experimentally determined factor and is subject to variations, the straight line relationship between torque applied and force achieved will always be assumed to be accurate [59]. The application of this relationship requires the long form equation, though, where there are three forms of long-form equations that are typically used, all of which yield the same results. These include the ISO 16047 equation which has been attributed to Kellerman and Klein, DIN946/VDI2230 equation and Motosh's equation [60].

Motosh's equation in Eq 2-8 below is in a format that is easiest to understand, with constituent terms that make up the equation for the constant, namely thread pitch, incline plane, thread friction, and nut underhead friction resistance.

$$T = F \left(\frac{P}{2\pi} + \frac{\mu_{thread} r_t}{\cos \beta} + \mu_b r_n \right) \qquad \text{- Eq 2-8}$$

Where,

T = Input torque (Nm)

F = Applied force (N)

P = Thread pitch (mm)

μ_{thread} = Thread friction coefficient

r_t = Effective radius of thread contact (mm)

β = Half-angle of thread form (30° for ISO threads)

μ_b = Nut underhead friction coefficient

r_n = Effective radius of head contact (mm)

Assuming that Motosh's equation is valid for threaded compression fittings as the considerations are the same, it can be rearranged to consider a system CoF value, which takes into account the potentially different values of thread and nut CoF to give one CoF value acting on the entire assembly as shown in Eq 2-9:

$$\mu_{system} = \frac{\cos\beta \left(\frac{T_{input}}{F_{opposing}} - \frac{P}{2\pi} \right)}{r_t + r_n \cos\beta}$$

- *Eq 2-9*

Where,

μ_{system} = Overall coefficient of friction for the assembly

β = Half-angle of thread form (30° for ISO threads)

T_{input} = Input torque (Nm)

$F_{opposing}$ = Opposing force (N)

P = Thread pitch (mm)

r_t = Effective radius of thread contact (mm)

r_n = Effective radius of head contact (mm)

The system CoF in Eq 2-9 from rearranging Motosh's equation then is directly affected by the input torque and instead of the force generated during tightening

for fasteners, the opposing force should be considered. This opposing force component is comprised of the material resistance from the swaging process. An increase in the input torque directly results in the proportionate increase in global CoF. This only explains what is happening in an ideal situation though, where issues such as coating wear are not taken into consideration.

Threaded compression fitting considered in this study

Threaded compression fittings which can be in the form of one or two piece ferrules are used in various industries including oil and gas, chemical, semiconductor, biotech, and so on for securing fluid tubing connections. These ferruled compression tube fittings can be used in a wide range of critical applications due to its ability to provide leak-tight seals, including instrumentation connections, hydraulic, pneumatic, power, refrigeration and various other applications that involve the transportation of fluid using either metal or plastic tubing [61]. Manufacturers often offer this system where reliability in high-pressure situations during the connection of metal tubing is required. Reliability is increased when fittings which come in separate units as the risk of the sealing surface rotating as the tightening force is applied is minimised.

A double ferrule compression fitting system is considered for this study. It is illustrated through the use of a cutaway section in Figure 2-6 and comprises of several key elements, including the fitting body, front ferrule, back ferrule, connecting tube and the nut. The system works on the basic concept of swaging which deforms the tube in the process, highlighted in Figure 2-7. During the tightening process, the nut travels in the direction of the fitting body and exerts a compressive force on the back ferrule. The back ferrule, in turn, transfers a compressive force on the front ferrule, and the connecting tube is intentionally

deformed, guided by the angled fitting body as the nut is tightened and holds the connecting tube in the fitting. The system is designed to create a liquid tight seal, resist loosening of the nut due to vibration and prevent blowouts when in either vacuum or pressure systems during its operational life [62].
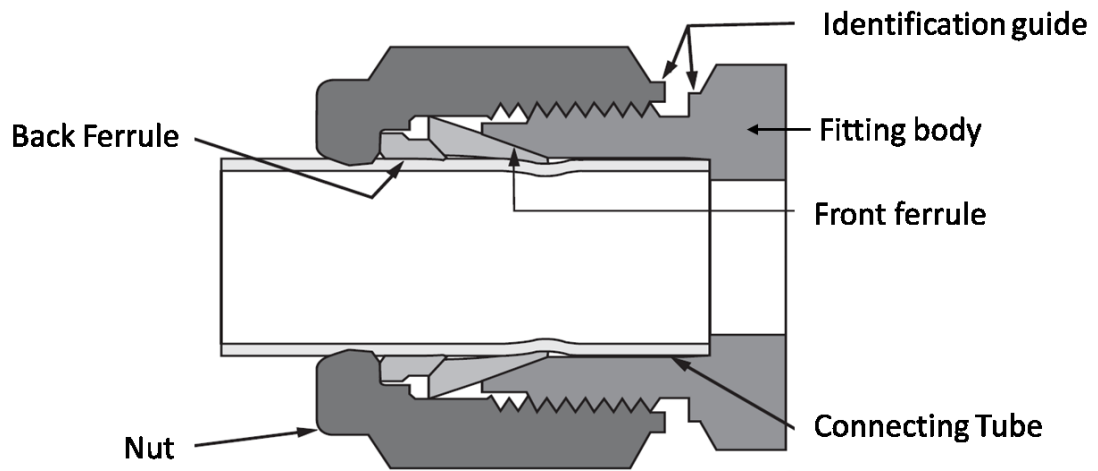
Figure 2-6 Cutaway section of a double ferrule compression fitting

Fittings suitable for use with metal tubing are typically made of the same metal as the tube. The inner diameter of the ferrules will be the same as the outer diameter of the tubing used. High performance, non-cost prohibitive applications such as instrumentation connections require metals with high corrosive resistance. These applications are critical in nature, where failures to the system will have potentially significant consequences to cost, time and even human life in extreme conditions. The main material of choice for most applications of this nature is austenitic stainless steels in 304 and 316 grades. Containing slightly higher amounts of molybdenum, 316 stainless steel has better overall corrosion resistance, higher pitting and crevice corrosion resistance in environments containing chloride when compared to 304. The increased performance makes it

cost effective when it comes to corrosion resistance and is relatively easy to fabricate.

The main drawback for the use of stainless steel in threaded compression fittings is its susceptibility to galling between unlubricated contact surfaces. A coating of silver is typically applied to the inner faces of the nut, including its threads to prevent galling and thus seizures during the make-up process of the compression fitting. Silver is also known for its tribological advantage of reducing the friction coefficient between the sliding contact surfaces [6]. Lubrication will be discussed in the next chapter sub-section. Furthermore, as a relatively noble metal, it is corrosion resistant, a desirable material trait for applications in highly corrosive environments.

One key difference to note between fasteners and compression fittings during the development of the self-lubricating coating is that there are limits to the CoF reduction in fastener coating. With very low CoF coatings, fasteners are prone to self-loosening in environments where it is subjected to external forces and slippage of the contact surfaces which has been the main subject of various studies [62-63].
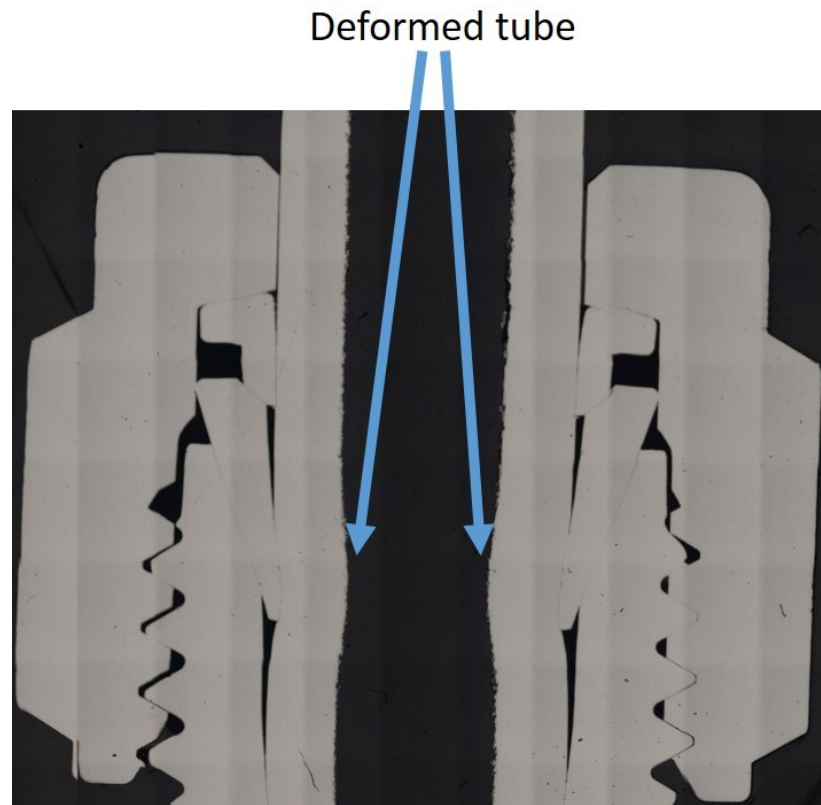
Figure 2-7 Compression fitting system - tube deformation post installation of compression fittings

2.2.4 Tribology of threaded compression fittings

Friction, Lubrication, and Wear

Lubrication forms an important part of tribological studies. As with any other machine, the adequate lubrication of screw threads is especially critical. In the event of inadequate lubrication, there is a risk of fasteners failing before its installation can be fully completed. This problem is further compounded by the fact that threads are difficult to lubricate due to poor or badly machined surfaces. Lubrication directly affects the CoF, and this has been the topic of interest for studies on fasteners [63], [65]–[67].

Although these studies have been focused on threaded fasteners of the bolt and nut type instead of threaded compression fittings, it can be argued that similarities exist between both the basic principles of operation and areas of contact. According to Gansheimer and Wessely, the majority of starting torque which is up to 50% is lost to head friction, followed by up to 40% of losses due to thread friction which means that only 10% of the torque applied is converted into the compressive force [68]. The authors also pointed out that the use of conventional oils and greases for thread lubrication are unable to perform due to the high pressures and low speed, resulting in oil seepage from the surfaces to be lubricated. In light of this, solid electroplated coatings can be tailored for use on fasteners.

As mentioned previously in this chapter, wear can be predicted based on its relationship to other tribological properties of a solid coating. As a system that is utilised on an intermittent basis, the solid lubricant coating for threaded compression fittings does not have to face the harsh conditions experienced by continually operated systems. Even so, it should be able to survive cycles of wear typically experienced through repeated installation and removal operations.

Make-up process (installation)

As opposed to threaded compression fittings, the issue of friction in threaded fasteners is one that has been studied in detail, where the conversion of torque input to the applied forces within the system is greatly affected by friction [67]. A practical technique for evaluating and verification of the force achieved for fasteners is the torque-angle curve. The torque-angle signature method is carried out through the examination of the tightening and loosening curves during the

installation process, through plots of torque versus angle during its installation and removal.

For threaded fasteners, the torque-angle curve can be used to identify torque to reach the bolt yield strength and structural integrity of fastener. There is a clear benefit in utilising this method for fastener joint assessment as the test is carried out during the assembly without the need for a load cell and without affecting the joint stiffness [63].

The torque-angle graph plots the torque exerted from the start of the assembly to when the fastener yields and can be used to understand the fastener behaviour during its assembly. The torque-angle curve for fastener assembly can be identified by Figure 2-8 four distinct zones as illustrated in Figure 2-8 [69]. Zone 1 is known as the rundown zone, Zone 2 is the alignment zone, Zone 3 the clamping zone and Zone 4 is the post-yield zone.

The rundown zone allows for the fastener nut to come into contact with the material surface which then leads into the alignment zone where fastener and material are drawn closer into a snug, settled position. Any prevailing torque from thread locking features such as thread deformations or inserts will show up in this zone. Shoberg has also noted that frictional drag as a result of parts misalignment, foreign material in the thread or out of tolerance threads will cause prevailing torque in this zone [69].

Rundown is followed by the alignment zone, where the fastener and mating surfaces are aligned in a stable, clamped situation. This zone is nonlinear owing to both macro and micro effects within this zone such as parts alignment, local surface roughness, coating deformations and thread deformations. The next

zone is the elastic clamping zone which follows a constant pattern. A key characteristic of this zone for threaded fasteners is the ability of this slope to be projected back to find its elastic origin. The product of angle-of-turn from the elastic origin can then be used to calculate the tension created by the fastener tightening process [69]. The post-yield zone at the end of the elastic clamping range signifies failure in the either the bolt or joint assembly. In threaded fasteners, the yield is used to verify the tension-angle coefficient for the tightening process. An example of the torque-angle signature curve is given in Figure 2-9 for an M12 bolt tightened to yield. The post-yield zone is not shown in the figure and this the yield of this bolt is approximately 135Nm at 210 degrees.

Figure 2-1 has been removed due to Copyright restrictions.

Figure 2-8 Generic torque-angle signature curve for fasteners showing the four distinct zones used to characterise the installation process of rundown, alignment, clamping and post-yield from Shoberg 2014 [69]

There is a benefit for the application of this non-destructive method to assess the assembly of threaded compression fittings as it could potentially identify defective assemblies prior to pressure testing. The main difference between using the torque-angle curve for threaded fasteners as opposed to threaded compression fittings is that although yield information for fasteners can be obtained, there is only a finite amount that the nut for compression fittings can travel because of its design. Although this is the case, excessive tightening during assembly will potentially restrict fluid transmission from a reduced inner tube diameter and causing unnecessary stress within the system by increasing the system pressure or result in thread failure.
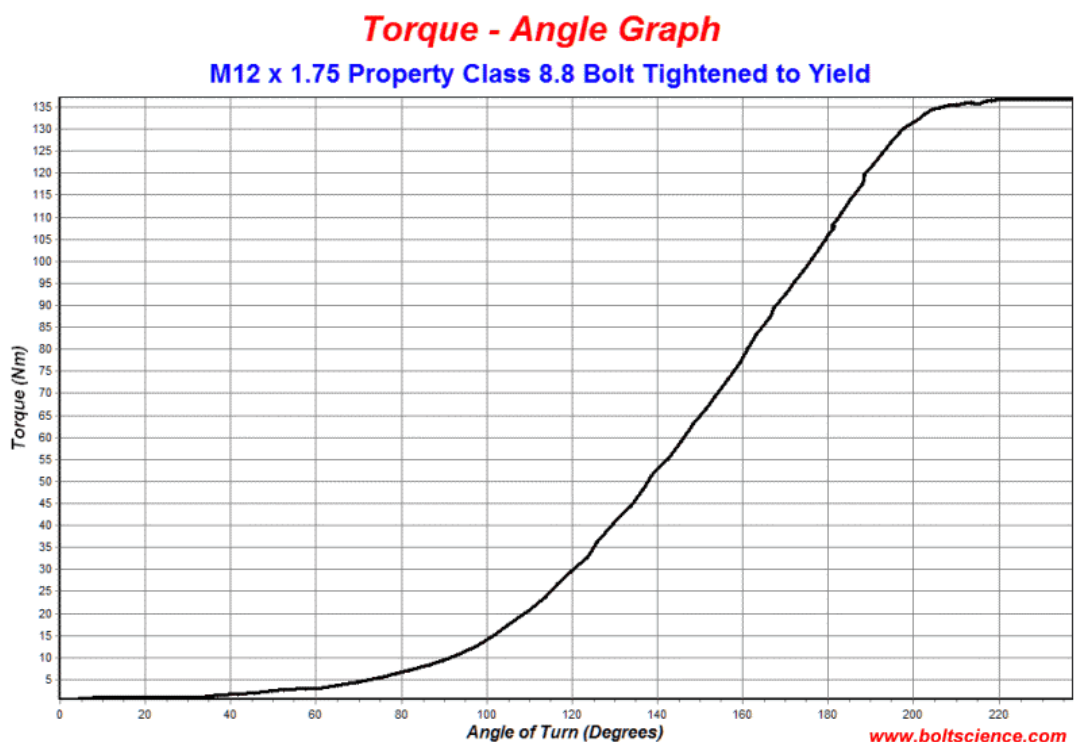
Figure 2-9 Torque - Angle Graph for an M12 bolt tightented to yield from Eccles 2016 [70]

2.3 Coating Deposition

The properties of a substrate metal can be altered through the use of surface coatings as part of the metal finishing process. These alterations may be to improve decorative or functional aspects of the substrate such as physical aesthetics, improved chemical resistance or even improved mechanical properties. Surface coatings which range from nanometre to micrometre thicknesses can be achieved through physical or even chemical thin film deposition methods. Although the outcome of both methods will result in a thin film being deposited on the substrate layer, physical deposition methods utilise mechanical, electromagnetic or thermodynamic phenomena while chemical deposition typically involves using a fluid or gaseous precursor [1]–[3]

The coating development carried out in this research will be focused on using electroplating. Electroplating is the use of an electrodeposition process to produce a uniform and dense coating that adheres well to metal or alloy surface using electrical current in a chemical process. The deposited coating is typically a more valuable material, and the process changes the physical characteristics of the substrate material. Although some coatings are for decorative purposes, the coating can also be used for protective purposes or even to enhance specific properties of the surface where the coating is deposited. The core of electroplating focuses on the electrolytic cell (electroplating unit). In the electrolytic cell, a current is passed through a bath containing the electrolyte. Pre-treatment and post-treatment processes are typically required to ensure the quality of the coating.

Electroplating is an important process that has been in use for over a century, and a wide range of metals can be deposited onto a conductive substrate material. Modern electroplating through necessary modification of the substrate material where required is carried out on a wide range of metal and plastics with the substrate material either being conductive or non-conductive. Through modern electrodeposition technologies, the properties of a less costly substrate material such as plastic to be modified through electroplating it with a more superior material, resulting in an extension of the superior properties of the usually more expensive metal such as a mirror metallic finish. Although it is a relatively cheap and versatile process, electroplating requires specialist knowledge, not just on the handling of aggressive and often toxic chemical solutions but also due to the complex relationships between the process steps and the final deposit quality. Dini provided a summary of electroplating factors which influence the metal deposit distribution as seen in Figure 2-10 [71].
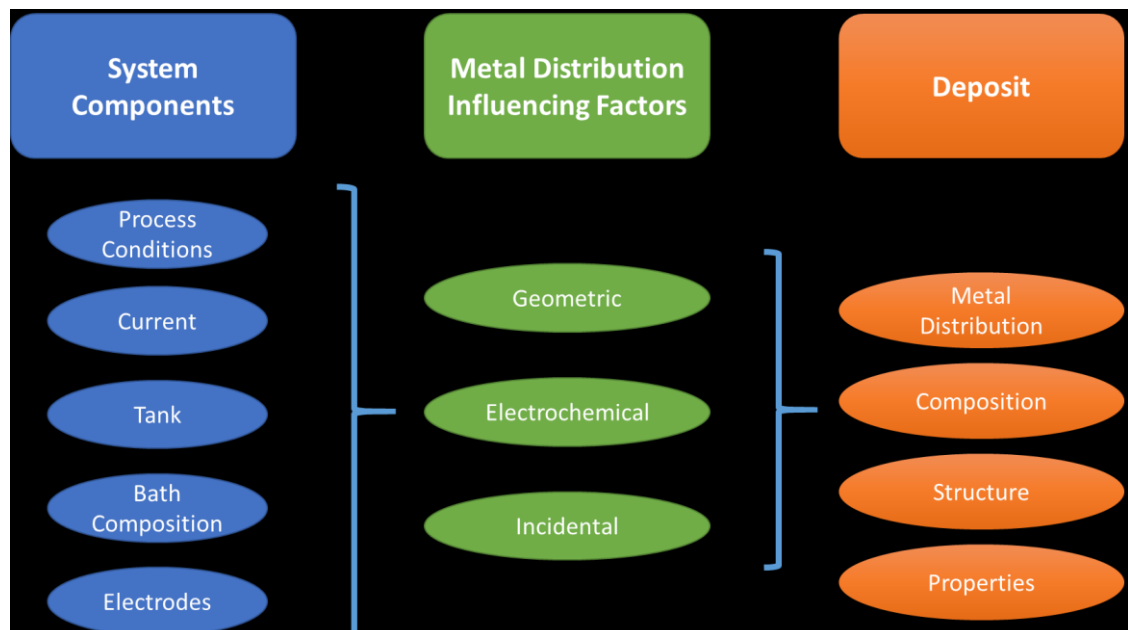
Figure 2-10 Metal distribution relationships and influencing factors for the electrodeposition process from Dini [71]

On the other hand, the flow of a typical electroplating process is shown in Figure 2-11. Due to the concentration and toxicity of electrolytes, chemicals and solvents used, treatment of the wastes generated during the electroplating process is necessary. Furthermore, the electroplating of metals such as silver and gold using traditional bath often contain cyanide, which is extremely toxic.
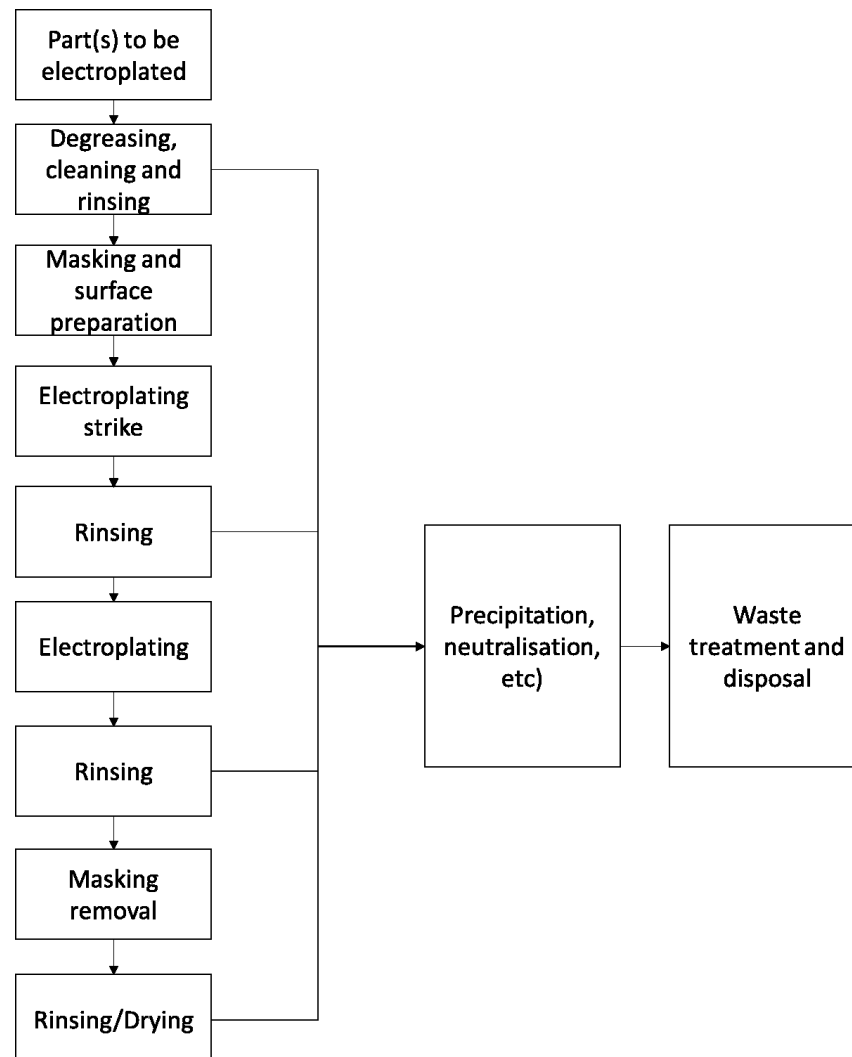
Figure 2-11 Flow of a typical electroplating process

The aim of this section is to provide an insight into silver electroplating and particle incorporation through electroplating also known as the electro co-deposition process. Specific focus areas in line with research objectives are the

topics of non-cyanide silver electroplating and methods for particle incorporation into the deposit to form a MMC.

2.4 Electrodeposition

Electroplating is the process of electrodeposition and electrodeposition is the depositing process of a substance through electrolysis [72]. Key electroplating process parameters include electrolyte composition, particle characteristics, current density, flow conditions and geometry of both the electroplating tank and electrodes [73].

A fundamental electroplating setup is shown in Figure 2-12 for silver. It is comprised of a rectifier which supplies the direct current via the two electrodes and the electrolyte (also known as solution or bath) which contains the dissolved metal ions. Electrolytes are ionic conductors whereby both ions and electrons move and common electrolytes used are aqueous acids, bases, and salts [74]. The plated object will be attached onto the cathode while the pure metal is attached onto the anode. The silver electroplating setup shown in Figure 2-12 utilises pure silver as the anode. The pure silver anode dissolves to replenish the silver ions that are deposited onto the plated object.
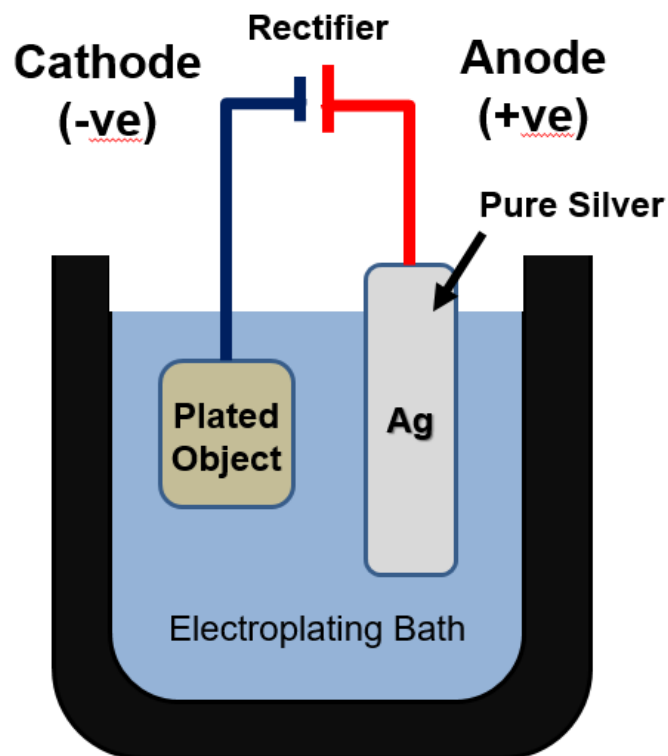
Figure 2-12 Silver electroplating cell

During the electroplating process, both the anode and cathode are immersed in an electroplating bath which contains an electrolyte as the electrical conductor. The current is carried by the ions in the electrolyte, and electrical conductivity closes the circuit. An electrical current is applied during the electroplating process. When the current is applied in the system, positive ions in the electrolyte move towards the cathode and negative ions move towards the anode. The workpiece is attached to the cathode or negative terminal which gives it a negative charge. The anode, on the other hand, can either be sacrificial or inert. Sacrificial anodes are of the same as the metal that is to be plated and it is dissolved to replenish the metal ions in the solution once it is depleted. Electrolysis occurs during electroplating as the direct electrical current applied to the electroplating solution is passed through the electrolyte and causes chemical reactions between circuit

and solution. The electroplating process can thus be carried out using either constant potential or constant current.

2.4.1 Faraday's Laws of Electrolysis

In 1833, Michael Faraday put forward his laws of electrolysis which has been fundamental in our understanding of the process. These have remained unchallenged and still form the basis of our current understanding of the process which can be expressed using Eq 2-10 and Eq 2-11:

$$Q = It = zFn$$

- Eq 2-10

Where,

Q = charge (Coloumb)

I = Current (A)

t = Time (s)

z = Change in oxidation state (g/Coloumb)

F = Faraday's constant (96485 Coloumb/mol)

n = Amount of oxidised or reduced substance (mol)

$$Q \propto \frac{zm}{M}$$

- Eq 2-11

Where,

Q = charge (Coloumb)

z = Change in oxidation state (g/Coloumb)

m = Mass (g)

M = Molar mass (g/mol)

Faraday's first equation shown in Eq 2-10, states that chemical change as a result of an electrical current is proportional to the quantity of electricity that has passed. This relationship is useful from a practical standpoint as the amount of chemical change can be predicted based on the measure of electricity passed within the system. The second equation shown in Eq 2-11, gives an inversely proportional relationship between the amount of different substances liberated using a given electricity quantity to its chemically equivalent weights. Practically, this means that based on the chemical weight of a substance, a prediction can be made as to how much it will be liberated using a given quantity of electricity.

2.4.2 Surface Preparation and Cleaning

The surface preparation of workpieces within any manufacturing process is critical and arguably even more important for electroplating processes. Workpieces which will be subjected to electroplating will typically undergo a series of pre-treatment processes. These will normally include cleaning the surface, modification of the surface as well as rinsing. The objectives of surface preparation are to remove any debris and contamination from the existing substrate surface such as film, dust, organic debris, mineral dust, oxide layers, and so forth. [75].

Poor surface preparation will result in issues with the electroplated layer such as poor adhesion and poor deposit quality. Adequate surface preparation of the workpiece being carried out will overcome these issues. Surface cleaning carried out removes physical contamination such as dust, film and debris left over from previous manufacturing processes. Surface cleaning can be carried out through either mechanical, chemical or both means depending on the severity and requirements for specific workpieces. Chemical cleaning typically includes degreasing using solvents, alkaline cleaning and even acid cleaning. Mechanical cleaning, on the other hand, is largely carried out through polishing and buffing processes. The advantages of polishing are that abrasives remove small amounts of the substrate metal and can be carried out to a consistent surface finish, useful if the substrate metal to be plated is highly reactive to the environment or if damages to the surface are present from previous processes.

Surface modification is carried out if changes in surface attributes are required. For materials that experience conductivity issues such as non-conducive or low conductive materials, this could include an application of a metal layer or surface hardening to improve conductivity. In certain cases, surface modification is carried out through the use of a strike. A strike process deposits a nanometre-thin coating which forms the base for subsequent electroplating operations. For substrate materials which possess compatibility issues which result in poor adhesive deposit properties, a strike can be used to improve the adhesion of the intended deposit metal.

Rinsing is an important process carried out when the samples (or workpieces in a manufacturing environment) are transferred between different electroplating solutions or after the final electroplating bath is carried out. The rinsing process

is intended to remove electroplating solution residue from the sample. In standard electroplating terminology, the residue known as drag out. Depending on the risks associated with the contaminated rinse water and environmental laws and policies, it might either be discharged to sewage systems or be treated before being discharged.

2.4.3 Electrolytic metal deposition methods

The electroplating process is one that can be carried out through several methods, namely through the use of a direct current method, pulsed current method or a pulsed reverse current method. Out of these methods, the methods of direct and pulse current methods will be explored in more detail. The advantages for electroplating as well as issues to be taken into consideration when using this method will be discussed alongside the issue of particle incorporation through electroplating in Section 2.6.

In an ideal electrolytic metal deposition process, the amount of electricity passed is directly proportional to the amount of metal deposited based on Faraday's law and can be calculated based on data from either of the electrodes. In reality, the electricity delivered to the electrodes will be used for other non-value added chemical reactions at the electrode. Within an aqueous solution, hydrogen evolution will occur at the cathode while the same will occur for oxygen at the anode from the following reactions:

$$2H_2O + 2e \rightarrow H_2 + 2OH^-$$

$$2H_2O \rightarrow O_2 + 4H^+ + 4e$$
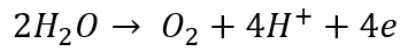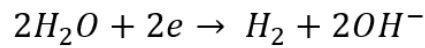
As the main goal is to achieve metal deposition, the conversion of the aqueous solution into its constituent parts are considered as losses within the process. To quantify this, the ratio of $\eta_{current} = \frac{W_2}{W_1} \times 100\%$ current efficiency is used, denoted by the formula in Eq 2-12.

- Eq 2-12

Where,

$\eta_{current}$ = Current efficiency

W_1 = Theoretical deposited weight

W_2 = Actual deposited weight

Direct current electroplating

The direct current electroplating (DCP) method is by far the simplest method of electrodeposition through the application of direct current and potential in an electroplating bath. DCP is carried out by the application of a direct potential and current in an electroplating bath, where the current source can be a battery or rectifier which converts alternating current to regulated low-voltage DC current.

Pulsed plating

Pulsed electrodeposition (PED) on the other hand is the swift alternating of current between two different values to create a series of pulses which are typically of equal amplitude, polarity, and duration that is separated by zero current [76]–[78]. PED can either be achieved through pulsed current methods, often denoted pulsed plating (PCP) or pulsed reverse current methods, and often denoted pulsed reverse plating (PRP). The benefits of PED over the DCP include that of improved throwing power, smaller grain sizes, reduced porosity, increased hardness and better ductility [79], [80].

PED through PCP can be achieved using a unipolar pulse current waveform as seen in Figure 2-13. The peak current is the maximum current applied; interval time is the time between pulses and pulse time is the duration in which the maximum current is applied. Components of the unipolar pulse current waveform include: pulse time (T_{on}), interval time (T_{off}), average current density (j_m) as well as pulse current density (j_p). Pulse time is where potential and current is applied, while interval time is when zero current and open-circuit potential is applied. According to Pearson and Dennis, three main parameters are required to enable characterisation of unipolar current pulses, which are pulse current density, pulse time and the interval time between pulses [79]. Detailed effects of PED variables towards electrodeposition have been summarised by Kelly [81]. Oscilloscopes are commonly used in conjunction with PED to visualise how well the pulse current waveform generator is able to control the output.
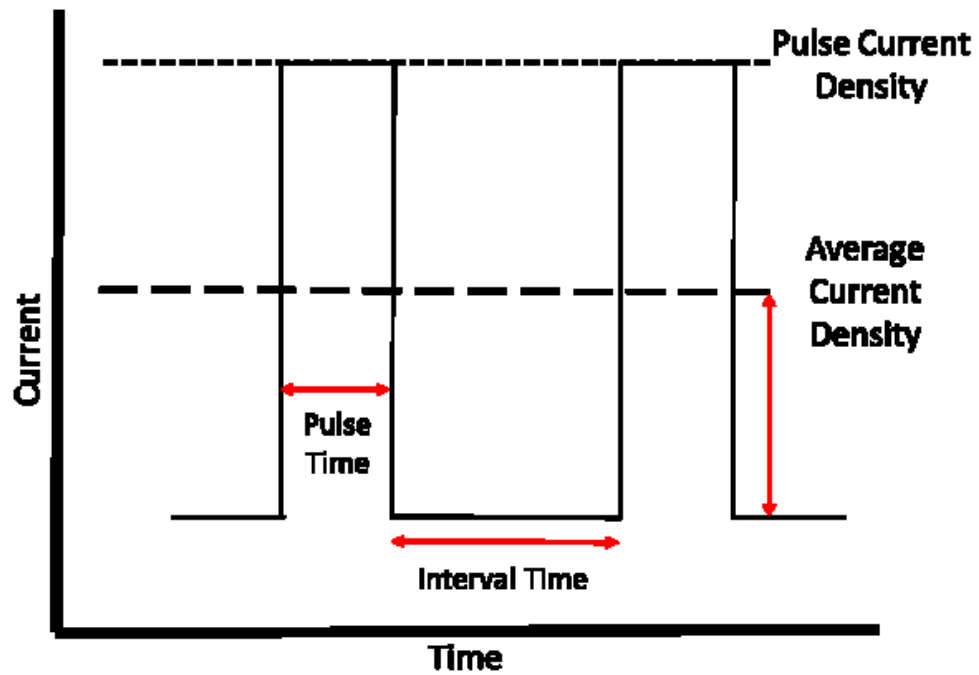
Figure 2-13 A typical unipolar pulse current waveform of equal amplitude, polarity, and duration that is separated by current pulses

From the peak current, pulse time and interval time, the average current density (j_m) and the percentage of time where the current is on (duty cycle) can be calculated based on the following relationships as defined in Eq 2-13 and Eq 2-14.

$$Average\ current\ density, j_m = \frac{j_p.\ t_{on}}{t_{on} + t_{off}}$$ *- Eq 2-13*

Where,

j_m = Average current density

j_p = Pulse current density

T_{on} = Pulse time

T_{off} = *Interval time*

$$Duty\ cycle\ (\%) = \frac{t_{on}.100}{(t_{on}+ t_{off})}$$

- *Eq 2-14*

Where,

T_{on} = *Pulse time*

T_{off} = *Interval time*

The PED process offers more control over parameters which can be adjusted independently and can withstand much higher instantaneous current densities [82]. PED affects the structure of deposited metal or coating by influencing the interplay between nucleation and crystal growth as part of the electro crystallisation process [83]. The application of a periodically changing current can be used to control these two processes above. This is achieved by controlling the negatively charged layer which exists in the cathode region. During DCP, restrictions from the layer which is charged to a defined thickness cause an obstruction to the ionic migration to the part. PED provides for the reduction of this obstruction by periodically disabling the applied current which in theory discharges the layer. The amount of layer discharge varies and can be controlled through PED frequencies. Furthermore, it is common belief that PED allows for the migration of ions to depleted high current density areas when current is turned off. Upon turning the current back on, a greater number of ions are available to be deposited.

When compared to DC plating, PED yields nanocrystalline coatings with improved surface appearance and properties, such as smoothness, refined

grains and enhanced corrosion resistance [19], [84]–[88]. PED currents can either be on-off (unipolar) or even reversed (bipolar) used along or superimposed on a DC feed [75]. There are four variable parameters which are critical to PCP. These are peak current density, average current density, interval time and pulse time; with one pulse cycle being a total of the interval and pulse time [89]. Control of the pulse cycles, specifically the pulse time, where current is applied is crucial to the success of the PCP process [38]. During the pulse time, an evenly distributed ion concentration is available for deposition. On the other hand, during the interval time, metal ions from the bulk solution are able to diffuse into the layer next to the anode [78]. By varying these critical parameters, the microstructure and properties of the deposited thin films can be controlled [80], [90]. The use of PED is also beneficial in the incorporation of particles within a deposit, details of which are discussed in Section 2.6.

2.5 Silver coatings

Silver is a precious metal with a melting point of 961°C that is resistant to most common acids but is weak towards nitric acid. As a noble metal which can be used as a replacement for gold in certain situations. It can be classed as an industrial metal due to its common use in various industries due to its excellent properties and relatively low cost compared to gold. These factors have resulted in its widespread use from coinage to non-cost prohibitive applications such as high-quality electrical conductors. Silver consumption for electronic and electric industries alone increased in use from 4.26 tons in 2001 to 6.21 tons in 2007 [91].

Furthermore, its metallic and shiny appearance makes it perfect for a wide range of applications, and not just for decorative applications such as silverware, but also for practical consumer applications such as mirrors. More recently the reflective and electrically conductive properties of silver have been harnessed for power generation applications such as photovoltaic solar panels [8], [92]. Other uses of silver include increasing wear and abrasion resistance, corrosion protection, aesthetics, and lubricity. Research has also highlighted the anti-bacterial benefits of silver for medical applications [5].

Silver coatings can be obtained through electroplating, where its characteristics are taken advantage of with a relatively low cost through the generation of a surface coating and the process is scalable at the same time. It was first achieved through a silver cyanide solution patented by the Elkington brothers in 1840 [15]. The silver electroplating process improves the properties of conductive metals through the thin film of silver deposited, which results in enhanced properties relative to the base metal [15]. The major drawback to the traditional bath solution introduced by Elkington is that it requires the use of cyanide as a key ingredient in the electroplating bath [14].

2.5.1 Chemical reactions taking place

During the silver electroplating process, the cathode where silver will be deposited is charged negatively. Electrons from the cathode transfer to the positively charged silver ions, thus releasing them as atoms of silver metal. Silver atoms then settle on the cathode surface and plate it. Based on Faraday's law of electrolysis, the same number of positive ions are required to be discharged on

the silver anodes to complete the circuit. The silver dissolves into the electrolyte and replaces the silver ions that have been deposited onto the cathode. In theory, the metal deposited on the cathode and the amount of metal sacrificed on the anode are at the same rate, as the uniformity of solution is maintained. During the crystallisation process, silver forms a face-centered cubic configuration.

Although alternatives to traditional cyanide silver plating techniques exist, traditional silver baths containing cyanide are still being referenced in recent texts and research [93], [94]. This chapter section will explore both cyanide and non-cyanide silver plating baths in more detail.

2.5.2 Cyanide silver electroplating

Traditional cyanide silver electroplating has not deviated much from Elkington's silver electroplating solution, however, it is worth noting that different electroplating solutions are optimised for individual applications and tailoring of properties, including deposit brightness, plating speed and quality of corrosion resistance, and so forth. These baths involve the use of cyanide complexes which have a requirement of free cyanide in the electroplating system to ensure that it works. Free cyanide in the plating solution plays several key roles. Firstly, it ensures that silver is soluble in the solution. Secondly, it is the electrolyte, and finally the anode is dissolved to ensure replenishment of the silver in the solution.

Cyanide silver plating used in commercial plating solutions typically contain 90-120g of free alkali cyanide per litre. Within this combination, metallic silver is comprised of between 25 – 40g/L, typically in the AgCN form of alkali silver cyanide or even sodium or potassium cyanide [17]. According to Morrissey,

potassium cyanide had become the norm for silver cyanide plating baths because of its increased solubility. The minimum operating pH for silver cyanide electroplating solutions are between 8.0 – 8.5 and the complex cyanide of silver is not stable if its pH is below neutral. If the pH falls below neutral, AgCN will form which is insoluble due to the hydrolysis. The formation of carbonate occurs in these alkaline cyanide systems, especially those with high concentrations of approximately 90g/L resulting in hydrolysis. The hydrolysis process causes dissolution of the anode thus resulting in deposit roughness. As a result of this, part of the operating process for this solution requires chilling the plating solution to 3°C and filtering out the excess carbonate; however, this only works for sodium cyanide solutions and not potassium based plating solutions. Alternatively, excess carbonate in potassium cyanide solutions can be treated using calcium cyanide or barium cyanide.

One of the drawbacks of the cyanide silver plating process is that it typically consumes a large quantity of fresh water which is used to rinse out the sample after electroplating. The large quantities of fresh water consumed is due to the cyanide ion being very surface active and hard to rinse out. Failure to completely rinse this out can cause issues such as staining. Furthermore, the treatment and disposal methods for silver cyanide electroplating wastes are both costly and are of detriment to the environment when successful silver electroplating using non-cyanide silver plating baths reported overcome this [14], [95]. The disposal of cyanide in industry is through further chemical processing. Cyanide disposal typically involves either complete destruction with chlorine gas or conversion into the less poisonous cyanate [14], [15].

Cyanide Silver Plating Dangers

Traditional silver plating methods used in industry increase the risk to health and safety as a result of the toxic cyanide component in the plating bath that forms complexes with silver [15], [96]. Cyanide is dangerous in either solid, liquid or gaseous form. Solid cyanide salts exist in the form of sodium or potassium cyanide. In liquid form, silver cyanide electroplating solutions contain cyanide ions which are corrosive to human skin and eyes. Both these solid and liquid forms of cyanide are extremely toxic and even lethal if ingested. In a manufacturing environment where silver cyanide electroplating baths are used, there is a risk of hydrogen cyanide gas being released when the solution pH falls below its recommended pH range or when the cyanide ions in the bath react with an acid.

Hydrogen cyanide gas is colourless and smells of bitter almonds. As a rapid acting poison, it can cause unconsciousness or death through suffocation. Long term exposure to the gas can cause cyanide poisoning resulting in symptoms of weakness, confusion, shortness of breath, headache, dizziness, seizures and even coma. Because of its level of toxicity, it is even categorised as an asphyxiant within a class of chemical weapons agents. During the processing of electroplating waste, even the sludge from cyanide solutions can cause poisoning, dermatitis, and nausea and has to be handled with appropriate care.

2.5.3 Non-cyanide silver plating

Due to its toxicity, cyanide alternatives to silver electroplating have been the topic of investigation for quite some time. The use of cyanide in silver electroplating

baths has traditionally been unavoidable due to its commercial feasibility as well as its ability to produce high quality electroplated surfaces which non-cyanide alternatives fail to do. In light of the problems associated with cyanide in silver electroplating baths, suitable and stable cyanide-free silver electroplating bath alternatives have been proposed over the years. Initial work for cyanide alternatives can be subdivided into three distinct groups by the type of compound used, namely simple salts, inorganic complexes and organic complexes [14]. It was only in the 20th century, though that cyanide alternatives to silver electroplating had a breakthrough. These baths were reported to be capable of producing mirror bright and ductile surface finishes while also being able to adhere sufficiently to substrates upon which the silver film is being deposited [16]. Initial attempts at eliminating cyanide from silver electroplating have failed to meet the quality of surface finish produced by a cyanide bath. Out of these cyanide alternative options, only the inorganic complex thiosulfate, and organic complex succinimide have been successfully adopted for selective commercial use [17]. In recent times, though, the non-cyanide silver plating baths have expanded through both academia as well as industry. These include patents filed as a result of industrial research and academia proposed alternatives which have investigated various complexing agents. These include variations in complexing agents related to initial work as well as newer proposals. To date, cyanide alternatives to silver electroplating have expanded to include complexes such as thiosulfate, succinimide, hydantoin, uracil, sulphite, ammonia, thiourea, HEDTA, 2-hydroxypyridine, ionic liquids, 5,5-dimethylhydantoin, trimetaphosphate, iodide and so on [97]–[117].

The issues typically associated with cyanide alternatives to silver electroplating include high costs of raw materials, especially for inorganic complexes, limited application of only a few metals, and poor adhesion without prior processing using a silver strike [17]. Strikes are special, micrometre or nanometer thin plating deposits of a compatible metal that will serve as a foundation for the subsequent plating process and sits between the main deposit and the substrate material. Morrissey and Blair have independently reported poor quality of deposits obtained from organic complexes, i.e. due to tarnishing, relative to the quality of deposits obtained from cyanide electrolytes [15], [17]. In addition to that, commercial operators who intend to use succinimide as a cyanide alternative for silver electroplating would have to periodically adjust the solution bath pH due to the hydrolysis of succinimide which reduces the operating pH of between 7.5 – 9 over time [118].

Analysis of cyanide alternative silver electroplating attempts are often focused on aspects such as the quality of the deposits through tarnish resistance, physical appearance or conductivity. Among the work carried out for the properties of silver deposits, the use of a non-cyanide succinimide complex found that thick, wear-resistant deposits are possible with compromised electrical resistivity [103], [104], [119]. These reported attempts at finding a cyanide alternative to silver electroplating along with the continued use of silver cyanide solutions in recent research provide evidence to support the fact that although cyanide alternatives are available, there is not a like-for-like replacement for cyanide in silver electroplating and like its cyanide counterpart, the plating bath has to be tailored to individual applications [9], [120]. Industrial silver applications that are often focused on aesthetics or electrical conductivity of the silver deposit represent a

knowledge gap owing to the forgotten tribological properties of silver. As such, the use of silver on threaded compression fittings requires a coating that is capable in its tribological properties.

2.6 Incorporation of inert particles in a MMC through electrochemical codeposition

Apart from electroplating pure metals such as silver, there has been a relatively new trend of incorporating other materials such as polymers during the electroplating process to form a metal matrix composite (MMC) [39]. The use of composite coatings where materials typically consist of two or more phases, when combined are able to exhibit properties that the individual materials are unable to. When this is carried out in the form of a coating, this becomes even more economical as materials of higher value can be used to improve the performance of the substrate material.

Research into MMC coatings has included the addition of polymers such as polytetrafluoroethylene (PTFE) particles, to produce a polymer composite surface coating with the advantage of being a metal coating with improved tribological properties due to the addition of the PTFE polymer. Polymers are attractive for being processed into thin films due to their low cost, versatility and ease of processing [121]. The polymer PTFE, in particular, is a fluoropolymer which has a low coefficient of friction but which also resists oxidation while retaining high thermal and chemical stability [122]. However, PTFE is not without its flaws, as it degrades rapidly when subjected to ionising radiation in ambient temperatures [123]. The degradation occurs as the polymeric chains are rapidly broken when

subjected to irradiation in the presence of air. As a polymer, it is also relatively soft in comparison to metals, and this directly affects its mechanical properties such as reduced load bearing capabilities which in turn accounts for higher wear rates when compared to metals. When it comes down to suitable material selection based on applications, PTFE excels in terms of tribological performance, where friction coefficients of around 0.05 have been obtained at high loads, low speeds, and moderate temperatures for directly applied thick (>10µm) PTFE coatings or interwoven PTFE fibres [124], [125]. Also, the self-lubricating properties of PTFE have resulted in its common use as a solid lubricant [126].

The first instance of electrochemical codeposition was in 1928 when Fink and Prince published their success in the codeposition of copper and graphite and research into various possibilities of successfully co-depositing of metal and suspended particles through electroplating baths have been reported on since [127]. Electroplating factors such as the geometry of the workpiece as well as bath agitation have been noted to be important the context of particle incorporation [39]. The benefits of MMC have also been commercially exploited and at present MMC coatings obtained through electroplating such as Nickel-PTFE (Ni-PTFE) are used for both its decorative and functional advantages over the standard nickel coating [128]. The incorporation of PTFE claim to have improved wear properties such as non-galling, dry lubricity, lower friction as well as improved corrosion resistance over existing coatings [128]–[131]. The work carried out by Pena-Munoz et. al. on the tribological properties of Ni-PTFE through electrolytic and electroless electroplating though a 10µm thick coating highlighted improvements in friction and wear. Interestingly this study showed that both methods had comparable frictional performance; however, the coating

life was improved for an electroless coating relative to an electrolytic deposited coating. This is a relevant finding as it brings to light the importance of coating life specification. A coating that is over engineered will have negative implications towards environmental sustainability in the increased use of raw materials and added processing as well as increased financial cost and manufacturing time. Considerations such as increased plating (processing) time are not mentioned within the context of coating development for the published papers and any improvements over tribological and wear properties could easily be overshadowed without holistic consideration of its impact.

On the other hand, research involving Ag-PTFE MMC coatings have been carried out for applications such as antimicrobial [32], conductivity [132] and improved corrosion resistance [8]. The successful codeposition of Ag-PTFE can be traced back to a series of patents filed by Helle et. al. in the 1980s. One, in particular, refers to the successful deposition of Ag-PTFE through electroplating for applications where low friction would be beneficial [133]. The authors were primarily focused on the chemical aspects of their patent, and thus a knowledge gap exists for the quantification of its tribological performance. Based on previous work, evidence exists to support the possibility of improving the tribological properties of a silver MMC such as improved CoF through the addition of the fluoropolymer PTFE which is already established in its use as a solid lubricant for various applications [126], [134].

A potential application of Ag-PTFE MMC coatings is for threaded connections, where the surface coating on threaded connections used for connecting valves and pipes is crucial to the sealability of the assembly as a whole. Key considerations for surface coatings on threaded connections include tribological

factors, galling (wear as a result of the friction and adhesion between sliding surfaces), aesthetics and potentially even load bearing capabilities depending on its application. Functional aspects such as the tribological qualities of the coating will affect the integrity and sealability of the connection during its assembly. On the other hand, the variation in galling resistance and friction affects the make-up torque and interface contact pressure of the assembly. Silver is a conventional, noble material used as a coating material when considering corrosion resistance with dry lubrication properties for non-cost prohibitive applications such as aerospace with improved benefits over Nickel [6]. It would be desirable for the Ag-PTFE MMC coating on stainless steel developed to exhibit improved dry lubrication properties and good adhesion. Furthermore, it is vital for the coating to achieve good coverage as defects in silver electroplating on stainless steel could be prone to corrosion which will ultimately lead to the failure of the protective film in harsh environments. There is also the potential for improved corrosion resistance through the embedding of PTFE particles in defects on the surface in the electroplating process [32].

The benefits of particle incorporation will be explored further in this section. However, those familiar with the PTFE polymer are also aware of the issues surrounding its handling during the incorporation process as it is chemically inert and has a low surface tension which will also be discussed.

2.6.1 Advantages and drawbacks of co-deposition

MMC coatings are defined as coatings consisting of particles in the second phase that have been dispersed throughout a metal matrix [75]. The matrix in this

instance is defined as the continuous phase in a MMC coating. The electrodeposition of a MMC coating occurs when a suspension of particles are co-deposited with the primary electroplated metal. The metal matrix often provides structural or physical strength to the coating while the composite second phase provides additional characteristics to the primary coating.

There are various advantages to the consideration of MMC utilisation within industry. Firstly, existing and often costly equipment can be reused after a relatively easy and low-cost conversion of conventional electroplating cells has been carried out. Furthermore, the benefits of electroplating are also realised in that it is a scalable process which carries industrial benefits in being able to support continuous processing, thus reducing costly changeovers and downtime. In addition to that, the process of electroplating is typically one of the final processes in metal finishing as limited post-treatment is needed if the production process is controlled, smooth and high-quality deposits can be obtained. Although various electroplating wastes are produced from the process, its volumes are relatively low as opposed to other techniques such as dipping or spraying. In the case of a silver MMC deposit through a non-cyanide bath, there is the added benefit of cyanide removal from the process and thus lower waste processing costs. Other advantages are that there is no need for specialist, high cost and high maintenance equipment such as high temperature or vacuum (as opposed to chemical vapour deposition or sputtering) and that the MMC can exhibit better properties as a result of the second phase particles.

On the other hand, there are several drawbacks to consider for MMC coatings. The introduction of particles does not overcome the core disadvantage of electroplating in terms of coating uniformity in that complex geometries will not

result in high uniformity of the coating. The addition of particles also limits the speed of the process. Processing speed for the electroplating operation in a manufacturing environment will be limited by the rate at which particles can be co-deposited. Lastly, particles which are to be incorporated into the second phase have to conform to the particle size limitations.

In short, the MMC can encompass a wide range of materials, including pure metals, alloys, ceramics and even polymers. Even though the co-deposition of the second phase is relatively robust, there are certain criteria that have to be adhered to, namely being insoluble to the electrolyte and wettable. Other than that, the second phase particle form can either be in a powder or fibre regardless of orientation or be conducting or non-conducting. The particles have to be continually suspended in the electroplating bath, and it has been suggested that an upper particle size of 40 µm in diameter should be adhered to [135].

2.6.2 Considerations for codeposition

The process of electroplating is sensitive to the effects of temperature, and it can be classified as being a critical variable in the electroplating process. Increases in temperature from an optimum temperature will increase the conductivity of the bath as the rate of diffusion, and ionic mobility is increased. Other potential effects of temperature changes include the evaporation and hydrolysis rates of the bath. Additive deposition rates may also be affected by changes in temperature. Due to the complexities of the potential impacts as a result of temperature changes, its effects can only be determined through trial and error, and this will vary with solution composition. Based on this, it is ideal to keep temperature as a controlled

variable with limited fluctuation from the optimal bath temperature. This has to be constantly monitored during the electroplating operation as the temperature of the bath will rise from its resistance to the passage of current. If the evaporative effect of cooling is insufficient, other methods of bath cooling will have to be considered. Apart from the effects of temperature, other factors to consider include the electroplating bath composition and pH. Inadequate control of these factors will result in issues relating to deposit quality. Through the application of a constant voltage or current in electroplating, the geometry of the part will affect localised current densities as well. Furthermore, in the context of continued bath use, electrolyte cleanliness, and bath ageing have to be taken into consideration. The use of appropriate filters to remove contaminants in the electrolyte and proper bath maintenance will ensure consistent deposit quality.

In terms of codepositing particles within the second phase as a MMC, issues such as particle type, concentration, shape, and size have to be considered. For the PTFE particle type, as it possesses a low surface tension, this can be overcome through the addition of a suitable surfactant. The surfactant reduces the surface tension of PTFE as it is suspended in the electroplating bath. One of the surfactants which have been used successfully for PTFE is the cationic fluoropolymer FC-4 surfactant [32]. There is a drawback to using surfactants, though, as it will also be incorporated into the MMC during electroplating. As such, it is imperative that compatible surfactants are used. Methods such as using high nanoparticle concentrations in the electrolyte solution, smaller sized nanoparticles, low concentration of electroactive species, the use of ultrasonification during deposition and even the use of PED can be considered to obtain high rates of incorporation for the dispersed particles [18], [75]. PTFE

particles rely heavily on adequate bath agitation to facilitate incorporation into the growing metal matrix as they are non-conductive without treatment.

There is the possibility for codeposition parameters also to affect suspension stability [136]. Suspension stability for spherical particles according to Stokes law is given by Eq 2-15.

$$v = \frac{2gr_p{}^2(\rho_p - \rho_c)}{9\mu}$$ *- Eq 2-15*

Where,

v = Velocity (m/s)

g = Gravitational acceleration (m/s^2)

r_p = particle size (m)

ρ_p = Particle density (kg/m^3)

ρ_c = Electrolyte density (kg/m^3)

μ = Viscosity (kg/ms)

According to this law, the stability of the suspension will increase when particle settling speed decreases. As such, Stoke's law dictates that particle size and density will have an impact on suspension stability, whereas bath conditions such as temperature and composition will dictate the density and viscosity of the electrolyte.

2.6.3 Models for foreign particle incorporation into MMC (particle codeposition)

Although particle codeposition was first carried out in the 1920s, attempts were only made to describe its mechanisms several decades later. The earliest

suggested mechanisms for the co-deposition of particles included that of electrophoresis, mechanical entrapment as well as adsorption. In 1962 an attempt was made to explain the process of electrochemical codeposition through Withers's work, where he proposed the role of electrophoresis in drawing particles with a positive surface charge to the cathode. Several years later, Martin and Williams proposed that mechanical entrapment of the particles in the growing mechanical layer occurred as the particles were transported to the cathode through bath agitation [137]. However, their proposal was rejected by Brandes and Goldthorp as they believed that an attractive force such as electrostatic force must be present to hold the particles for a sufficient period for incorporation into the metal matrix.

The 1970s saw a breakthrough in theory with Guglielmi's model for the codeposition of inert particles in a MMC which was warmly received and forms the basis of our current understanding [138]. Guglielmi proposed that the codeposition process was as a result of a two-step process of both electrophoresis and adsorption. The first step is a physical one which involves the loose particle adsorption onto the cathode surface. In this state, they are in equilibrium with the suspended particles, even though they are still surrounded by a cloud of adsorbed ions. The second step is a chemical one involving the irreversible adsorption of the particles on the cathode through loss of the ionic cloud through the electrical field present at the cathode. As the deposited metal is growing, the particles are incorporated into the MMC due to the strong adsorption.

Celis, Roos and Buelens [33], [139] carried out further development to Guglielmi's model. The model proposed by the authors was that the adsorbed double layer

forms around each particle in bulk solution which is illustrated in Figure 3-5. These particles are transferred to the hydrodynamic boundary layer through forced convection and particles arrive at the cathode by diffusion. As the free and adsorbed ions are reduced, the particle becomes entrapped when a fraction of the ions originally adsorbed are reduced.

Other models for particle incorporation include the model proposed by Hwang and Hwang which is similar to Guglielmi's model with differences of three current densities being identified [29]. The rate of particle codepositon is determined by electrode reactions of adsorbed species on the particles.

In 2002, Bercot et. al. developed a mathematical model for the codeposition of PTFE into a Nickel MMC based on Guglielmi's model of particle incorporation [20]. Although the authors did not mention the use of a surfactant or their method for obtaining a dispersed, stable PTFE suspension, they reported reproducible results using direct current and mechanical stirring methods.

Figure 2-14 has been removed due to Copyright restrictions.

Figure 2-14 Model of particle incorporation proposed by Celis, Roos and

Buelens [31], [140]

2.7 State of the art silver composite coatings

Silver has been traditionally used for its aesthetic properties but in recent times, silver in the form of Ag-PTFE MMCs have been exploited for its other lesser

known properties for a variety of applications such as power generation and biomedical.

The use of silver in the power generation industry is to take advantage of its excellent properties. Research has found nano silver structures to have excellent electronic, magnetic, optical, thermal and catalytic properties, which are in turn influenced by its size, shape, morphology and crystallinity [141]–[143].

Fu et al. reported successful deposition of Ag-PTFE on stainless steel through nicotinic acid and bi-pulse electroplating [8]. The Ag-PTFE coating was used within a fuel cell, where their focus was on increasing the contact angle of water on the coating, which is beneficial for water management of the fuel cell stack. The authors found that the embedded PTFE did not affect the corrosion resistance of the silver plating and later concluded that the PTFE particles were embedded into the defects of the Ag coating during electrodeposition and this reduced the defects on the overall coating. Within their published work, the authors neglected to state the parameters and conditions used during electroplating, and the scope of their published paper did not include an assessment of other coating properties such as porosity, thickness, adhesion, tribology or wear resistance.

On the other hand, Zhao et al. reported their research into the development of a Ag-PTFE MMC coating with anti-microbial and anti-corrosion properties through the use of electroless plating for biomedical applications [32]. Their developed coating was focused on creating a biomedically safe coating for use in the human body which would have the benefits of preventing bacterial infection through a low surface energy. Thus, research carried out by the Zhao et al. were focused

on evaluating the surface energy through contact angle measurements and bacterial adhesion tests. The researchers tried 3 different solutions and 5 different surfactants to obtain the Ag-PTFE coating and found the coating thickness to be between 1-2 micrometres. The authors provided an SEM micrograph of a uniform, rough silver deposit which coincide with low amounts of PTFE incorporation. The authors later claim improved PTFE deposition which had a smooth deposit appearance; however, this claim was not supported with any SEM micrographs. In relation to PTFE incorporation using surfactants, Zhao et al. later reported a linear relationship between PTFE in the plating solution with incorporated PTFE in the Ag-PTFE MMC and concluded that the FC-4 surfactant showed best performance in uniformly dispersing the inert PTFE particles within the plating solution. The work also concluded that the corrosion performance of Ag-PTFE was improved over 316L stainless steel. Again, due to the scope of the work limited information about the other properties of the coating was provided.

The morphology of deposited silver dictates the overall surface morphology of the Ag-PTFE deposit as silver is the only conducting material in the context of electrodeposited Ag-PTFE. Experiments carried out by Liu et. al. to understand the morphology of silver deposits relative to applied current density found that a low applied current density resulted in the formation of silver aggregates occurred, while dendritic morphological silver deposits were created at higher densities (Liu et al. 2015). The experiments carried out by Liu et al. were focused on the creation of dendritic deposits of silver to take advantage of its conductive properties. However, the authors only reported on a limited number of coating properties which limit its applicability for tribological applications, where properties such as coating thicknesses are critical. Within the context of

tribological applications, the use of silver aggregates would be more suitable as opposed to silver dendrites due to load bearing requirements of the nanostructures.

Research carried out on Ag-PTFE coatings have thus far been limited to specific applications in power generation and biomedical, where specific coating characteristics have been investigated and coating deposit refinement techniques have not been fully investigated. One specific coating deposit refinement technique is the utilisation of PCP, where authors such as Shanti et al. have found improved coating thickness uniformity with less porosity and finer grains over DCP [144]. Earlier work carried out by Shanti et al. using PCP frequencies of 10, 25, 50 and 100Hz with a constant 120s plating time found an inverse trend in the deposit thicknesses with frequency used and concluded that good quality deposits with low porosity and fine grains have been obtained from low peak current density and higher duty cycles [120]. Gaps in the works published by the authors include that of coating characterisation, where mechanical coating properties such as adhesion would be of great benefit.

Among the non-cyanide silver electroplating baths available, Ren et al. reported their successes in obtaining good quality silver deposits using a thiosulfate bath on a copper substrate with good adhesion results [145]. The adhesion tests carried out were as per the QB/T 3821-1999 standard which is based on the international ISO 2819 standard for testing adhesion of electrodeposited and chemically deposited coatings on metallic substrates which only details a method for qualitatively evaluating a coating. On the other hand, silver deposits with increased microhardness over conventional cyanide silver plating of similar thickness have been reported using a non-cyanide succinimide bath. The

research carried out by Jayakrishnan et al. through their work on electroplating silver on a copper substrate using a succinimide bath found that current efficiencies of up to 98% were possible at controlled pH and temperature and reported that the resulting silver coating exhibited with a microhardness of 75.2 Vickers, which was harder than 60.3 Vickers for a conventional cyanide plating [96]. Within the publication, no meaningful images of the surface morphology were provided and characterisation of the resulting coating such as adhesion and tribology were not considered. The wear of a coating is impacted by the hardness of the coating, and there is a benefit for a having a harder silver deposit in the context of a silver coating on stainless steel and thus the succinimide bath warrants further investigation.

In terms of tribology for silver coatings, Jang and Kim Investigated dry sliding friction experiments with soft metallic coatings including silver and concluded that optimum film thickness for silver to be between 7 to 10 nm [146]. The limitation of the work was that it was only carried out under low load contact sliding on a relatively soft silicon substrate. It was only quite recently that Tronci and Marshall assessed the behaviour of silver as a low friction coating in aerospace fasteners and found the thread friction to be between 0.1 – 0.14 as a result of shear flow of silver coating during the assembly process [147]. The assembly tests carried out by Tronci and Marshall utilised liquid lubrication on the bolt prior to assembly and thus the CoF values obtained were not of dry sliding. Furthermore, it has not been clarified if a cyanide silver or non-cyanide silver electroplating method was used during the electroplating of the nuts and the application is limited in the context of this thesis.

2.8 Coating testing and evaluation

Adhesion is a key characteristic of a deposited coating and there are various methods for the assessment of coating adhesion, including the use of pressure sensitive tape, acceleration testing, electromagnetic stressing, shock wave testing, tensile and shear testing, laser techniques, acoustic imaging, indentation tests and scratch testing, with the scratch test having the widest commercial use [148], [149]. The scratch test not only provides the provision of assessing adhesion, but the cohesive and tribological characteristics are also able to be obtained for both industry and research. This test was introduced in the early 1980s and is carried out by moving a diamond indenter across the surface to be tested at a constant velocity, typically with a linearly increasing load. The scratch testing method is able to highlight adhesion failure of the coating through failure modes such as coating detachment, through-thickness cracking, plastic deformation and cracking in the coating [149]. A variation of this technique for tribological analysis of coatings is by using a sliding sphere [49], [150].

Where the characterisation of a coating primarily involves its tribological properties, tests such as pin-on-flat or pin-on-disc methods have been utilised for characterising coatings [146]. This method is well suited for the tribological and wear assessment of thick coatings and offers a variety of wear mechanisms.

In terms of standards, ISO2819:1980 is commonly used for testing the adhesion of metallic coatings on metallic substrates deposited using electrodeposition or chemical deposition. This standard is limited to qualitative tests carried out on the deposit coating and as such, the comparison of 2 or more coatings using this standard is limited by the biases of qualitative data comparison and apparent lack of quantifiable resolution. As such it is much more suitable for applications within

an industrial context where process parameters have been fully established, as opposed to within a research and development context.

Threaded compression fittings are used as connecting components within a wider system for the transmission of a media under pressure. Component robustness is challenged through pressure testing to the relevant pressures which are dependent on the size and wall thicknesses of tubing used. Furthermore, the major manufacturers for threaded compression fittings have not included the test methods or standards utilised in the testing of the coatings on the compression fitting nuts in published literature. Moreover, deterioration of threaded connectors due to tightening operations is recognised as a failure mode for pressure tests [151]. On the other hand, the importance of the tightening process towards the creation of a successful assembly is widely acknowledged for threaded fasteners. Threaded fasteners are tested to various standards, key among which is the ISO16047:2005 standard, which determines the tightening characteristics of threaded fasteners as well as its associated parts. The applicability of this standard is towards fasteners made of carbon or alloy steel with ISO metric internal or external threads per ISO 68-1. The standard takes into account CoF of contact areas during assembly as it impacts on the overall tightening process, which is in turn directly affected by the interactions between surfaces due to lubrication.

2.9 Summary of the chapter

This chapter has provided a review of existing knowledge in relation to coating deposition as well as key tribological concepts relevant to threaded compression fittings.

As electroplating is typically carried out as part of finishing operations, a key consideration prior to electroplating is surface preparation and cleaning to ensure deposit quality and adhesion to the substrate. This chapter has also highlighted the development of non-cyanide silver plating methods which has progressed over the years to be of equivalent quality to traditional cyanide electroplating methods. In addition, although the incorporation of PTFE into silver to form Ag-PTFE composite coating had previously been successfully attempted, there are knowledge gaps in achieving this using a succinimide silver bath and more importantly the quantification of its tribological performance.

In relation to key tribological concepts relevant to threaded compression fittings, an overview was provided for threaded fasteners, and a comparison between fastener types was carried out, since studies relating to threaded fasteners are more established. Issues such as the effects of screw thread profiles in the capability of converting torque into linear motion were also considered. All the issues discussed in this chapter have provided the basis for identifying the main issues surrounding the tribological testing and lubrication of fasteners which will be used in the self-lubricating coating development process in the following chapters.

Furthermore, the literature review has highlighted several gaps in current knowledge which this research is aimed at addressing. Firstly, traditional

research into non-cyanide silver electroplating has been focused on the aesthetics of the coating for decorative applications. Modern research on the other hand, has exploited the antibacterial properties of silver for biomedical applications along with its conductive properties in the power generation applications have shown promising results. There is an opportunity to better characterise the physical properties of a non-cyanide silver coating. Secondly, silver has been used as a low-friction coating for aerospace fasteners. However, the low-friction coating is used in conjunction with liquid lubricants during assembly. Moreover, electroplated silver with embedded PTFE is not novel. The opportunity therefore lies in understanding the dry sliding tribological properties of silver and silver-composite fabricated using environmentally friendly methods. Thirdly, pulsed plating is advantageous in depositing harder coatings with a fine grain structure and is advantageous in embedding foreign particles. There is therefore an opportunity to characterise silver deposits using a non-cyanide process using pulsed plating. Fourthly, threaded compression fittings of a ferruled type have been in use for decades with silver used as a solid lubricant in dry sliding conditions during assembly. These silver coatings are typically carried out using traditional silver plating parameters, and there is an opportunity for non-cyanide alternatives to replace the environmentally detrimental process associated with traditional silver electroplating. Finally, leading manufacturers of threaded compression fittings stipulate a qualitative rotational angle target in addition to a qualitative "feel" of torque during assembly. Present day understanding of fasteners have highlighted the importance of both angle and torque targets during assembly and it would be advantageous to quantify the process.

The next chapter details the methodology used for coating development and experiments carried out in achieving the aims and objectives of the research.

Chapter 3 Coating synthesis and analysis

3.1 Introduction

The literature review in Chapter 2 provided key information concerning existing knowledge on threaded compression fittings, current knowledge on electroplated coatings, and the incorporation of particles into a silver MMC. The literature review on threaded compression fittings provided key aspects to consider for the various aspects involved in the make-up process of these fittings. On the other hand, the literature review on electroplated coatings provided general hints on aspects that would be worth considering for non-cyanide silver MMC electroplating.

The analysis was carried out after each set of experiments and the key learnings from the analysis were used to inform further experiments that were carried out. This gradual but systematic coating development method forms the basis of meeting the project aims and objectives. This chapter subsequently details the methodology for the experimental work that was carried out in the development of a self-lubricating composite coating for threaded compression fittings

3.2 Methodology

The development of the self-lubricating composite coating is spread across three stages as seen in Figure 3-1. Stage 1 comprises of the initial development of the coating, which covers aspects such as trials using different voltages, varying PTFE bath content and substrate surface modification and subsequently a structured investigation of variables to find the optimum bath variables for a coating which meets the aims and objectives of the research. Stage 2 involves further coating refinement and this involves the utilisation of surfactants, pulsed plating and an investigation into the utilisation of strikes. The final stage, is an assessment of the coating for use in threaded compression fittings. As performance data for the existing coating is not provided by manufacturers, commercial cyanide silver coatings are compared alongside a non-cyanide silver and the Ag-PTFE coating developed as part of this research.

Framework for the development of a self-lubricating non-cyanide Ag-PTFE composite coating for threaded compression fittings (TCFs)
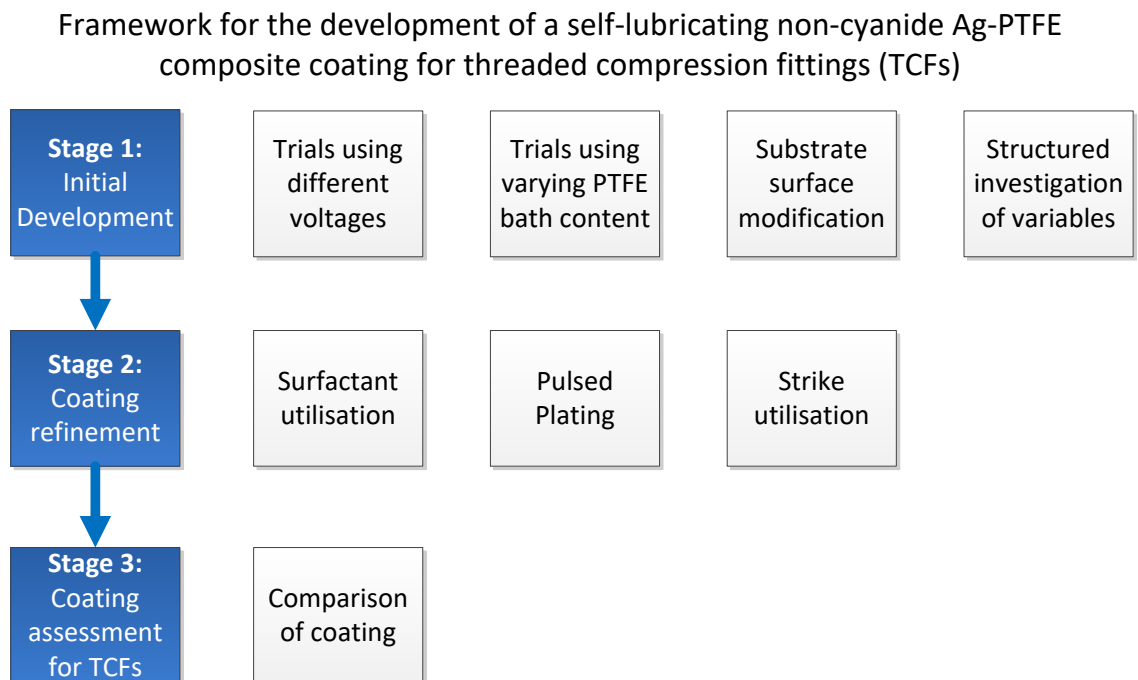
Figure 3-1 Framework for the development of a self-lubricating non-cyanide Ag-PTFE composite coating for threaded compression fittings

3.3 Cleaning and surface preparation

Surface preparation plays a key part for laboratory testing of samples to ensure that surface conditions remain constant throughout. Furthermore, it is also a key part of ensuring a consistent and acceptable surface quality during the electroplating process. For cleaning, an alkaline cleaner was employed containing sodium hydroxide, sodium carbonate, tribasic sodium phosphate, and sodium metasilicate with concentration listed in Table 3-1. Sodium hydroxide is commonly used as an ingredient in the manufacture of soaps and detergents. Sodium carbonate on the other hand is used for cleaning and polishing silver. Tribasic sodium phosphate is widely used in formulations of consumer grade soaps and detergents as a cleaning agent. It is commonly used for cleaning and degreasing of oils left over from the manufacturing process. Lastly, sodium silicate can improve the ruggedness of the solution by forming a coating of silicates on the detergent granules.

The samples to be cleaned were immersed in the cleaning solution, and the entire solution was put in an ultrasonic bath for 600s. The acid etching and surface activation were carried out using 5% w/v HCL acid. Deionised water was also used for cleaning and rinsing the samples where necessary. The acetone used during sample cleaning and surface preparation was of analytical grade. For surface roughness investigations, grit sizes of 320, 400, 800 and 1200 were considered. The substrate would be subjected to 10 manual cycles of polishing in a direction perpendicular to the linear tribometer test and its surface analysed before electroplating.

Table 3-1 Alkaline cleaner composition

Composition	Concentration
Sodium Hydroxide (g/L)	25
Sodium Carbonate (g/L)	30
Tribasic Sodium Phosphate (g/L)	15
Sodium Metasilicate (g/L)	20

3.4 Coating Synthesis

Initial trial and error were carried out to understand better the potential for obtaining a successful silver deposit. This was conducted using a similar alkaline non-cyanide silver plating solution based on successful attempts of obtaining succinimide silver electroplating deposits at a plating time of 600s [103]. The succinimide silver electroplating bath is made from two distinct parts. The first part of the electroplating bath comprises of a silver nitrate and succinimide solution resulting in a neutral pH of approximately 7. An aqueous potassium hydroxide solution is then added to increase the alkalinity of the bath to meet the pH requirements. The trial and error was then carried out for both temperature and pH to ensure that a realistic operational range was present not just for subsequent experiments but also for the bath to be used within industry. Temperature was varied in 1°C increments while pH in 0.5 increments. Each trial was carried out one at a time on 3 samples based on a nominal temperature of 30°C with a tolerance of +/-2°C and a nominal pH of 9 +/-0.5 to ensure that a coating could be successfully obtained on 304 stainless steel plates using a constant voltage of 0.5V. A successful coating on the substrate is visually

observed as a uniform, off-white deposit on the substrate. All samples trialled showed success in having a deposited coating.

The succinimide bath that was chosen for further study had the bath compositions as summarised in Table 3-2. Further developments of the electroplated coating were carried out on the same 304 stainless steel plates. Specifications, physical properties and elemental compositions of the plates are listed in

Table 3-3. For the non-cyanide silver plating bath, succinimide added acts as the complexing agent to the electrolytic solution. The PTFE used was supplied by Sigma-Aldrich with particle sizes quoted by the manufacturer with average particle sizes of 0.22μm, 60wt.% dispersion in H_2O.

Table 3-2 Variables that were investigated for the Ag-PTFE surface coating

Composition	Ranges
Silver Nitrate (g/L)	17-34
Succinimide (g/L)	50-80
Potassium Hydroxide (g/L)	12-14
Solution pH	8.5 – 9.5
Temperature (°C)	28 – 32
Current Density (A/dm^2)	0.13 – 0.15

Addition of PTFE into this succinimide silver electroplating bath and subsequent success in obtaining a Ag-PTFE MMC has not been previously reported to the knowledge of this author at the time of conducting the experiment. As such, trial and error using a moderate addition of 5% PTFE in the bath was carried out on 3 samples to understand if PTFE can be successfully incorporated. Subsequent EDS analysis of the plated samples was carried out as part of the SEM analysis to determine the presence of PTFE $(C_2F_4)_n$ through carbon and fluorine elements on surface characteristics of the stainless steel substrate. This showed success in PTFE incorporation within the MMC through the detection of fluorine element in all the samples.

Through reflection of experiences obtained through one-at-a-time trial and error, the author decided to seek a more structured method for investigating subsequent variables that could impact on the tribological performance of the coating. These factors include theoretical coating thickness controlled through voltage, time and bath conductivity as well as PTFE incorporation controlled through PTFE concentration in the bath and the hydrodynamic conditions in the bath that are affected by bath agitation speed. These are discussed in more detail in Section 3.4.2.

Table 3-3 Specifications, physical properties and elemental composition of the

304 stainless steel plates

	Criteria	Values
Specifications	Dimension (H x W x D)	25 x 12 x 1 mm
	Material Type	304 Stainless Steel
	Finishing	As machined
	Surface Roughness Ra	Approx. 2.0 µm
	Hardness (Vickers)	129
Physical Properties	**Physical Property**	**Value**
	Density	8.00 g/cm³
	Melting Point	1450 °C
	Thermal Expansion	17.2 x10^-6 /K
	Modulus of Elasticity	193 GPa
	Thermal Conductivity	16.2 W/m.K
	Electrical Resistivity	0.072 x10^-6 Ω .m
Elemental Composition	**Element**	**Weight %**
	Carbon (C)	0.08 Max
	Chromium (Cr)	18 – 20
	Iron (Fe)	66.345 – 74
	Manganese (Mn)	2 Max
	Nickel (Ni)	8 – 10.5
	Phosphorus (P)	0.045 Max
	Sulphur (S)	0.03 Max
	Silicone (Si)	1 Max
	Nitrogen (N)	0 – 0.11

3.4.1 Usage of strikes

The challenges associated with electroplating stainless steel are widely known in the metals finishing industry, and this is typically overcome by the use of appropriate strikes. Furthermore, the current commercial silver electroplating process also involves the use of a silver strike before carrying out the electrodeposition of the main silver coating. The main objective for using a suitable strike is for ease of depositing the main coating, especially when it comes to metals that are well known to face difficulties in the electroplating process. Strikes are inefficient processes of metal deposition, and the use of strikes results in releasing gases such as hydrogen at the cathode in aqueous solutions. The release of hydrogen also has the effect of further cleaning the cathode before depositing the main layer. As a result, it would be easier to electroplate silver directly onto metals such as silver, copper, and nickel as opposed to stainless steel. Therefore, strikes were investigated as part of the research into the development of the self-lubricating coating.

The copper and nickel strikes obtained from the Universal Metal Finishing Guidebook considered during the research process are listed in table 3-2 and table 3-3 respectively along with operating parameters [152]. The silver strike used is chemically comprised of the succinimide non-cyanide plating solution with the exception of current density, where an increased current density of 2 A/dm^2 was used.

Table 3-4 Copper strike composition and operating conditions from the

Universal Metal Finishing Guidebook [152]

Component	Concentration/ operating parameter
Copper Sulphate	7.5 g/L
Sulphuric Acid	3% w/v
Current Density	2 A/dm^2
Temperature	Room temperature

Table 3-5 Woods nickel strike composition and operating conditions from the

Universal Metal Finishing Guidebook [152]

Component	Concentration/ operating parameter
Nickel Chloride	45 g/L
HCL Acid	10% w/v
Current Density	2 A/dm^2
Temperature	Room temperature

3.4.2 Coating development through full factorial experiments

A systematic approach was required to identify the appropriate parameters to achieve a coating of acceptable quality. Trial and error one-at-a-time methods would prove to be inefficient and consume significant amounts of resource to

investigate the factors that affect the electroplating process. Instead, design of experiments (DoE), which is a powerful and efficient method to investigate various factors affecting complex processes such as electroplating using trial and error methods can be utilised. DoE also provides a method for systematic investigation of all factors and interactions between variables and is more reliable and complete than one factor at a time experiments.

As the objective of carrying out the DoE was to screen the variables, a two-level factorial design is suitable [153]. This allows the investigation of how the variables affect the intended outcomes in the presence of other variables. Furthermore, full factorial experiments allow complete and systematic study of interactions between variables in addition to identifying significant variables. The outcome expected of the full factorial experiments is an understanding of the interactions between the variables and its impact on the outputs of silver and PTFE incorporation, as well as establish the significance of PTFE incorporation towards tribological performance of the coating.

The experimental design of full factorial experiments revolves around three aspects of the process, namely the factors, levels, and response. Within the context of the experimental design, the inputs to the process are considered factors for the experimental design. Factors can typically be classified as either controllable or uncontrollable variables, and only controllable variables are considered as factors. The abundant literature available for electroplating discussed in previous chapters and previous trial and error experiments were paramount in mapping out and deciding the process factors which would be chosen for further study. The levels can then be defined as the setting or settings for each factor, with a minimum of 1 level required per factor. The responses, on

the other hand, are the measured outputs from the experiment and will be studied in detail, and these include CoF measurements, adhesion, and the inclusion of PTFE into the MMC. The method for obtaining these results as well as its significance is discussed in their respective sections.

A full factorial consisting of 5 variables with two levels per variable was carried out. The objectives of the full factorial experiments were to review and determine the effects of these variables on the overall quality of the deposited coating as well as PTFE incorporation into the MMC. Variables considered include voltage, agitation speed, coating time, potassium nitrate presence and the PTFE content in the bath. The variables and associated levels are shown in Table 3-6. The consistency of the electroplating bath during the production process was achieved using a master batch, which was adjusted for pH consistency before being decanted into smaller beakers for the individual electroplating operations. The full factorial experiment process flowchart provides a graphical overview in Figure 3-2. 3 test plates were electroplated for each sample set to be used for testing purposes.

A pragmatic approach for using the two-level full factorial experiments is to use extremes of process settings for each variable. The key output of tribology will be affected by voltage, where it has been established that 0.8V is the maximum voltage that can be applied through initial trial and error experiments carried out as reported in Chapter 4, while the minimum of 0.5V was used as it has been established as this would successfully result in coating deposition. The maximum coating time on the other hand is 600s as originally reported. Based on Faraday's law, halving the plating time to 300s would theoretically halve the theoretical coating thickness, and it would be of interest to compare the effects of this. On

the other hand, potassium nitrate is commonly used to improve conductivity in an electrolyte and it is viable to consider the effects of improved conductivity towards the resulting coating. In terms of PTFE content and bath agitation speed, previous trials showed success in PTFE incorporation through addition of 50mL/L worth of PTFE at 100 RPM. By using the structured two-level full factorial approach, the effects of doubling the amount of PTFE in the bath and bath agitation speed towards incorporation within the MMC its tribological effects can be studied.

Table 3-6 Summary of variables for the full factorial experiments

Factor	Setting 1	Setting 2
Voltage (V)	0.5	0.8
Agitation speed (RPM)	100	200
Coating Time (s)	300	600
Potassium Nitrate Presence (g/L)	0	16.7
PTFE Amount (mL/L)	50	100
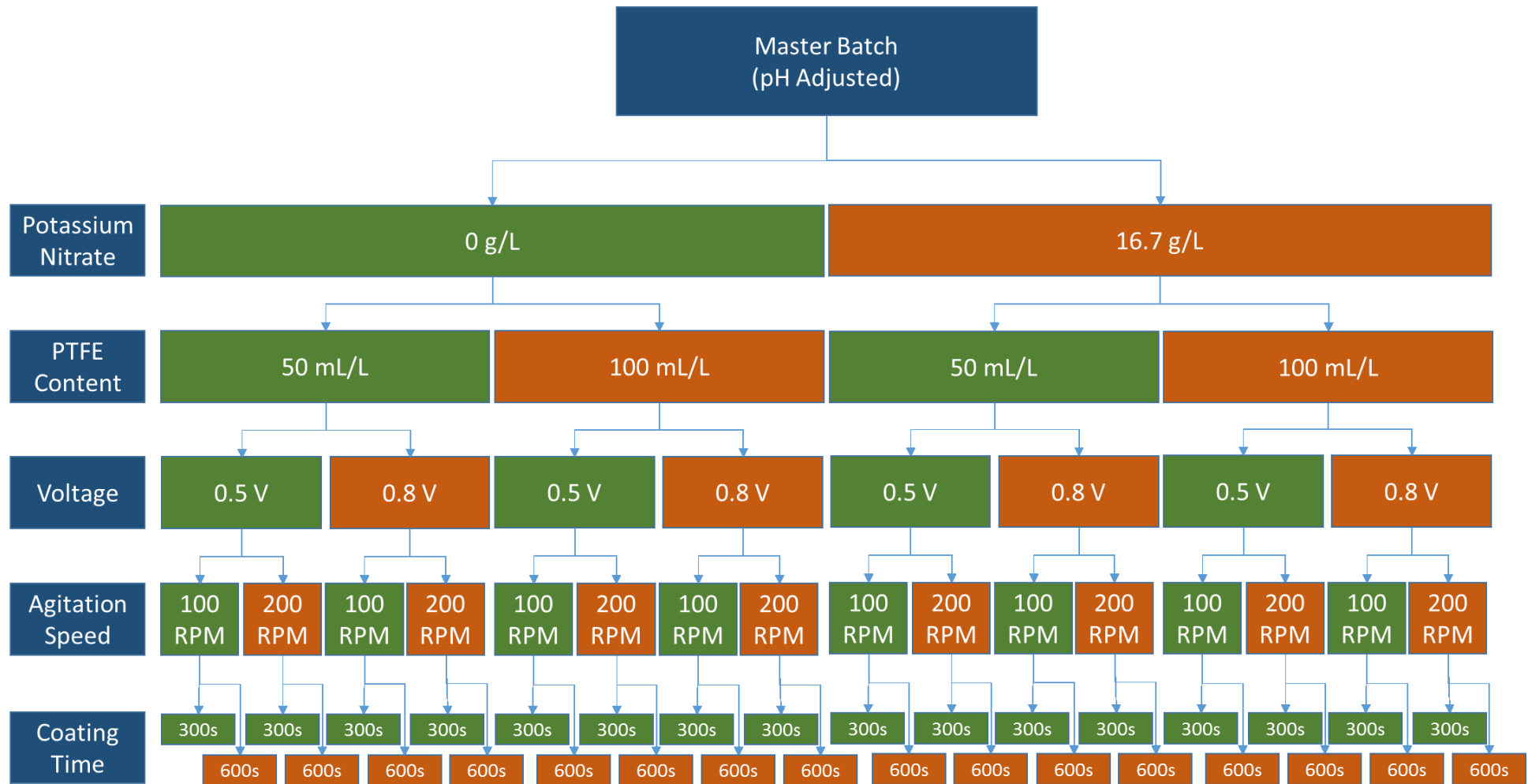
Figure 3-2 Electroplating bath fabrication flowchart

3.4.3 Coating development after full factorial experiments

The full factorial experiments provided the parameters for obtaining a coating which could be further developed to meet the project aims and objectives. The lessons learned from these experiments were used to inform subsequent experiments.

A good quality coating has to provide lubrication to the contact regions during repeated make-up attempts without the use of external or added lubrication. To be able to provide lubrication over repeated make-up attempts, the relatively soft coating has to resist wear, as an exhausted coating would ultimately result in direct stainless steel on stainless steel contact, resulting in galling and potentially seizure of the assembly.

The coating development also included investigation into the use of pulse plating. These were carried out using a rectifier that was capable of generating the required pulse waveforms thus a BK Electronics Model BK9174 was used.

3.5 Microscopy

Microscopy was used for several purposes. Firstly it was used to examine the surface roughness of the substrate material prior to electroplating in determining the effects of surface roughness on frictional performance. Furthermore, optical microscopy was used to observe the extent of the wear on the sample after testing was carried out. SEM and EDS were also used to determine silver and PTFE surface coating content after electroplating.

3.5.1 SEM & EDS

The SEM microscopy was conducted on the JEOL 6500 and JEOL 7100 instruments available at Plymouth University. This included inspecting the surface morphology and determining the silver and PTFE surface coating content in wt% using EDS analysis. The elements of interest were silver (Ag) as well as both fluorine (F) and carbon (C) from PTFE with chemical formula $(C_2F_4)n$. Quantitative data from the EDS analysis were compiled and compared across all the full factorial samples analysed with averages from three random sites on each sample at the same magnification levels.

3.5.2 Optical

The inspection of parts at low level magnification levels of up to x100 was carried out using several optical microscopes available at Plymouth University. These included the Olympus BX-41 and Olympus BX-60M optical microscopes.

3.5.3 Surface roughness

The examination and quantification of the substrate surface roughness prior to electroplating was carried out. The equipment used was an Olympus LEXT OLS3000 Laser Confocal microscope. This was carried out to ensure a similar surface roughness on the pre-plated samples as well as to identify the surface roughness achieved through surface modification activities. Through the LEXT Laser Confocal Microscope at Plymouth University, a three-dimensional profile of the surface topography for the test plates was obtained as seen in Figure 3-3.
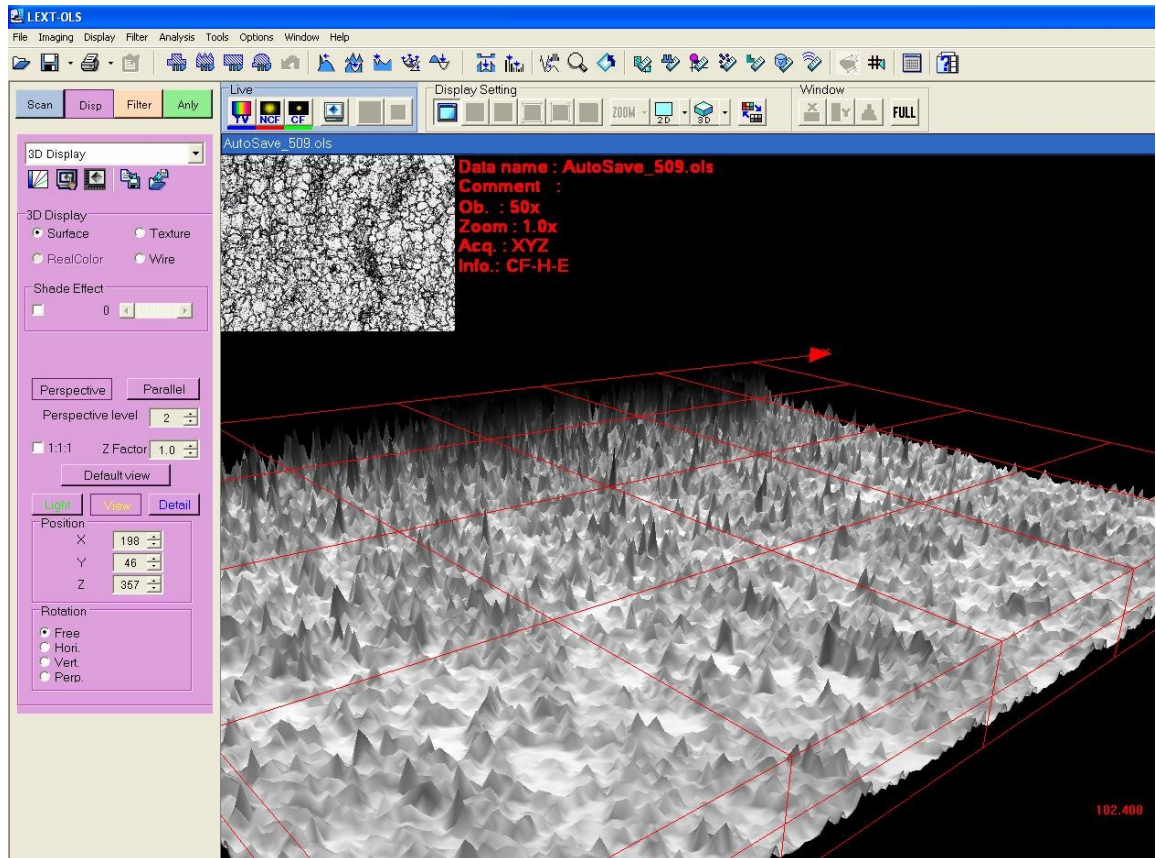
Figure 3-3 Three-dimensional surface topography obtained from the LEXT laser confocal microscope used to measure surface roughness

3.5.4 XPS

As part of the microscopy analysis, XPS was carried out in order to better understand the surface chemistry of the Ag-PTFE electroplating. The XPS microscopy work was carried out by Newcastle University's NEXUS facility as part of the EPSRC access scheme. As such, only a small number of samples could be tested at NEXUS due to the limited availability of the facility. Initial results from the SEM and EDS analysis was used to determine the selection of samples to be analysed; these included a control sample of pure electroplated silver fabricated using the non-cyanide electroplating process.

3.6 Tribology

Although Rabinowicz's definition of a self-lubricating MMC is based on foreign particle incorporation which can be obtained through microscopy or chemical analysis, this author believes that it is still necessary to determine the quantitative tribological performance of each coating through obtaining its CoF so a comparison can be made. The main objective of experiments carried out on the linear tribometer is then to determine this value for the coatings as part of the development process. This involves sliding a pin across the coating surface and applying contact pressure through the cycles.
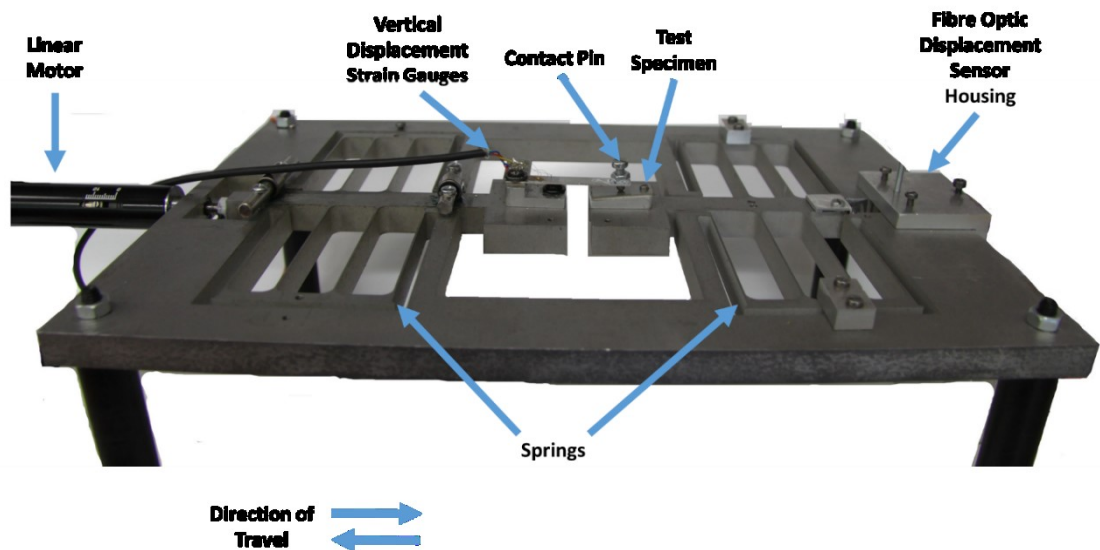
Figure 3-4 The bi-directional linear tribometer

The tests to determine the CoF were carried out using a bespoke bi-directional tribometer as illustrated in Figure 3-4. The test rig comprises of an aluminium base plate supported by two horizontally constrained flexure spring platforms, where one platform can move relative to base plate using a linear motor. The relatively low sliding speeds of the tribometer minimises temperature changes at

the pin/coating interface and mitigates variation in frictional properties due to temperature variation in PTFE polymer as part of the experiment. The cantilever beam is mounted to the actuator platform, with strain gauges mounted on the cantilever. With the test pin located on the end of the cantilever, the deflection that occurs during sliding provides a normal force reading.

In this test, the sample is mounted at a set 5° from horizontal with the replaceable, 3mm diameter, grade 10 AISI 52100 chrome steel spherical friction pin (Hardness: 60-67 HRC) resting on the sample at the datum state as illustrated in Figure 3-5. The forward sliding motion as the actuator is engaged displaces the pin upwards as it travels across the surface of the test sample, mounted on the second flexure. The combination of forward action and angled test base results in the increase of a normal force. The horizontal force provided by the actuator through the sliding pin also displaces the second flexure and provides the horizontal frictional force component. An optical fibre detects and measures this deflection to enable horizontal and frictional force calculation. Calibration is carried out on both the cantilever and optical fibre to ensure accuracy of output readings. The various criteria for the tribometer experiments are listed in

Table 3-7.

Although this method for tribological testing is not commonly utilised, it has a benefit over tribology experiments such as pin on disk of capturing varying normal force during each test cycle to detect variations of CoF with contact pressure. This is a much more appropriate method of experimental testing for a coating that will ultimately be utilised for threaded compression fittings, where varying contact pressures are prevalent during the make-up of the assembly. Additional details

on the design of the test rig can found in the original work carried out by Le et. al. [154].
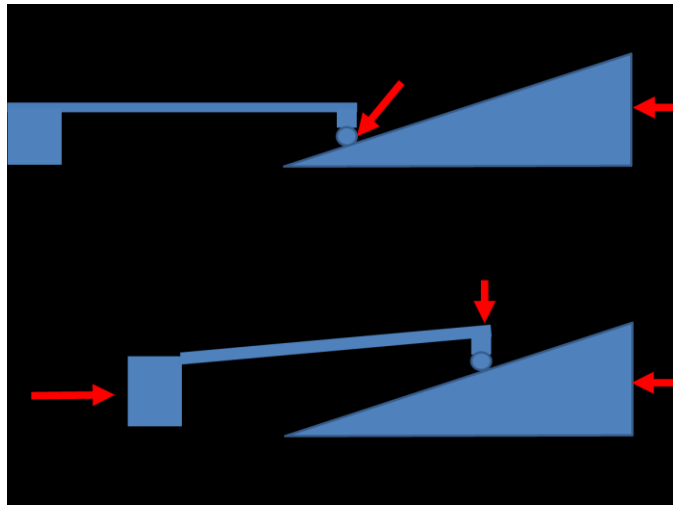
Figure 3-5 Stages of operation for the linear tribometer

Table 3-7 Criteria for experiments carried out on the linear tribometer

Sliding velocity:	12mm/min
Sliding distance:	13mm
Number of cycles:	8 (16 passes)
Total sliding distance:	208mm
Data sampling Rate:	1 Hz
Number of tests:	3 random sites per sample

Developmental work was carried out to ensure that the linear tribometer was capable of delivering repeated and reliable output data throughout all of the

experiments. Upgrades were carried out to the hardware including the use of shielded cables for signal transmission to prevent electrical and electronic signal interference, the addition of a signal filter and amplifier as well as a standalone Wheatstone bridge. After the upgrades to the existing equipment were made, a linear relationship of voltage to weight was observed from the calibration of both the strain gauges and fibre optic displacement sensor within required force range. In addition, a consistency of output results were obtained during multiple calibration runs for both the strain gauges and fibre optic displacement sensor. The calibration of the system suggests that the tribometer is capable of producing reliable and repeatable output results. The friction coefficient was calculated based on the forces acting on the sample surface with friction pin resting on top. The acquisition of voltage output data from both the strain gauges and fibre optic sensor were through Labview 2012 version 12 which was linked to a National Instruments NI USB-6210 data acquisition module. All of the experiments were carried out at room temperature. Instructions for the data collection and maintenance information for the linear tribometer were created and are attached in Appendix 1.

The experiments carried out on the tribometer are based on Hertzian elastic theory with the assumption of plastic deformation during the contact process. This is due to the average Hertz pressure of 700 MPa achieved during steel-on-steel sliding of the wear pin [155]. This is also backed by the fact that the Ag or Ag-PTFE coating is soft relative to either the tribometer pin or the substrate.

Microscopy analysis of the coating post-test was carried out to study the effects of the sliding tribometer pin on the coating as well as substrate. Tribological theories relating to wear and lubrication are used to characterise the frictional

performance of each coating under the cyclical wear process. The sliding pin is inspected under a microscope before and after each wear cycle to establish its surface conditions. A replacement pin or fresh pin surface is used in the event of cyclical wear or any other forms of wear being present on the surface of the pin.

3.7 Adhesion

Figure 3-6 The Instron tensile testing machine

Adhesion tests were conducted using an Instron tensile testing machine as illustrated in Figure 3-6 with a maximum force transducer capacity of 5000N. ANSI 304 stainless steel rods of 6mm diameter were fabricated with a hole in one end to allow a metal wire to be attached to the machine. The other end of the

stainless steel was polished to a mirror finish and thoroughly ultrasonically cleaned using acetone and the alkaline cleaning solution prior to being attached to the sample using a Vishay general purpose adhesive. Care was taken to ensure that an appropriate amount of adhesive was used during the mounting of the sample. After curing of adhesive between the test rod and the sample, the Instron machine test profile was set to carry out the tensile test at a speed of 2mm/min. Alignment was carried out in both X and Y directions, with the test carried out in the Z direction as illustrated in Figure *3-7*.
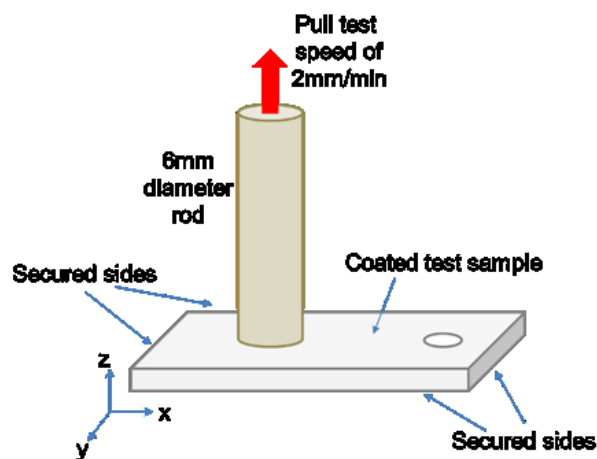
Figure 3-7 Schematic of the adhesion test experiment

Maximum yield forces were noted for each of the coatings tested. The adhesion strength was subsequently calculated by dividing the maximum yield force of the coating by the area of rod as shown in Eq. 3-1 below.

$$P = \frac{F}{A}$$ *- Eq 3-1*

Where,

P = Adhesion strength (MPa)

F = Maximum yield force (N)

A = Area (mm^2)

3.8 Weighted decision matrix

A weighted decision matrix was used in order to rank the experimental outcomes based on the criteria to meet the project aims and objectives. The use of this enables the quick and systematic identification of relationships between predefined criteria and the measured outcomes. This method is used in numerous forms within various industrial functions from design to manufacturing and is not limited to use in specific industries.

The intent of the decision matrix is to identify one or more suitable coating(s) to be taken forward for further tribological study through the torque test. Weightings for each criteria will be between 0 and 9. In the decision matrix, each criterion will be given a score of either 0, 1, 3 or 9; where higher values for weighting or score indicate higher favourability towards the coating. Once each of the criteria has been scored, going row by row, the score in each criteria column is multiplied with the relevant criteria weighting. This product of the criteria score and weighting is then totalled to form the final score for a particular coating option. This can be better understood from the illustration provided in Figure 3-8.

Criteria	Weighting/ Coating	Coating 1	Coating 2	Coating 3	Coating 3	Coating 5
Criteria 1	9	9	0	3	3	1
Criteria 2	4	3	1	1	1	9
Criteria 3	7	1	3	9	3	3
Criteria 4	3	1	9	1	9	3
Total		103	52	97	79	75

$$(9 \times 9) + (4 \times 3) + (7 \times 1) + (3 \times 1) = 103$$
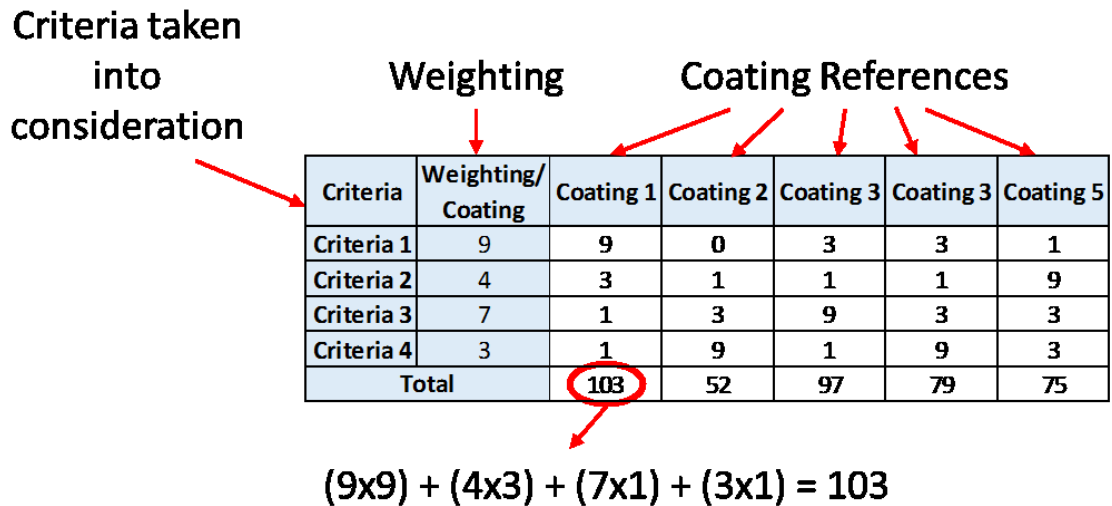
Figure 3-8 Example of a weighted decision matrix used

3.9 Torque Experiment

The performance of non-cyanide Ag and Ag-PTFE coatings were tested along with the commercially available cyanide silver coated nuts through a torque experiment. The basic profile measurement for the nut thread is provided in Appendix 3. Based on the assembly instruction for the compression fitting provided by the manufacturer, the whole compression fitting assembly should be made up and the nut tightened to finger tight prior to applying torque using a torque wrench. An angle target of 450 degrees is provided for making up the specified assembly without any specific torque specification. To ensure a consistent finger tight value is achieved across the experiments, all the nuts are pre-tightened to a value of 2Nm. For the reassembly process, although certain manufacturers state that lubricants may be applied if required, none will be applied for all the experiments.
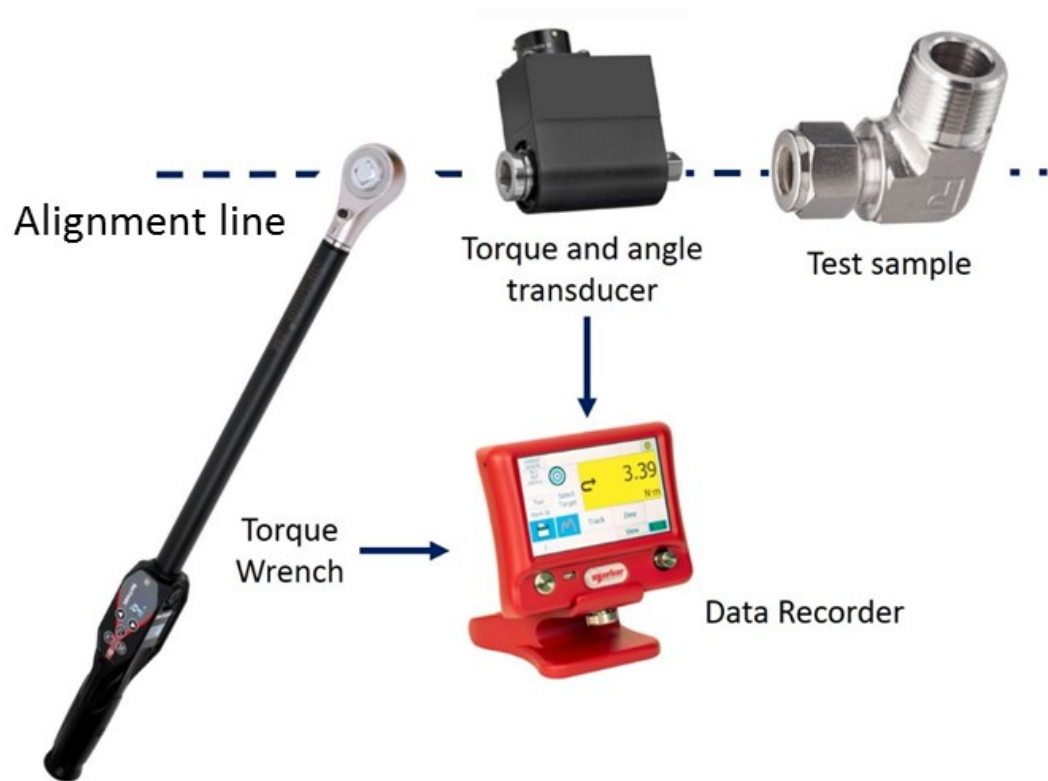
Figure 3-9 Torque experiment equipment setup

Each of the nut coatings were tested for 5 attempts using the equipment setup as shown in Figure 3-9, through the reuse of the nut and testing at constant velocity of 5° per second. Prior to testing, the test parts (nut, front ferrule, back ferrule, body and tube) were thoroughly cleaned using acetone and alkaline solution to remove any residual contamination from the manufacturing and electroplating processes. The body of the test sample is securely fastened using clamps and the equipment and parts are aligned on the x and y-axis. Manual application of torque was carried out using the torque wrench. The torque and angle signals from each attempt were recorded using the data acquisition and recording TL Box supplied by Norbar. The output of the torque experiment is subsequently used to model the tightening process based on torque output across the 450 degrees. The torque-angle curve is typically used for determining fastener strength in threaded fasteners where torque applied will translate to a

clamping force. On the other hand, the torque applied for threaded compression fittings is used for swaging and this method is proposed to compare the torque required as part of the assembly make-up for different nut coatings. This torque angle curve is further described in Section 2.2.4. Traditionally used to model the tightening process of threaded fasteners, this method is proposed to evaluate the swaging process of threaded compression fittings. This method is advantageous in that data is collected on-line during the make-up of the threaded compression fittings, it is a non-destructive test and it also highlights the areas of resistance during make-up. Areas of resistance are indicated by higher torque input requirements which could highlight issues during assembly make-up. As torque is applied to threaded assemblies which in turn imparts clamping or swaging forces, the drawback of this method is the lack of data in relation to force that is being applied.

Each coating variation was repeatedly tested to overcome variability in testing, manufacturing finishes and tolerances. An assumption is made that constant tightening velocity was used during the tightening process. Detailed specifications and data sheets for the equipment can be found in Appendix 3. Each nut is allowed to rest for a minimum of 5 minutes between installation and removal. Furthermore, after a set of installation and removal experiment has been carried out, the nut is allowed to rest for a minimum of 15 minutes during part changes and equipment recalibration. These periods of resting are to allow the nut to dissipate any increases in temperature as a result of frictional heating.

The assumption is made that the coating is tested through this experiment based on a worst-case scenario basis. During its normal lifecycle, a nut is typically installed only once and removed for inspection or other purposes when necessary.

During refitting, it is typical of the ferrules already attached to the tube through initial installation to be re-used. The nut therefore only needs to secure the already clamped ferrules back onto the body without being subjected to the high initial installation stresses.

3.10 Summary of the chapter

This chapter has detailed the methods used to obtain and analyse data from experiments with the intent of achieving the research aims and objectives. This includes details such as the cleaning and surface preparation prior and between electroplating processes or experiments. The coating synthesis introduced the formulation and parameters of strikes used during the coating development. Details for the full factorial experiments carried out were also provided. Furthermore, analysis methods for issues concerning tribology and adhesion which is used to determine the tribological performance and coating suitability for threaded compression fittings have also been discussed. The results of the experiments using these methods will be discussed in further detail in chapters 4 and 5.

Chapter 4 Initial coating development

4.1 Introduction

Developmental stainless steel plates were used to determine the performance of the succinimide silver coating deposits through the methodology detailed in the previous chapter to meet the project aim of developing a suitable coating for use in threaded compression fittings.

This chapter starts off with characterisation of the deposit obtained from the non-cyanide succinimide silver bath because of voltage changes. Subsequent investigations were carried out on effects of PTFE incorporation into the MMC because of increased concentration. The chapter then progresses into detailed investigation into aspects such as the effects of surface roughness on particle incorporation and its tribological effects.

The results from the structured investigation of variables through the 2-level full factorial experiments carried out are also presented in this chapter. The overall findings from this chapter are used to inform the subsequent development step of coating refinement.

4.2 Surface morphology

Based on the silver electroplating bath solution using succinimide salt as an alternative to cyanide, a trial and error method was used to deposit a pure silver layer. Using a constant voltage process with agitation speed of 200 RPM and 600s plating time, voltages of 0.5V, 0.8V and 1.0V were trialled. Coating quality was assessed based on coating presence, coating uniformity and overall visual appearance. Coating presence is clearly visible based on a discolouration of the initial sample where silver was successfully deposited. Secondly, the surface morphology of the deposit was considered, where a uniform coating has to be obtained for it to be considered successful. Finally, visual appearance was considered, where a coating should be smooth and in appearance.

The electrodeposition process was carried out after the sample surface had been degreased, cleaned and etched based on the process steps detailed in the previous chapter. Visual inspection of the 0.5V and 0.8V samples immediately after electroplating was that they were bright and smooth. On the other hand, the deposit from the 1.0V process was rough and dark as shown in Figure 4-1, with agglomerates around the sharp edges. This was due to an overpotential within the bath, resulting in an uneven deposit which was flaky and easy to remove which discounted this variable from further investigation.
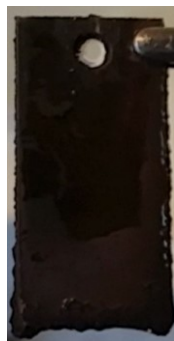
Figure 4-1 Rough and dark deposit from the 1.0V succinimide bath

On the other hand, the coating deposited using 0.5V and 0.8V were similar in surface morphology and showed a successful and uniform distribution of silver on the sample surface. A representative SEM image is shown for the 0.5V coating deposit in Figure 4-2, which suggests that the succinimide silver electroplating bath can deposit a thin but consistent silver deposit. The uncoated substrate surface was provided for comparison and can be seen in Figure *4-3*.

Due to the relatively short amount of electroplating time, the thin coating was deposited on the grain surface and did not manage to obscure the grain boundaries. Although the deposited silver coating grains were varied in size, a refined deposit was achieved with the majority of sizes being under the 100nm magnitude, although several large particles of sizes greater than 100nm were also observed. Furthermore, due to the relatively thin coating, elements such as iron (Fe) and chromium (Cr) can be picked up from the substrate due to EDS analysis. The silver particles deposited are globular in nature, and they can be seen to be adhering to the contours of the substrate material. Shown in Figure 4-4 these silver globules are approximately 100nm in size. Globules smaller and larger than 100nm are also present on the surface.
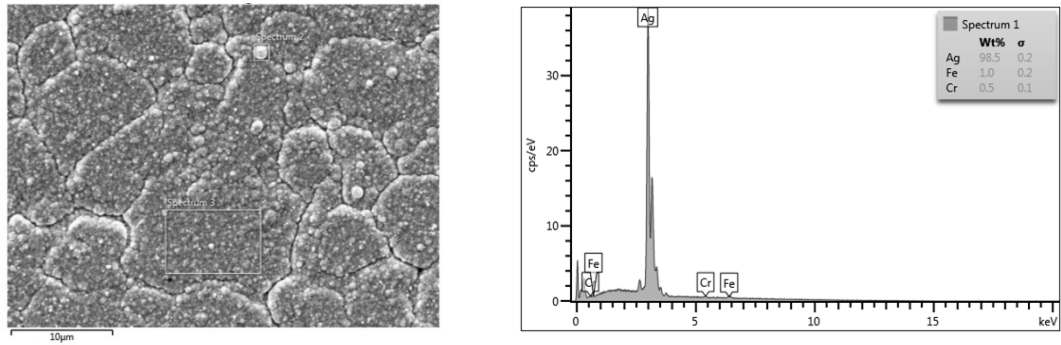
Figure 4-2 SEM image at x5000 magnification (left) and associated EDS spectrum (right) showing uniform distribution of silver on the sample surface using the succinimide electroplating bath at 0.5V as well as high contents of silver deposit
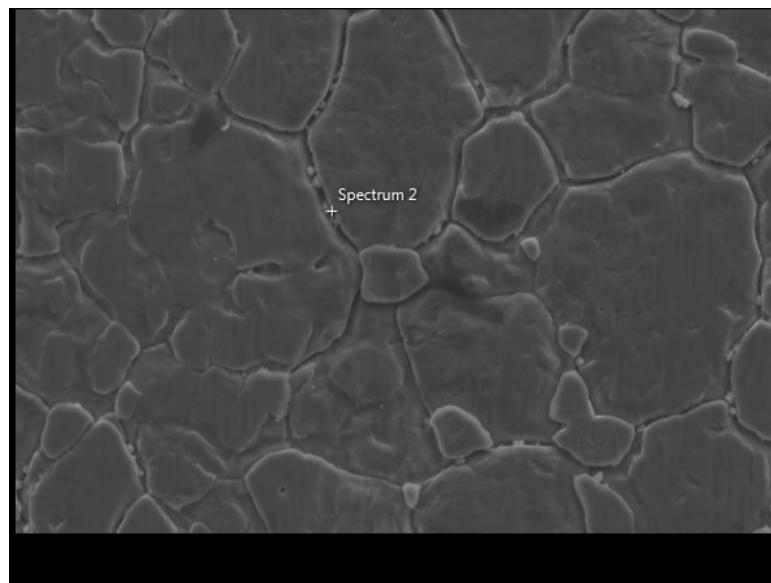
Figure 4-3 Surface morphology of the uncoated substrate

An initial inspection of the surface morphology is illustrated in Figure 4-4 for the control sample of pure silver electroplating. This was conducted to establish the effectiveness of the succinimide electroplating bath. At 40,000x magnification, the surface morphology is comprised of nugget like silver particles. These silver particles demonstrate good adherence to the substrate by covering all the

substrate surface area, even at such as high magnification, suggesting that succinimide is a suitable cyanide alternative to silver electroplating.
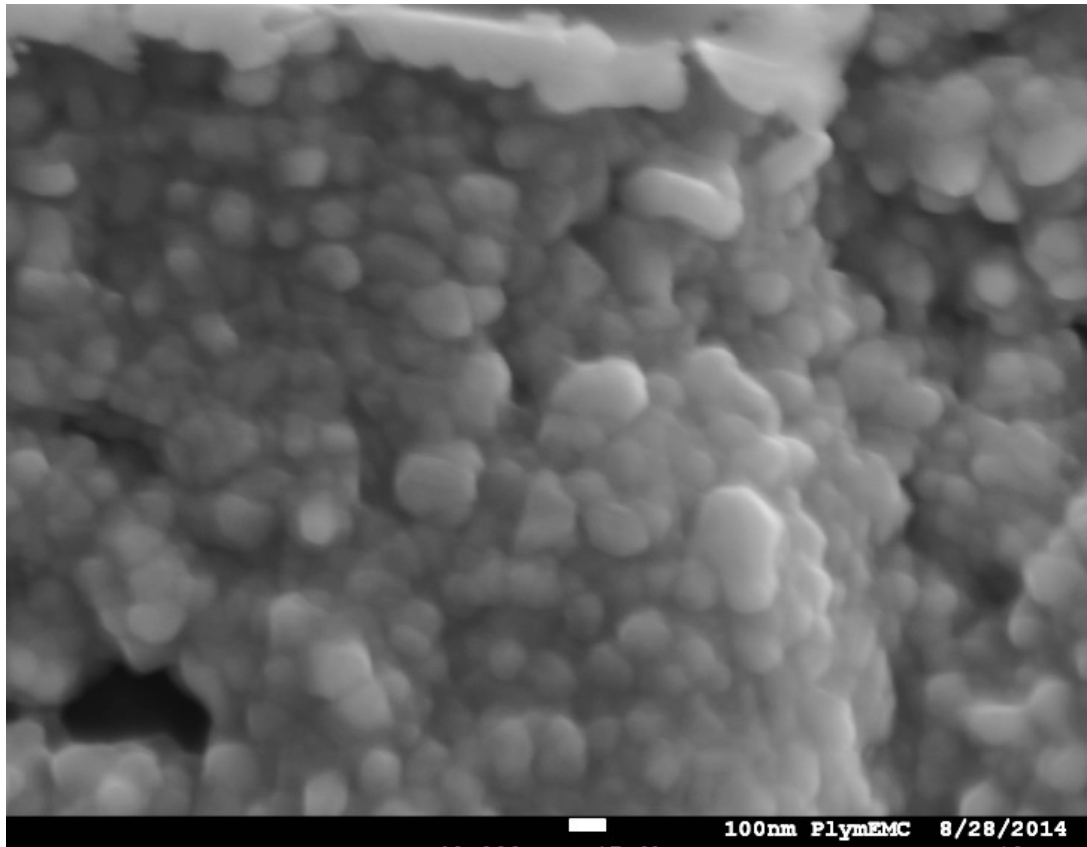
Figure 4-4: SEM image of the pure silver deposit at 40000x magnification

The uniform non-cyanide Ag plated obtained using a succinimide bath was then subjected to testing on the linear tribometer to obtain its CoF performance. An average CoF value of 0.3 was obtained for both 0.5 and 0.8V, which was an improvement over the CoF values on the uncoated surface of 0.6 as illustrated in Figure 4-5. Average CoF was based on data collected for the entire run and the information obtained from the succinimide bath for pure silver will be used as a benchmark for subsequent development and experiments. The CoF performance of the pure non-cyanide Ag coating was consistent over the ramping normal load

while the non-coated surface exhibited relatively constant CoF but subsequently suffered from erratic performance towards the end of the 8 cycles. Inspection of the sample post tribometer testing under an optical microscope showed surface roughening and evidence of galling which occurred on the surface of the non-coated substrate which could be used to explain the erratic CoF results observed towards the end of the tribometer test.
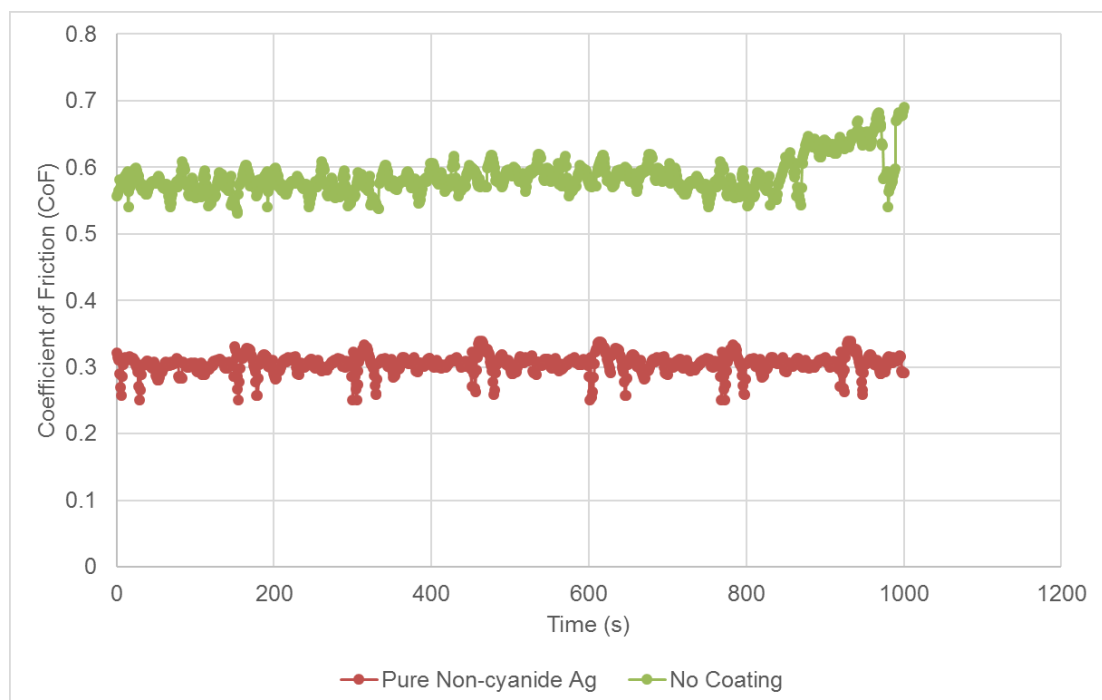
Figure 4-5 CoF comparison of eight cycles, for non-cyanide Ag coated surface and non-coated stainless steel surface

4.3 Effects of PTFE concentration in the bath

The next challenge was to incorporate PTFE into the silver MMC through electroplating. Early efforts to incorporate the aqueous PTFE particle suspension were through direct addition into the bath. EDS analysis subsequently carried out showed that even though substantial amounts of up to 100mL/L of suspended PTFE particles were included in the bath, the fluorine element detected on the

substrate did not manage to surpass 4wt%. Surface morphology of the Ag-PTFE was visually identical to that of the pure silver deposit. This was to be expected as the untreated PTFE particles are inert and can only hope to be transported to the growing metal deposit through conditions in the electroplating bath. Furthermore, the relatively low amounts of incorporated PTFE did not manage to improve the CoF. This led to the next aspect of investigation, which was carried out to understand the effects of surface roughness on particle incorporation. The incorporation of composite PTFE particles will alter the surface morphology of the coating, thus affecting its frictional properties and as such both aspects will be studied to meet the aim of the project which is to develop a self-lubricating coating.

4.4 Effects of substrate surface roughness on deposit and particle incorporation

As only a thin layer of the Ag-PTFE coating will be deposited through electroplating, optimal substrate conditions should exist for optimal particle incorporation. The effects of substrate surface roughness on particle incorporation were studied using the rectangular test plates. The average initial surface roughness values were measured using the LEXT laser confocal microscope to be approximately Ra 2.401. These values indicate that the substrate surface is rough. However, rough surfaces are advantageous from the perspective of galling. According to Rabinowicz, rough surfaces are less prone to galling and even in the event of galling occurring, its effects on the surface damage are reduced [45]. Furthermore, the author also believed that roughness troughs act as lubrication reservoirs to prolong the self-lubricating properties of the coating.

Surface modification was carried out on test plates. The plate surface was polished using sanding paper by following the process as described in the previous chapter with the intent of studying effects of smoother surfaces towards particle incorporation and also CoF performance of the coating. Post surface modification, roughness measurements were averaged based on 3 samples per variant across 5 random sites per sample.

Visual inspection of the test plate surfaces after polishing showed visibly deep score marks left on the surface caused by abrasive wear as a result of the operation, with different grades of sanding paper used showing either finer or rougher score lines. The surface roughness analysis carried out on the LEXT laser confocal microscope, on the other hand, showed that the average overall surface roughness had decreased to between Ra 0.807µm and Ra 1.551µm.

To understand this, the method of measuring surface roughness has to be taken into consideration, where both amplitude and frequency of the surface dips and peaks are taken into consideration. During the polishing surface modification process, the abrasive particles of varying sizes on the sanding paper would have different effects towards the substrate. Larger abrasive particles had increased the magnitude of the peaks and dips. The result of this is visually observed through score lines. On the other hand, smaller abrasive particles would have evened out the asperities that existed on the surface through sliding abrasive wear and the mapping of the surface using a laser highlighted the fact that the overall frequency of the peaks and dips had decreased.

Figure 4-6 shows the Ag-PTFE deposit on an 800 grit polished surface. Due to the relatively thin coating deposited, score lines on the substrate due to the

polishing process can still be visually observed. The results of the experiments are summarised in Table 4-1, and SEM and EDS analysis carried out noted an inverse relationship between PTFE incorporation and surface roughness. The inverse relationship between grit size and measured surface roughness was unexpected, but can be explained based on the polishing process carried out. Due to the low polishing cycles, the lower grit sizes (which corresponds to a larger average abrasive particle size) were able to remove more of the substrate material. Higher grit sizes, on the other hand, were unable to remove as much of the substrate, and the original surface conditions still existed, resulting in the registration of larger Ra values.

Results from the linear tribometer showed that the decreased surface roughness coincided with an increase in CoF to between 0.35 and 0.45. Analysis of wear track post-testing showed that the Ag-PTFE coating had been fully removed from the main pin contact area of the wear track which is consistent with the observations from previous experiments.
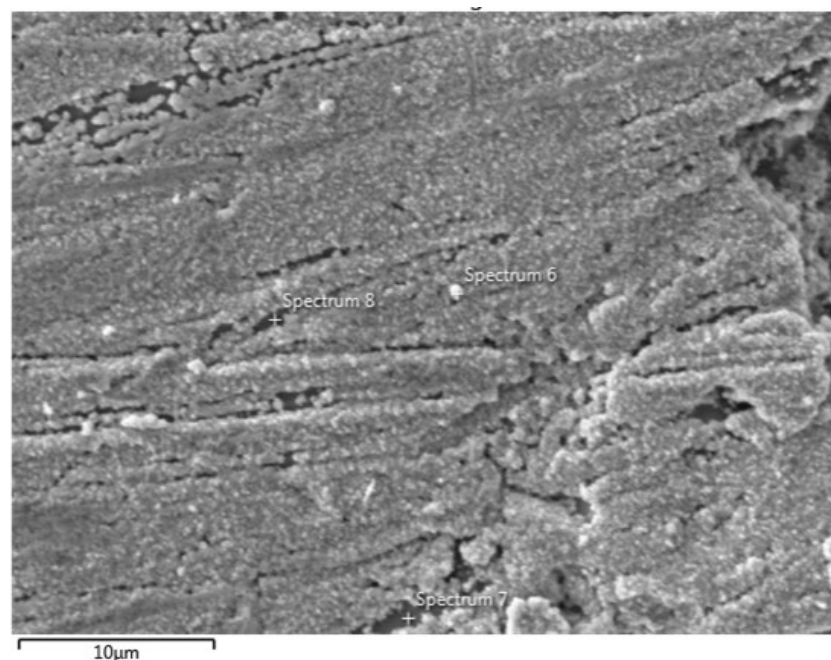
Figure 4-6 Ag-PTFE deposit on modified surface

Table 4-1 Summary of results for substrate surface roughness after polishing and its associated CoF performance

Polishing (Sanding Grit Sizes)		N/A - As manufactured	800	400	320
Measured Surface Roughness, SRa (μm)	1	2.381	1.251	1.223	0.779
	2	2.512	1.577	1.154	0.781
	3	2.311	1.824	1.238	0.861
	Avg	2.401	1.551	1.205	0.807
	St. Dev	0.083	0.235	0.036	0.038
PTFE (fluorine wt.%)	1	3.874	2.954	2.252	2.652
	2	3.746	2.895	1.899	1.181
	3	3.840	2.821	2.179	1.296
	Avg	3.820	2.890	2.110	1.710
	St. Dev	0.054	0.054	0.152	0.668
Coefficient of Friction, CoF	1	0.265	0.343	0.331	0.454
	2	0.293	0.345	0.417	0.441
	3	0.312	0.362	0.362	0.455
	Avg	0.290	0.350	0.370	0.450
	St. Dev	0.019	0.008	0.036	0.006

(Note: Higher grit sizes indicate finer abrasive particles while higher surface roughness values indicate rougher surfaces)

The phenomena of increased particle incorporation as a result of increased surface roughness can be explained using frictional forces acting on the PTFE particles as proposed by Hovestad et.al. [26]. Considering the local surface roughness of the substrate as a series of peaks and recesses, it is crucial in ensuring particles are incorporated within the MMC. A low local surface roughness based on a relatively flat surface will reduce the probability of particle

incorporation while a higher local surface roughness provides the environment in which the particles will be able to be incorporated.

On the other hand, the phenomena of decreased CoF as a result of a higher SRa has also been observed and reported by Sedlacek et. al., where the authors noted high surface SRa values coinciding with lower CoF values [57]. The tribometer test on the substrate is illustrated in Figure 4-7. The polished substrate would have a lower SRa value and thus result in higher CoF values. Incidentally, the electrodeposited layer is in the form of a thin coating and would conform to the contours of the surface topography of the substrate material. In terms of wear, as the experiment is carried out, abrasive wear would occur, resulting in removal of material as the wear pin slides across the surface. This changes the surface topography, resulting in CoF fluctuations. As such, the CoF results utilised were averages from the steady-state CoF.
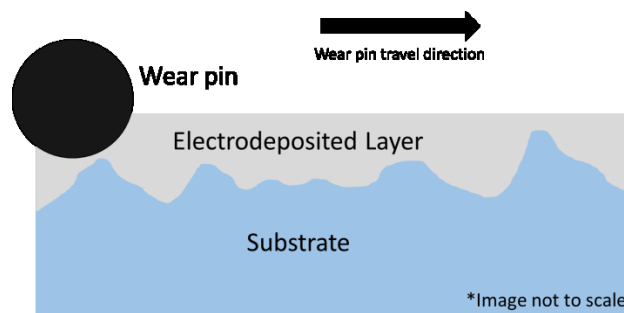
Figure 4-7 Illustration of tribometer test on the substrate

The results based on substrate surface roughness have shown that the existing substrate layer performs favourably albeit by a small margin. This is also beneficial in a commercial environment as it reduces the amount of pre-processing required before the coating process.

4.5 Full factorial experiment results

The full factorial experiments were carried out in an attempt to study the effects of the input variables towards the outputs of surface morphology, particle incorporation, adhesion and tribological performance. Details of the experiments carried out can be found in section 3.4.2 of the previous chapter.

All of the samples were thoroughly cleaned based on the cleaning regiment stated in the previous chapter. During the experiments, the potential was kept constant, with current being allowed to fluctuate. The current outputs achieved throughout each experiment run and between runs were measured and calculated to be between 0.13 A/dm^2 and 0.15 A/dm^2. The rectifier used for these experiments was the Rapid Electronics DC power supply model HY3003D. After the electroplating process, all the samples were thoroughly rinsed with DI water, dried labelled and kept in air-tight sample bags for further testing and analysis.

4.5.1 Characterisation of the deposit and surface morphology

The first observation is carried out towards visual appearance. Although it is not a critical criterion for the coating's intended application reported in this study, it does, however, highlight the differences in chemical bath composition towards the visual appearance of the coating deposit. Figure 4-8Figure 4-8 shows the visual differences between a tarnished and bright sample.

Figure 4-8 Tarnished sample (left) and bright sample (right)

Differences in surface morphology were also observed as a result of bath parameter changes. The typical surface morphology for the Ag-PTFE MMC coating (obtained at 5000x magnification) is illustrated in Figure 4-9**Error! Reference source not found.**. At this level of magnification, the grain boundaries of the substrate are clearly visible, and the plated thin film layer was able to cover minor pits and imperfections on the substrate. The failure of the plated layer to cover larger pits and imperfections suggest that the coating is in the form of a thin film of nanometer to micrometer thickness, which corresponds well to the theoretical deposit thicknesses of between 0.48 microns to 1.15 microns. Larger silver particles are visible as being spherical in shape, bright and light coloured. In general, the plated coatings were observed to have full coverage of silver particles in varying sizes.
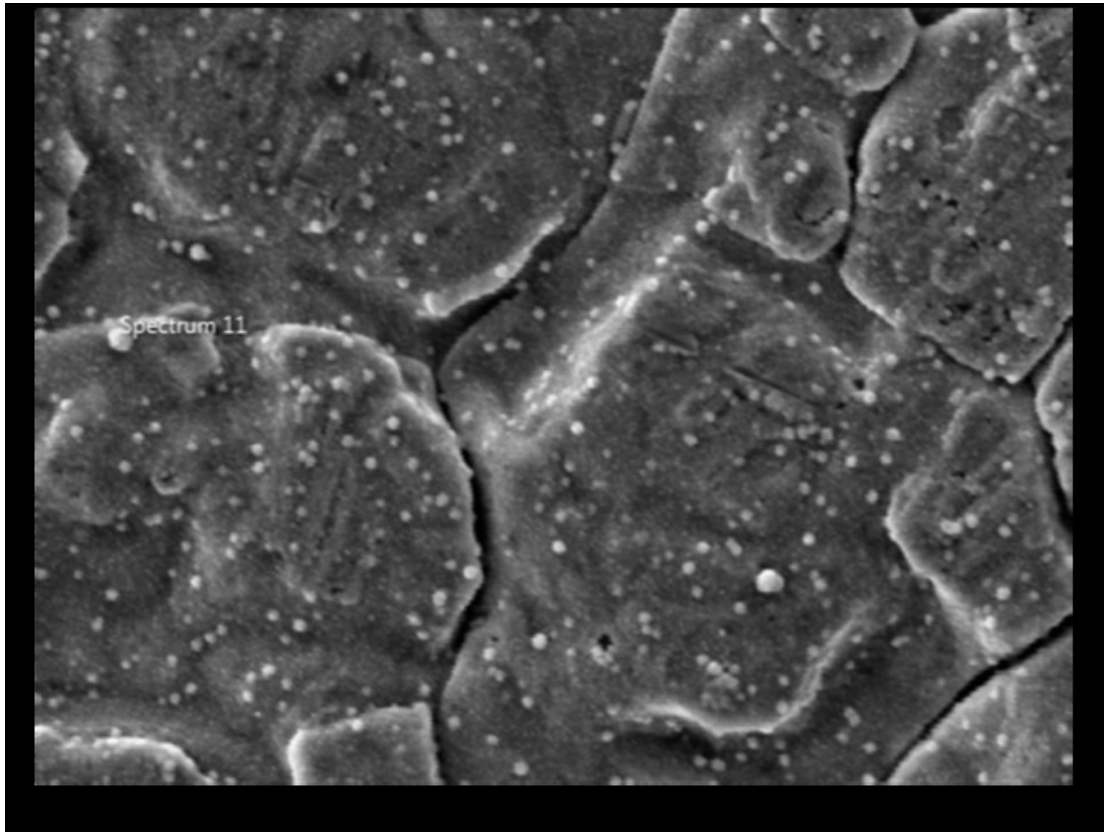
Figure 4-9 SEM image at 5000x magnification showing grain boundaries of the

substrate layer and evenly distributed silver particles as being spherical in

shape, with larger silver particles being bright and light coloured

The different bath conditions yielded varying results for Ag-PTFE coverage of the

substrate. Typical poor distribution of plated particles on the substrate surface is

illustrated in Figure 4-10. The poor distribution has resulted in clusters of

randomly dispersed silver particles on the substrate being visible at 30,000x

magnification. This can be attributed to less than optimal bath variable conditions

for electroplating, low surface tension for PTFE and less effective surfactant in

the bath. On the other hand, typical good distribution of plated particles on the

substrate surface is illustrated in Figure 4-10. Good distributions indicate optimal

bath variable conditions for electroplating, and Ag-PTFE particles of varying sizes

adhere fully to the substrate surface. By controlling the bath variables during electroplating, the quality and thickness of the coating can be fine-tuned. The surface morphology of a good quality Ag-PTFE coating obtained by Zhao et. al. has been included in Figure 4-12 as a comparison [32]. The quality of coating adhesion on the substrate surface based on varying bath conditions has also been quantified using adhesion tests methods discussed in the previous chapter.
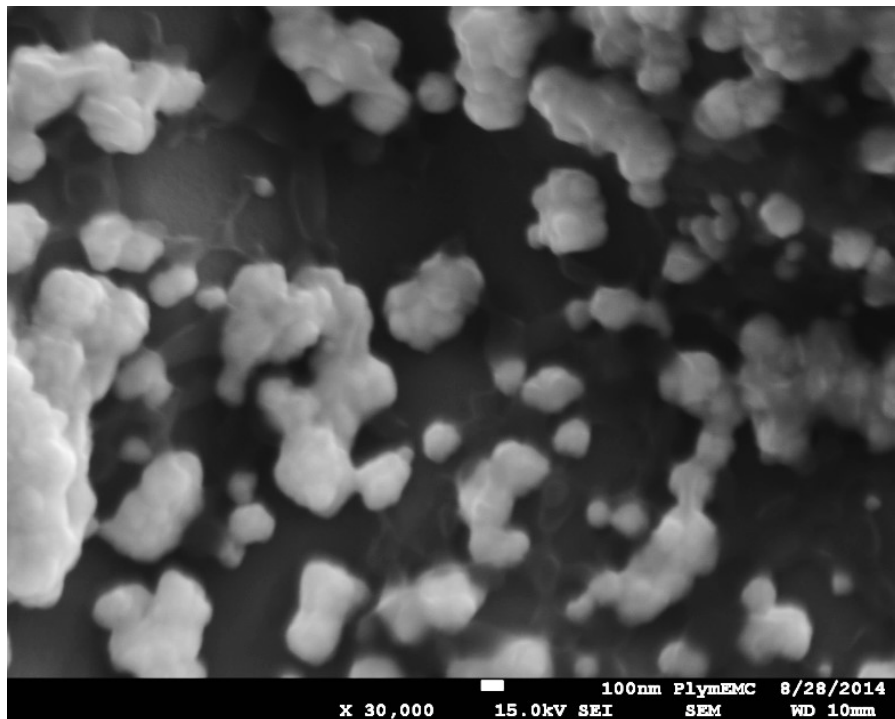
Figure 4-10 SEM image at 30000x magnification showing random clusters of dispersed silver on the substrate in a poor quality Ag-PTFE coating
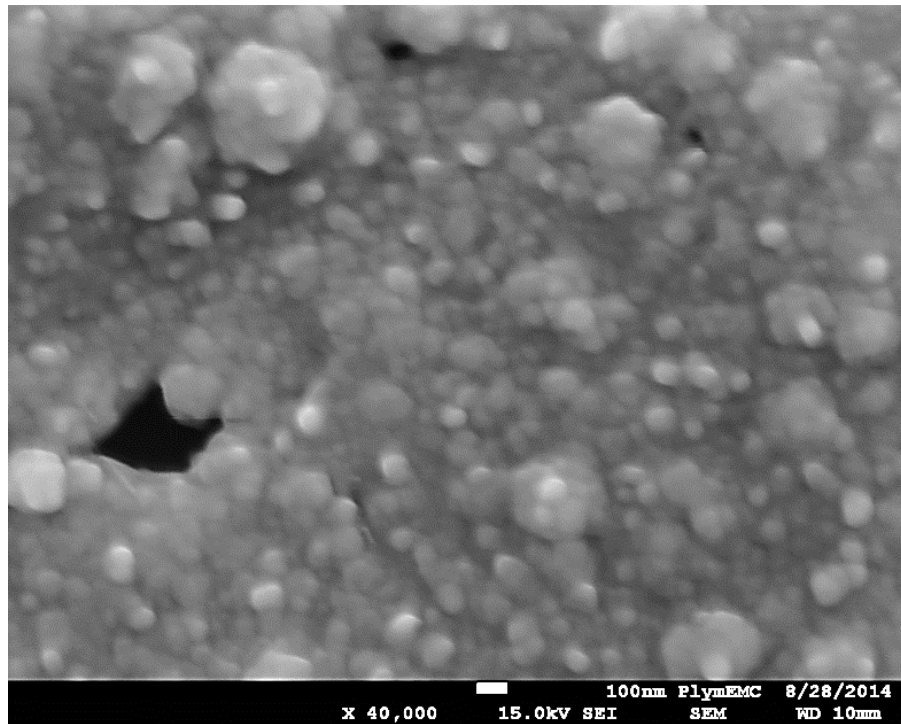
Figure 4-11 SEM image at 40000x magnification showing uniform Ag-PTFE

coating of varied particle size in a high-quality Ag-PTFE coating
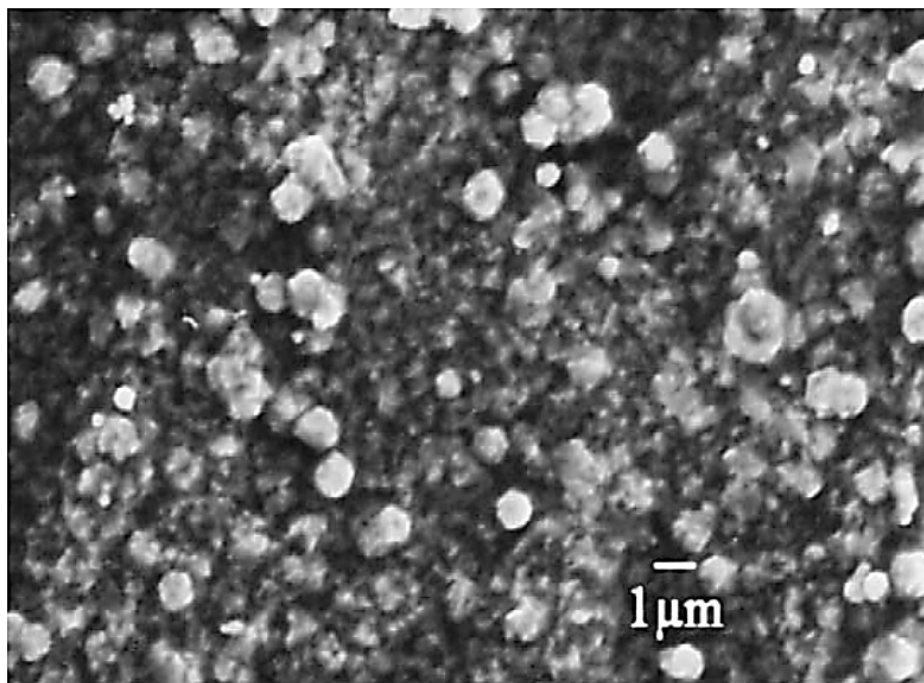
Figure 4-12 Surface morphology of Ag-PTFE coating obtained by Zhao et.al.

[32]

One of the key variations observed between coatings is the difference in coating deposit "roughness". Figure 4-13(a) shows a visibly rougher coating when compared with the smoother deposit obtained in Figure 4-13(b). An assumption that all the other chemical bath factors which have the potential to impact deposit roughness are consistent throughout can be made based on the controlled bath parameters. As such, the differences can be explained by another variable which had been experienced fluctuation during the process, which is current density. As a constant voltage was applied during the electrodeposition process with the current allowed to fluctuate, certain samples would be deposited using a higher current density had a higher overpotential value. This is significant because the over-potential directly affects the rate of nucleation. A low nucleation rate would result in a larger space for the crystal nucleus to grow. With this in mind, and tied in with the bath effects will result in the different deposit nucleus sizes and thus uneven surface conditions.

(a)   (b)
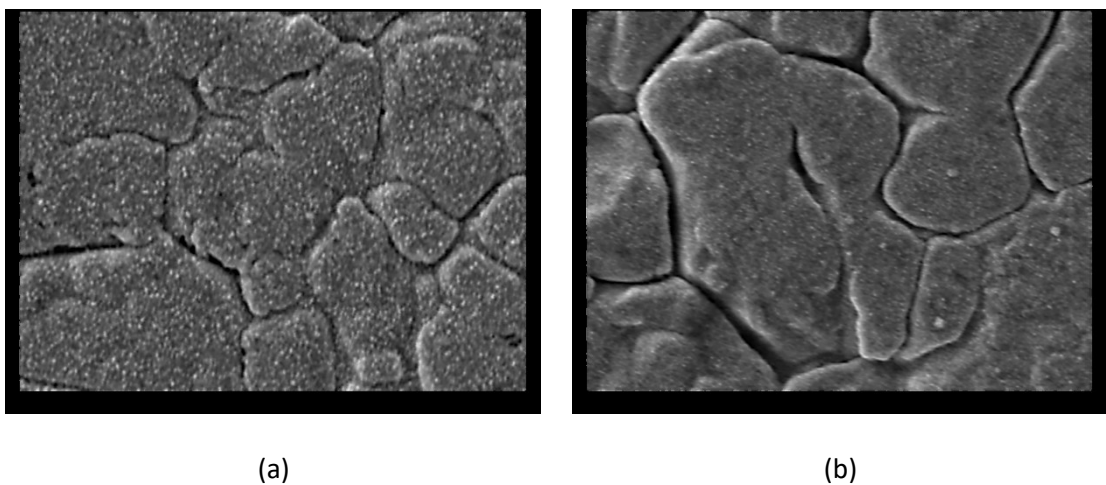
Figure 4-13 Visible variation in deposit "roughness" observed at 5000x

magnification

A variation in deposit roughness has the potential to impact the CoF of the coating directly. To obtain a relatively even surface, a synchronous rate of nucleation could be sought by increasing the current density. However, previous research has found that if the nucleation rate is too high, larger grains and thus an increase in surface unevenness will occur because of the phenomenon of sharp micro-discharge angle [145].

EDS Analysis

EDS analysis was carried out alongside SEM in an attempt to confirm and quantify the elements present in the deposit. Based on the EDS wt.% analysis, silver and fluorine content on the surface of the samples were between 87.99 wt.% - 99.82 wt.% and 0.18 wt.% - 12.01 wt.% as illustrated in Figure 5-9 and Figure 5-10 respectively. Firstly, this confirms that a composite layer has been successfully plated through the succinimide bath and electroplating process. Secondly, the presence of both silver and PTFE in varying amounts throughout the coatings have also confirmed that the variables investigated were, in fact, pivotal in the particle incorporation process, and this warrants the further investigation of these factors in meeting the project aim.
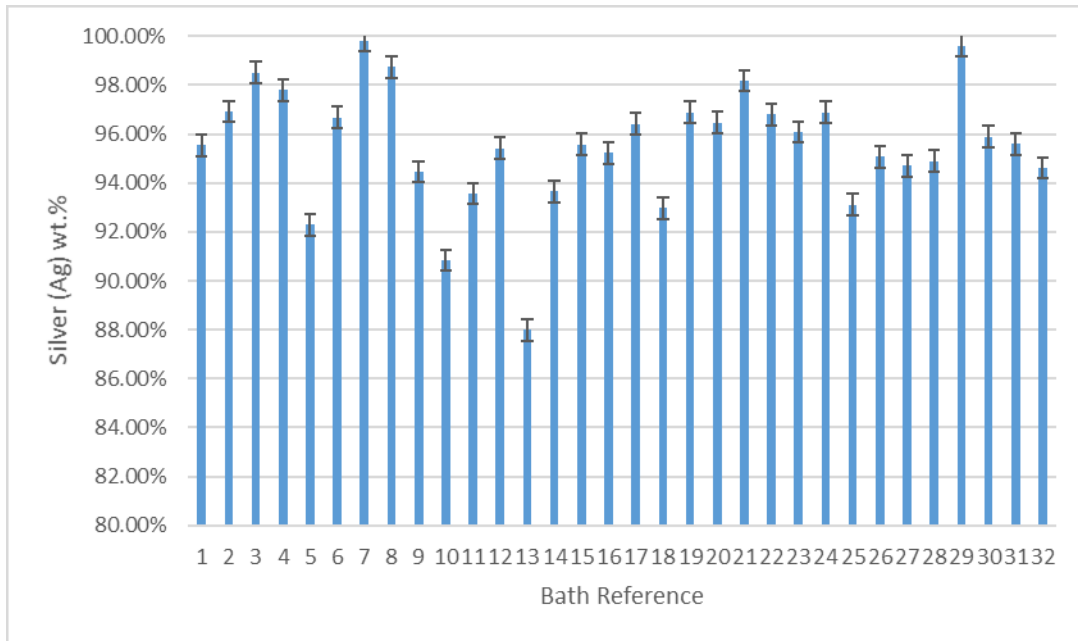
Figure 4-14 Silver (Ag) wt.% by bath reference suggesting success in the non-cyanide alternative bath for silver electroplating
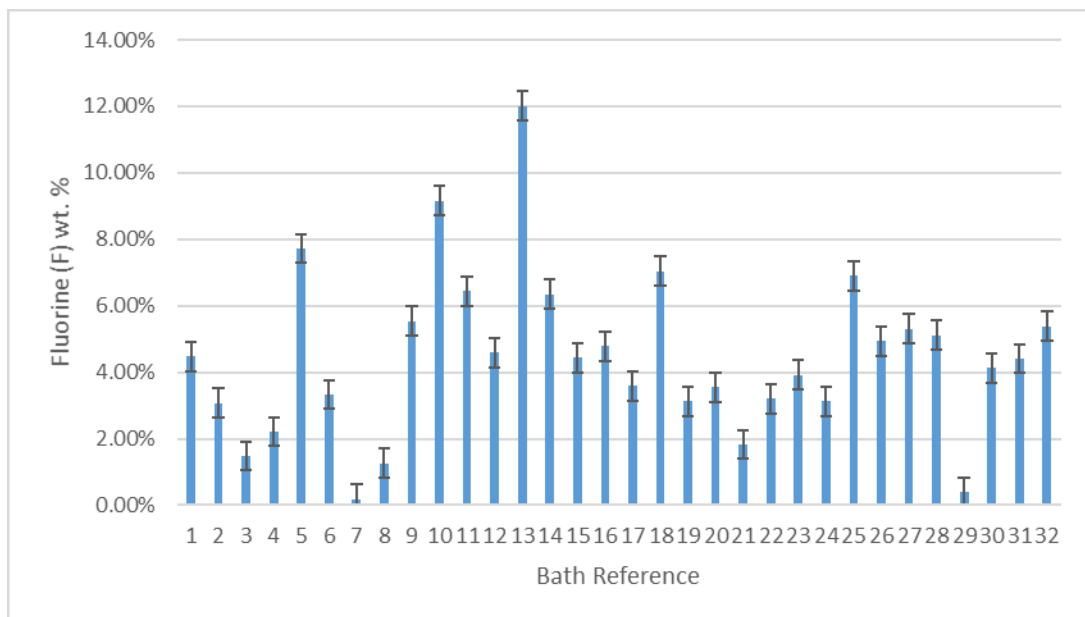
Figure 4-15 Fluorine (F) wt.% by bath reference indicating the success of Ag-PTFE synthesis through a non-cyanide electroplating bath

One of the variables considered during the full factorial experiments was the quantity of dispersed PTFE in the electroplating bath. Direct comparison of PTFE incorporated to the amount of PTFE added into the electroplating bath was made by keeping the other variables in the bath constant as seen in Figure 4-16. The fixed variables are listed in Table 4-2. Observations based on the figure are firstly, that the magnitude of PTFE variation is relatively consistent based on the fixed variables from group 2 to group 8. Secondly, although the figure shows that the overall trend leans towards the fact that more PTFE in the bath equates to more PTFE incorporated, there are several conditions where this does not apply, namely in groups 10 and 11.

It can therefore be concluded that the amount of PTFE added into the electroplating bath to the amount of PTFE incorporated into the deposit is dependent on factors other than its concentration within the bath. The data obtained from this study supports findings from established literature that bath electroplating parameters are critical in electroplating without the use of suitable and bath compatible surfactants [140]. It is likely that without the presence of a suitable surfactant during the Ag-PTFE electroplating process, the PTFE particles struggled to overcome the surface tension required for good adhesion and subsequently good electroplating quality. Furthermore, there is also the issue of particle transportation to the cathode surface, where in the context of these experiments are the electrolyte flow conditions which are in turn affected by agitation speed.
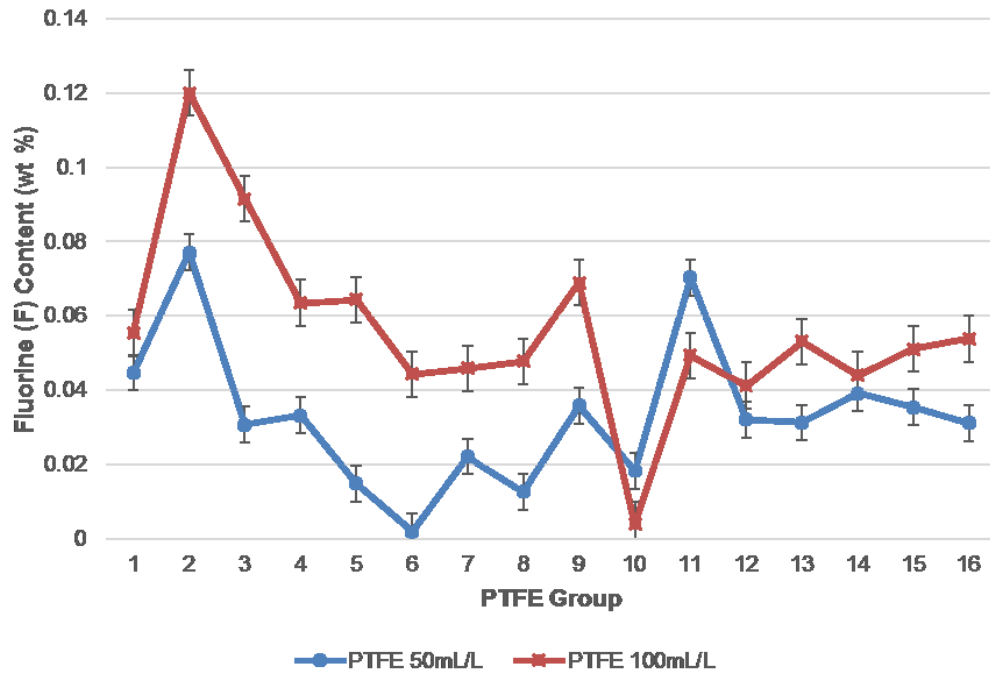
Figure 4-16 Comparison between PTFE incorporated with PTFE concentration in the electroplating bath

Table 4-2 List of fixed variables by group

Group	Time (s)	Voltage (V)	Speed (rpm)	Potassium Nitrate Content
1	300	0.5	100	Yes
2	300	0.5	100	No
3	300	0.5	200	Yes
4	300	0.5	200	No
5	600	0.5	100	Yes
6	600	0.5	100	No
7	600	0.5	200	Yes
8	600	0.5	200	No
9	300	0.8	100	Yes
10	300	0.8	100	No
11	300	0.8	200	Yes
12	300	0.8	200	No
13	600	0.8	100	Yes
14	600	0.8	100	No
15	600	0.8	200	Yes
16	600	0.8	200	No

The quantitative comparison of element data obtained from the research with the electroplating bath variables initially suggests that the samples with the highest amounts of Ag (and inversely lowest amounts of PTFE) occur when no potassium nitrate is added to the bath. However, the presence of potassium nitrate has also contributed to the opposite extreme in the results for having the highest amount of PTFE on the plated surface. Due to the inconclusive data, it can, therefore, be concluded that potassium nitrate addition into the electroplating bath is not a critical factor in the Ag-PTFE electroplating process.

Interaction Plots

Quantitative elements data from the EDS analysis was used to generate interaction plots in Minitab 17. Interaction plots are useful for visualising potential interactions between the considered factors. In this case, the other factors considered for the full factorial experiments include agitation speed, plating time and voltage. Parallel lines that exist within an interaction plot indicate no interaction while a greater slope indicates that there is a greater degree of interaction.

Interaction plots for both silver (Ag) and fluorine (F) were generated using Minitab for the factors and responses considered in the full factorial experiment. Considering the interaction plot for silver shown in Figure 4-17, there appears to be an interaction between time and voltage, where the data suggests that more silver is detected with the increase in voltage and time. This is to be expected and is consistent with Faraday's law of electrolysis, which states that increases

in both voltage and time will increase the coating deposit thickness, regardless of additives in the bath such as PTFE.
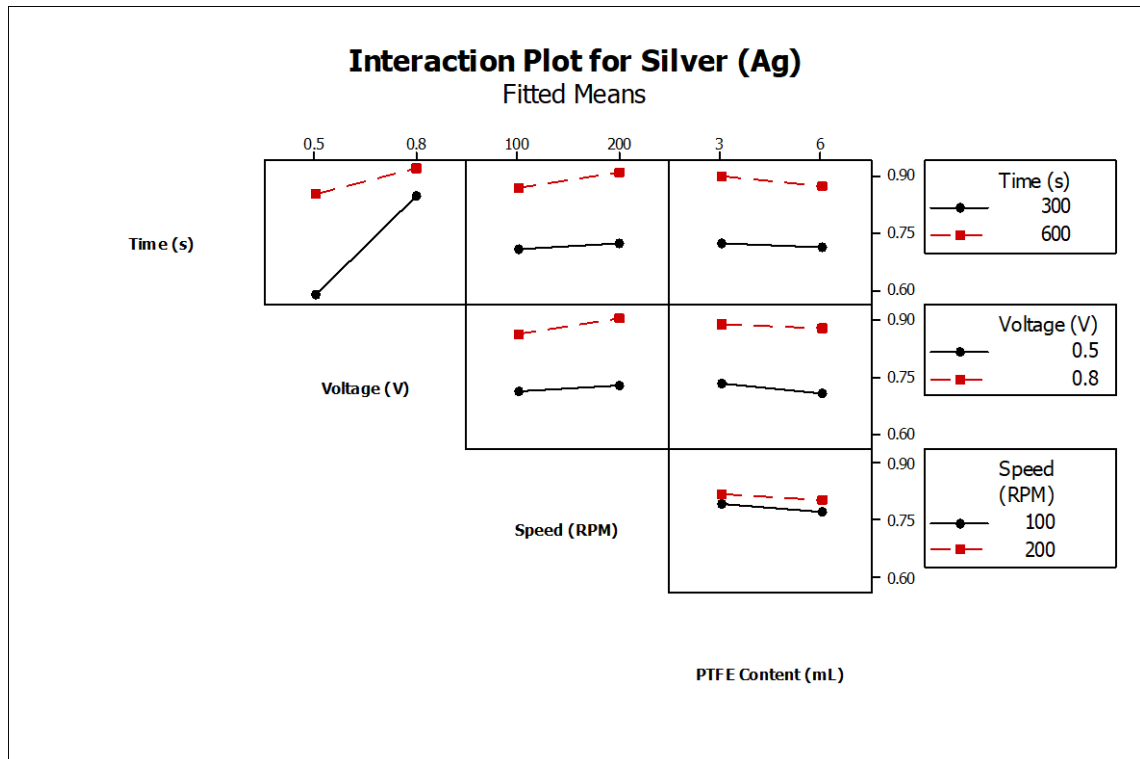
Figure 4-17 Interaction plot for silver (Ag) element based on quantitative EDS data

Based on the interaction plot for Fluorine shown in Figure 4-18, the interaction plots suggest that for t=300s there is an inverse relationship between applied voltage and PTFE incorporation. As the voltage increases the amount of Fluorine decreases. For t=600s, the results suggest the opposite of this and PTFE incorporation increases when the higher voltage is applied. To make sense of this, it is vital to understand that voltage directly influences the current density and thus nucleation rate of the conductive silver during the deposition process. It is possible that in the relatively short plating time of 300s, effects of nucleation rate and deposited silver were unfavourable for PTFE incorporation and the

opposite occurred at a longer plating time of 600s. In addition, there would also be other unmeasured changes in the resistance of both the bath and the substrate. Furthermore, when considering the effects of low voltage and agitation speed, a drop in incorporated PTFE was experienced when the speed increased. The opposite phenomena was observed when a higher voltage was introduced. The combined effects of nucleation rates and agitation speed would have also resulted in the differences between PTFE incorporation observed for voltage and speed.

When considering the factor of PTFE content within the electroplating bath, the general conclusion that higher PTFE content in the bath will result in the higher incorporation of PTFE particles within the MMC can be drawn. The data suggests that this has occurred regardless of time, voltage and agitation speed. There is also the inference based on the data that although a relatively substantial amount of PTFE had been considered for the experiments, (with a minimum of 50mL/L of PTFE added to the bath) the saturation point of PTFE within the deposited layer has not been met. If the saturation point of PTFE content in the bath were met or exceeded, no changes would be observed to the incorporation of PTFE into the MMC.

One of the variable interactions remained relatively unchanged when considering PTFE incorporation. The combination of changes in speed and time only produced marginal increases in particle incorporation. This is confirmed by previous studies on particle incorporation which found that increased agitation results in increased incorporation due to the increase in particle transfer from the bulk electrolyte to cathode surface [156]. This is only applicable assuming the

thresholds of particle incorporation have not been exceed, as otherwise particles would be ejected from the cathode surface before incorporation [147-148].

It should be noted that while factors of applied time, voltage and speed play a vital role in particle incorporation, the results from the interaction plots cannot be analysed in isolation as there are other aspects to be considered for particle incorporation into the silver MMC. Furthermore, it should also be noted that within the electroplating bath, PTFE is the only component not to be replenished.
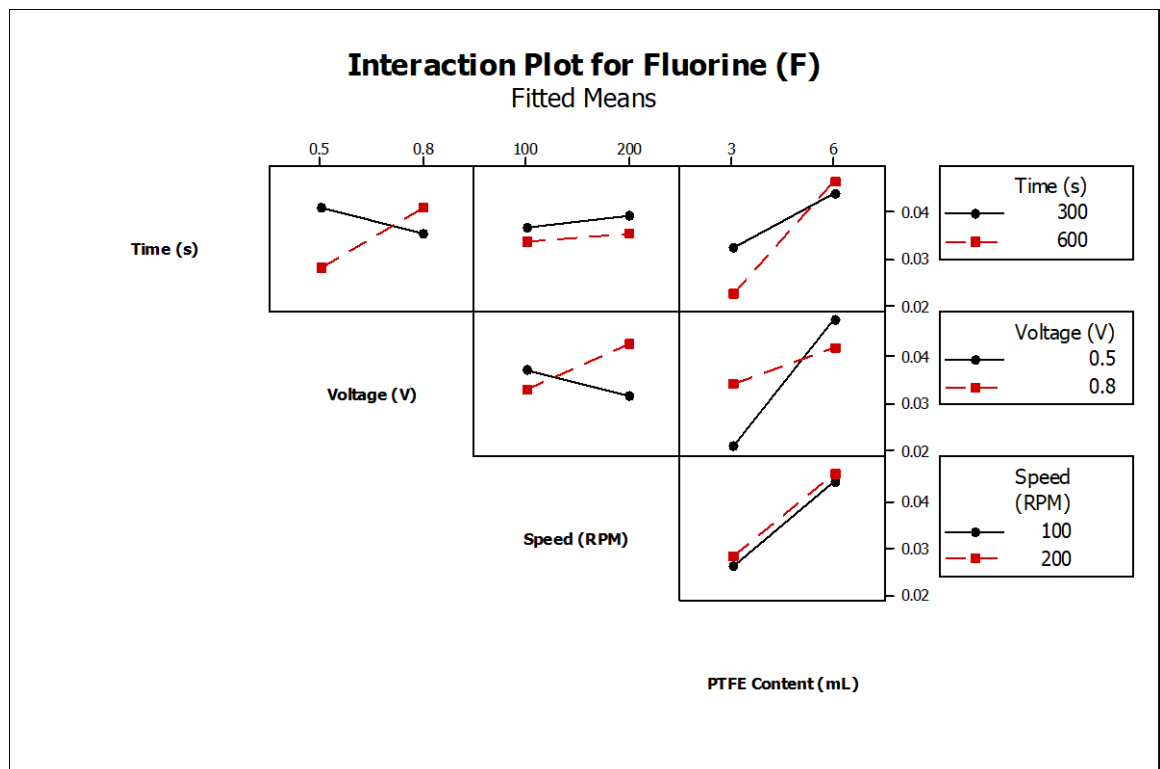
Figure 4-18 Interaction plot for fluorine (F) element based on quantitative EDS data

Although Carbon (C) was to be considered in the initial design of the experiment, it was not subjected to further analysis due to several reasons. Firstly, the 304 stainless steel substrate contains carbon in trace amounts which can be picked

up through the EDS analysis, and this was confirmed through the elements analysis of an uncoated sample plate. Due to the micro-coating thickness, the EDS analysis X-Rays can easily penetrate the coating and reveal elements of the substrate. This is evident as elements from the substrate layer such as Chromium (Cr), Nickel (Ni) and even Iron (Fe) were picked up during the analysis. In addition to that, the presence of carbon in the substrate had also skewed the interaction plot for carbon. It is expected that the patterns exhibited by the carbon interaction plot to mirror that of fluorine if the detected carbon is indeed only from the coating.

4.5.2 Experiments on the linear tribometer

In achieving the intention of obtaining the coating performance measured through CoF values, the 32 sets of samples were mounted and tested on the linear tribometer.

Friction coefficients were higher at the start of the tribometer run as well as during changes in direction. This was to be expected as the friction pin would have to overcome static friction before moving and thus dynamic friction would take over. Runs carried out on the tribometer to establish friction coefficients showed dynamic friction coefficients of between 0.23 and 0.51 was achievable between samples tested, with an average of 0.34 across all the samples. These results have been summarised in Figure 4-19. The best friction coefficient was obtained from bath reference 30, under plating parameters of PTFE 100ml/L, Plating time 300 s, Agitation speed 200 RPM, Voltage 0.8 V with no potassium nitrate added.
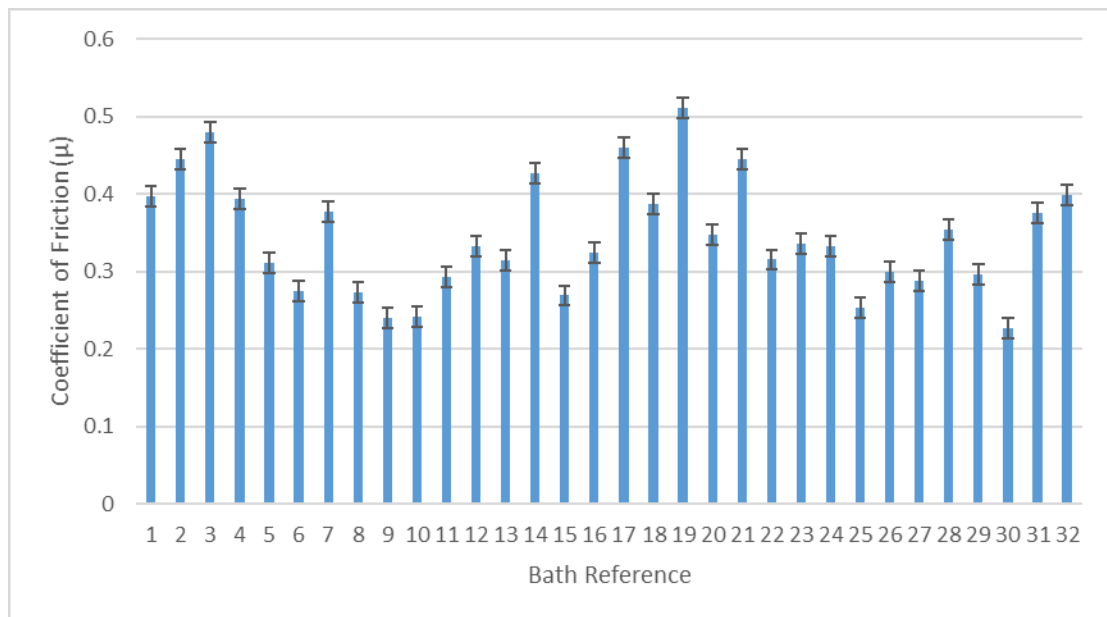
Figure 4-19 Coefficient of friction by electroplating bath reference for Ag-PTFE

with an average of 0.34 and range of between 0.23 and 0.51

The friction data for pure silver electroplating control samples produced using the same succinimide process, on the other hand, resulted in friction coefficients of 0.6. The results indicate that the Ag-PTFE MMC coating offers improved overall tribological performance over a pure silver electroplating. The friction coefficients obtained from different electroplating baths indicate the potential of reducing the friction coefficient by up to 62% by varying different bath parameters. It also suggests that optimisation of bath parameters might be able to improve the coating quality and tribological performance further.

CoF values were calculated based on an average of the CoF values recorded upon achieving steady state. A representative graph of the CoF is shown in Figure 4-20.
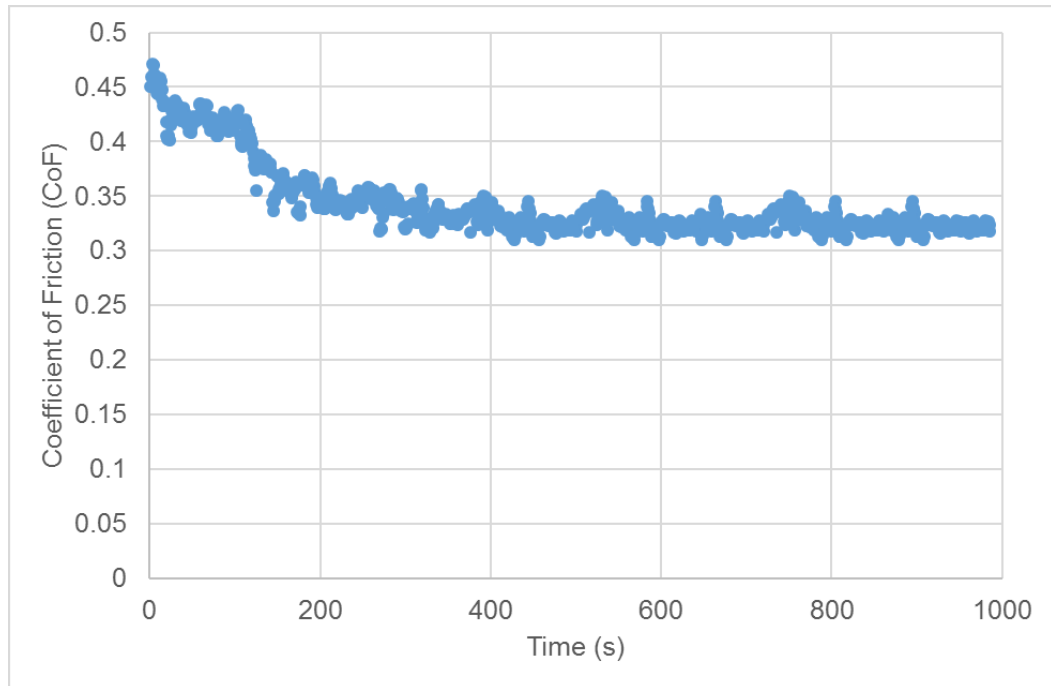
Figure 4-20 Gradual decrease in CoF observed prior to reaching steady state

Further analysis of the data obtained shows no correlation between amounts of PTFE on the surface with the friction performance of the coating. All the samples tested on the tribometer were not subjected to additional surface finishing prior to testing. Therefore, one possible cause of this might be varying surface roughness obtained after electroplating, which is a potential area for future research.

Both the wear track and wear pin were studied under the optical microscope after carrying out experiments on the linear tribometer for evidence of galling. Galling is likely to occur when the coating is completely removed, resulting in metal on metal contact. Occurrences of galling would be visible on the sample as substrate adhesive wear and occurrence of material transfer from the substrate to the wear pin would be visible.

The wear scar was inspected using an optical microscope after the sample was tested using the tribometer as shown in Figure 4-21. Most of the coating appears to have worn through around the areas of highest contact pressure from the friction pin, resulting in the appearance of the shiny stainless steel substrate below and leaving a visible wear scar of approximately 155μm in width. Although most of the coating has worn through, no visible evidence of adhesive material transfer exists either on the substrate or the pin countersurface in this instance.

Subsequent phenomena of wear observed on both the test plates as well as the steel ball bearing used will be discussed in this chapter section.
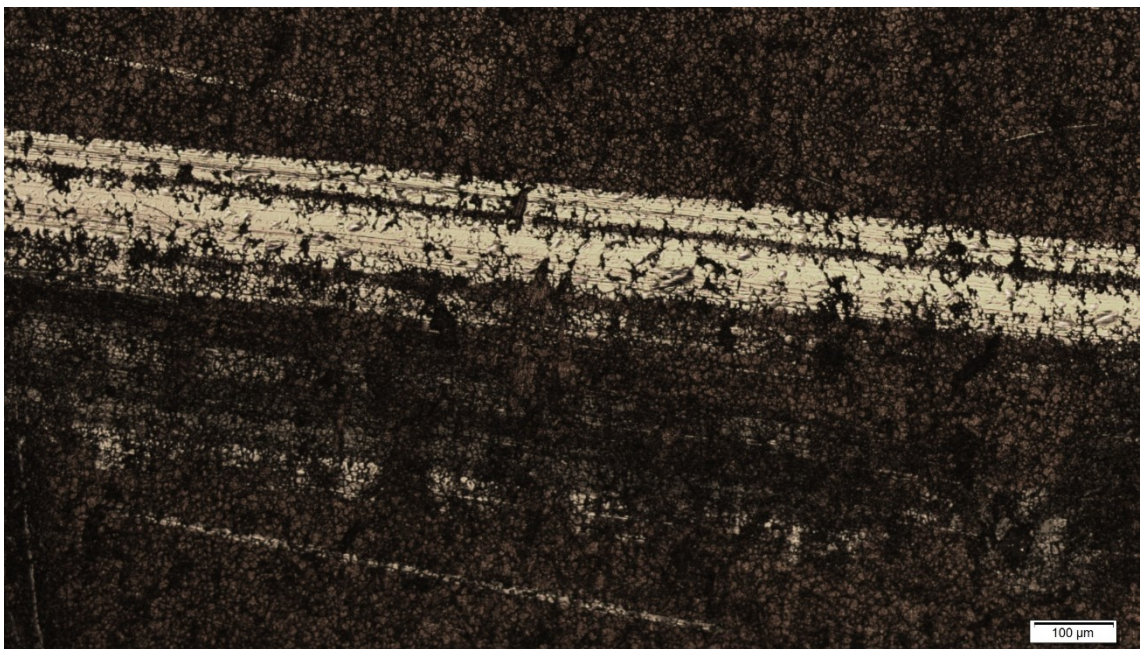
Figure 4-21 Wear scar from the tribology test based on a sample from full factorial experiments

Parameters: PTFE 100ml/L, Plating time 300 s, Agitation speed 200 RPM, Voltage 0.5 V, Potassium nitrate 16.7 g/L

Wear Pin

Surface fatigue wear was the dominant wear mechanism on the wear pin characterised by the formation of a pit on the pin contact area as shown in Figure 4-22. This would initially start out as a series of cracks as a result of repeated sliding of a single area over the track and would then spall revealing a pit. This was expected as the wear pin has to undergo repeated cycles of loading and unloading and was overcome by the frequent inspection and rotation of the wear surface.
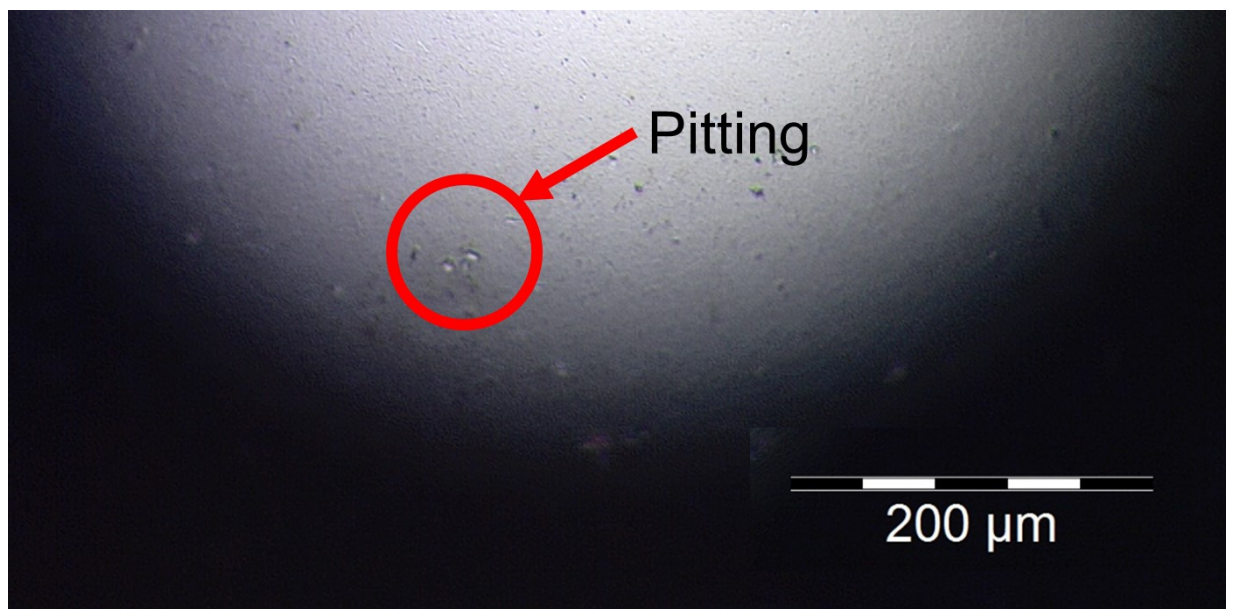
Figure 4-22 Pitting and remnants of transfer film on pin

Coating and Substrate

Adhesive wear of the coating resulting in coating material transfer to the wear pin counter-face was observed as seen in Figure 4-23 for the coating. Although pure PTFE material transfer on the transfer pin is relatively hard to be observed owing to the low surface energy causing it to fall off easily as previously reported [159],

trace amounts of the coating material were observed on the counter-surface which was removable as shown in Figure 4-24. The material transferred onto the pin contact surface area would have aided in the reduction of pin resistance during the sliding wear experiment and thus CoF observed. The other mechanism of adhesive wear was observed between the substrate and wear pin shown in Figure 4-255. The thin coating was fully removed but the substrate oxide surface layer was not broken through in this instance. The areas which are out of focus indicate a small portion of substrate adhesive material transfer to the wear pin during sliding. This is the start of substrate material transfer and galling build-up.
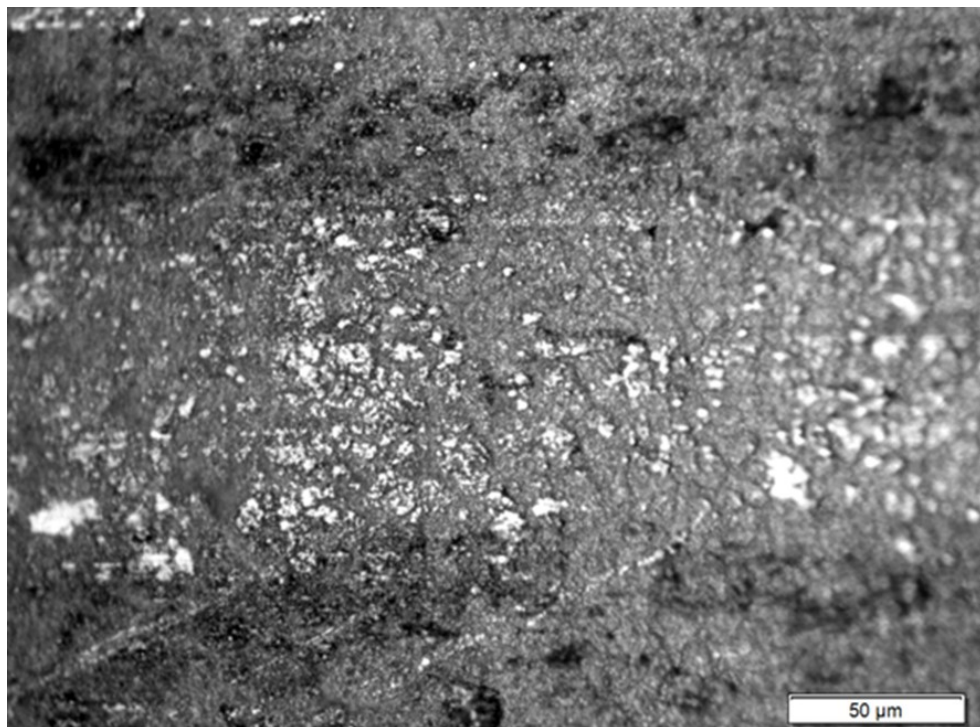
Figure 4-23 Adhesive wear observed on the coating resulting the transfer of material from the coating onto the counter-surface DoE 28a x50
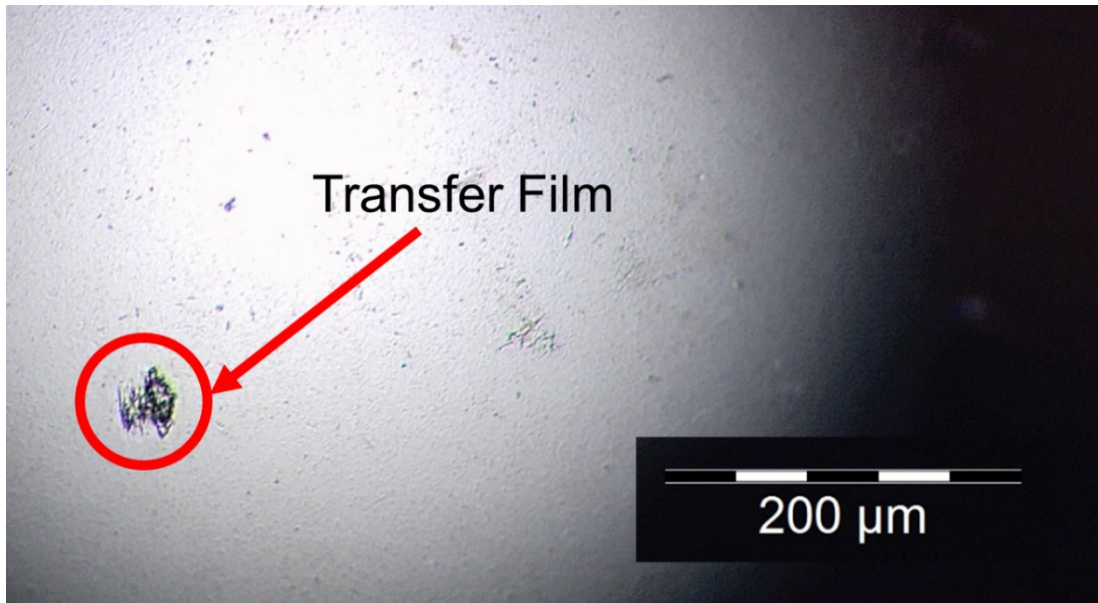
Figure 4-24 Transfer film observed on pin countersurface
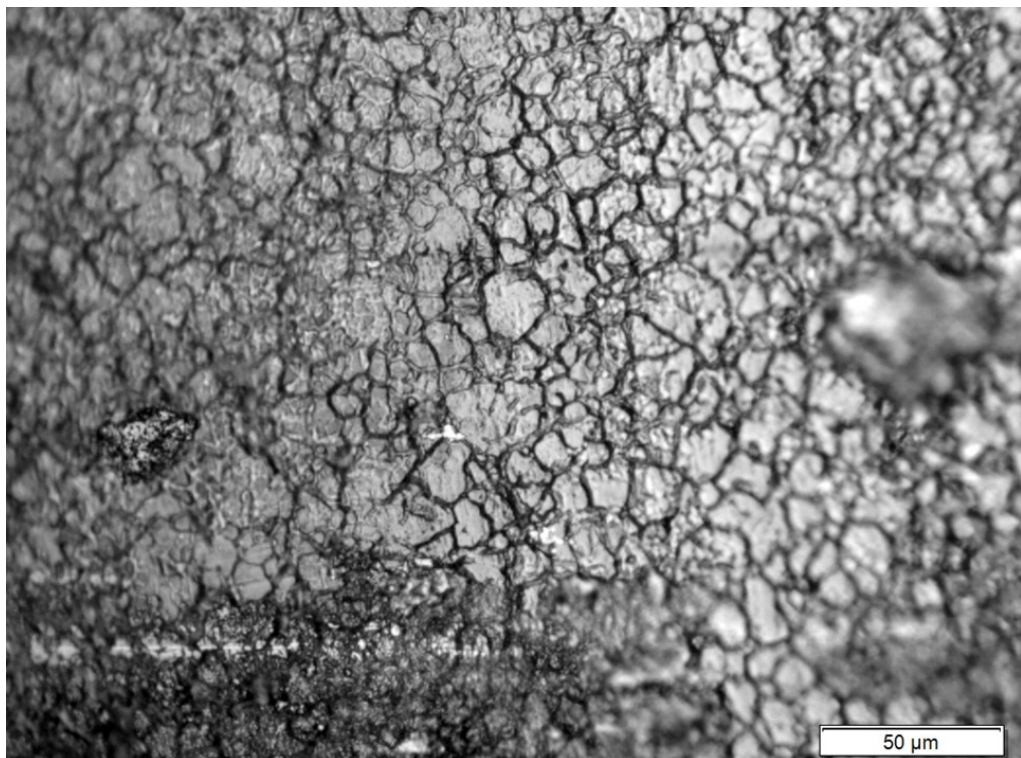
Figure 4-25 DoE 21 x050 – Adhesive wear observed

Apart from adhesive wear, the other wear mechanism relating to both the coating and substrate was abrasive wear. Based on the visual inspections carried out, abrasive wear can be grouped into two distinct types. The first type of abrasive

wear is due to imperfections in the substrate material as can be seen in Figure 4-26. The thin coating deposited was not sufficient in masking substrate surface imperfections such as dips in the surface. As the wear pin encounters the dips, the wear pin removes the coating from the substrate asperities exposing a bare substrate. Small, hard debris that are trapped between the wear pin and its contacting surface result in the score marks observed. This type of abrasive wear is typically limited to the region of substrate imperfections.

The second type of abrasive wear observed creates visually deep grooves in the substrate material. The observations made of the plates and wear pin can conclude that this type of abrasive wear occurs primarily due to large, hard debris being trapped on in between the sliding surfaces. The other instance of this occurrence as seen in Figure 4-27 coincides with the surface fatigue wear on the wear pin as previously illustrated in Figure 4-22. It is believed that hard pin material would have fragmented due to fatigue spall, leaving the pits observed. The hard material when trapped between the sliding surfaces which would then plough the observed grooves into the substrate.

Figure 4-26 DoE 001a x50 Abrasive wear due to the substrate imperfections
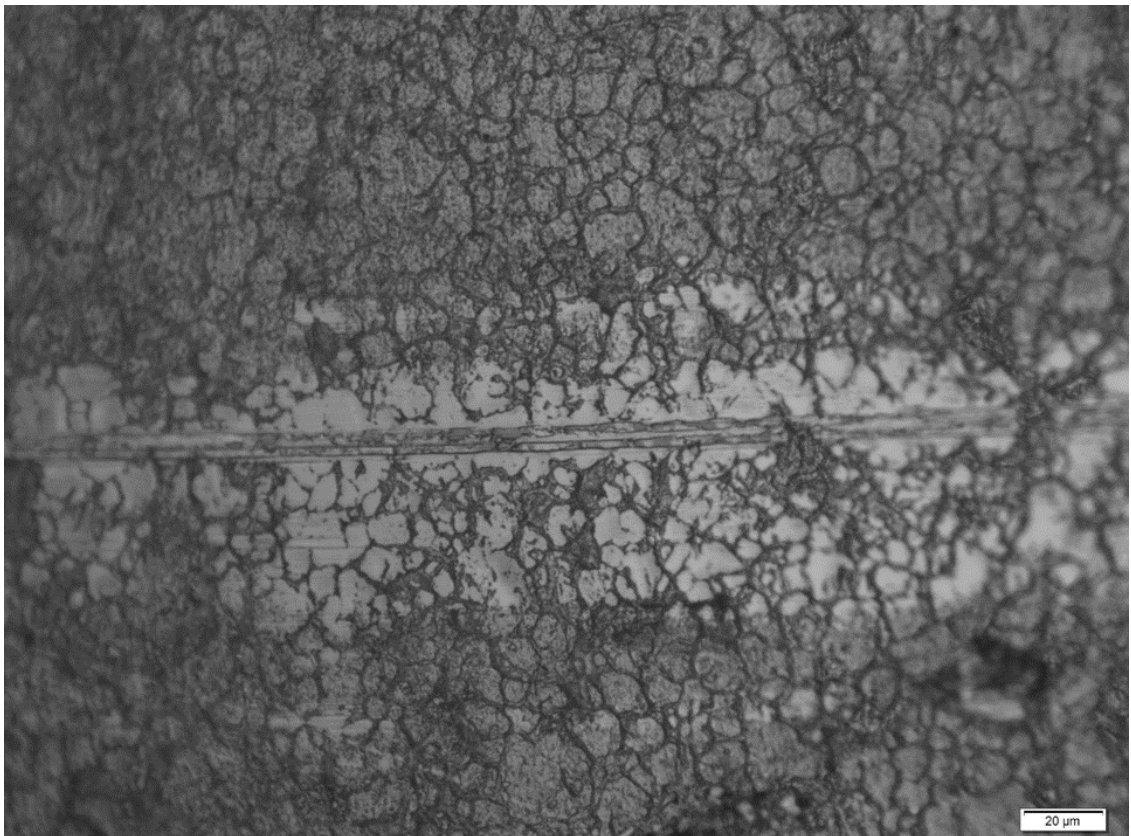
Figure 4-27 DoE 008a x050 Abrasive wear resulting in scoring on the substrate

It should be noted that the theoretical deposited thickness of the coatings for the full factorial experiments based on Faraday's laws of electrolysis and electroplating parameters range from 0.48 to 1.15 microns. This is substantially lower than the minimum 25 micron thickness used for hardness and wear rate measurements carried out by Le et. al. [154]. Variation in CoF values represent the ability of coatings in successfully forming a transfer film and preventing adhesive wear between the substrate and the pin which will ultimately result in galling.

In summary, samples generated from the structured full factorial experiments were subjected to tribological testing on the linear tribometer. The findings indicated that a reduction of CoF to 0.23 was achievable when compared with the CoF for the pure non-cyanide silver coating, although adverse CoF results of 0.51 were also observed. Wear and galling of the samples was studied as it could contribute to the variation in CoF obtained from the samples. Inspection of the wear scar from the tribology tests showed evidence of galling on samples where the coating was completely removed, which resulted in metal on metal sliding and thus adversely impacting the CoF. Abrasive wear was also observed on samples where the wear pin encountered surface fatigue, which is not unlikely if the coating had poor wear characteristics resulting in prolonged metal on metal contact. On the other hand, evidence of transfer film formation was found on the sliding countersurface (wear pin), which provides an explanation towards improved CoF performance..

4.5.3 Adhesion

Adhesion tests carried out showed maximum adhesion strength of 2.5 MPa was achievable between the Ag-PTFE sample runs illustrated in Figure 4-27. On the other hand, the maximum adhesion strength for pure silver electroplating of 4.5 MPa was achieved. The comparison of data suggests that a reduction of approximately 44% in maximum adhesion strength is a result of PTFE addition into the electroplating process. The review of electroplating bath parameters with electroplating adhesion performance has concluded that there is an inverse relation between the PTFE content in the electroplating bath with the electroplating adhesion performance. The higher amounts of PTFE in the electroplating bath which resulted in lower adhesion performance might be due to the lack of a suitable surfactant to ensure adhesion of PTFE particles during the electroplating process.

Furthermore, the adhesion data suggests that there is no direct correlation between adhesion and friction coefficients in this instance. Based on the data obtained, it can be concluded that high adhesion strength between the surface coating and the substrate will not result in low frictional coefficients due to increased wear resistance.
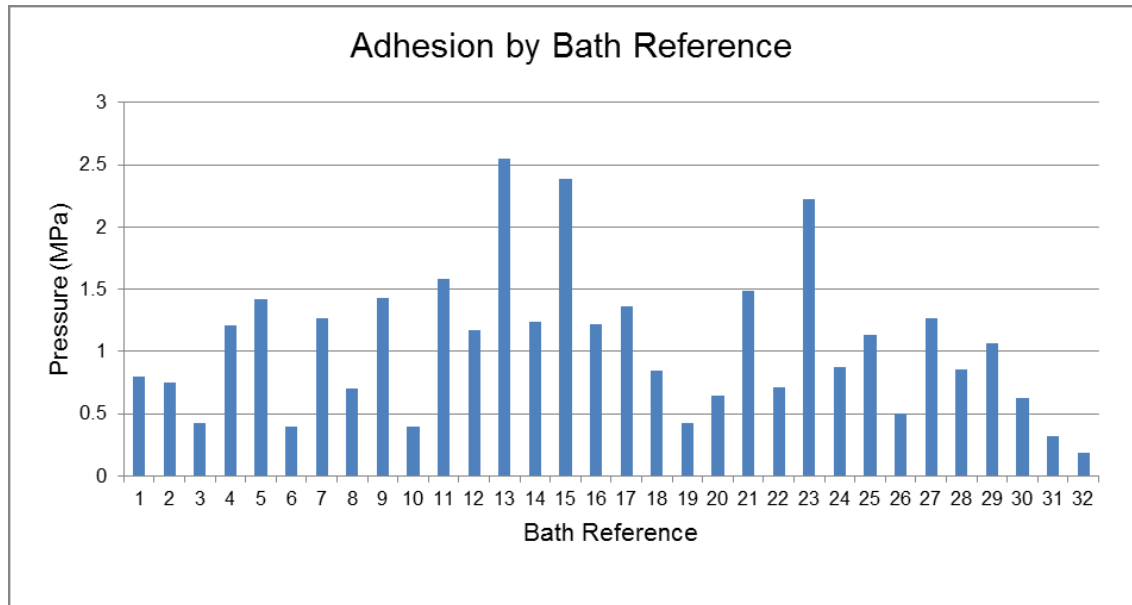
Figure 4-28 Adhesion performance by electroplating bath reference with a range of between 2.5MPa and 0.2MPa

4.5.4 Summary of the full factorial experiments

The full factorial experiments were able to provide valuable insight, not just in terms of how each electroplating bath performed in relation to required criteria, but also provided insight into other areas which will affect the ultimate of the performance such as surface morphology and particle sizes.

It is difficult to assess the relative importance of the considered variables on codeposition, and the decision matrix method had been used to enable a decision to be made as to which bath parameter would be considered for further study and development based on the output of coating performance. The highest decision matrix score was reserved for CoF performances of <0.25, >10 wt% Fluorine for particle incorporation, >1.5MPa for adhesion strength and for no observed galling. The full scoring for each key criteria by output range is detailed in Appendix 2.

The key criteria of the full factorial experiments and its associated scoring for each criterion by full factorial experiment reference are tabulated in Table 4-3. Alongside the best performance, reserve developmental baths and the lowest performing coating was identified. The best overall performing coating would be developed further. The baths highlighted as reserve would be used as potential future consideration while the weakest overall coating would also be studied in detail to understand the possible reasons for its overall weak performance.

Table 4-3 Key criteria of the full factorial experiments and its associated scoring

Coating Ref / Weighting	Criteria				Total
	CoF Performance	Wear	Particle incorporation	Adhesion	
	9	7	5	3	
1	1	1	1	1	24
2	0	1	1	1	15
3	0	1	0	0	7
4	1	1	1	3	30
5	1	1	3	3	40
6	3	1	1	0	39
7	1	1	0	3	25
8	3	1	0	1	37
9	9	3	3	3	126
10	9	1	3	0	103
11	3	1	3	9	76
12	1	1	1	3	30
13	1	1	9	9	88
14	0	1	3	3	31
15	3	1	1	9	66
16	1	1	1	3	30
17	0	1	1	3	21
18	1	1	3	1	34
19	0	1	1	0	12
20	1	1	1	1	24
21	0	1	0	3	16
22	1	1	1	1	24
23	1	1	1	9	48
24	1	1	1	1	24
25	9	3	3	3	126
26	3	1	1	1	42
27	3	1	3	3	58
28	1	1	3	1	34
29	3	1	0	3	43
30	9	9	1	1	152
31	1	1	1	0	21
32	1	1	3	0	31

(Note: The green highlighted cell indicates highest overall tier score, orange highlighted cells indicate potential future considerations for development and red highlighted cell indicate lowest overall score)

Important lessons were learned during the course of carrying out the full factorial electroplating experiments and highlighted several key opportunities for improvement in methods for future experiments. One key lesson was in relation to the constant potential method used. The surface morphology observations drew attention to how the current density fluctuations affected the sizes of the deposited particles. A constant current density would allow adequate control of deposit quality. Having a constant current density would also be beneficial for the future development of the coating. The full factorial experiments were carried out on test plates of the same geometry; however, the coating would have to be ultimately electroplated onto a nut which had a more complex geometry and hence replication of the Ag-PTFE onto the nut would be easier with a constant current density and potential allowed to fluctuate.

In summary, samples were electroplated using the full factorial method for determining the effects of identified variables towards the deposit characteristics. Although the best CoF achieved through this process is 0.23, there is still scope for further improvement of this through improving the friction and wear properties by increased incorporation of PTFE particles.

4.6 Summary of the chapter

This chapter reports on the results obtained from the initial coating development. After a uniform silver deposit was successfully obtained from the succinimide non-cyanide silver electroplating bath, trials were carried out using voltages of 0.5V, 0.8V and 1.0V. Similar visual characteristics between 0.5V and 0.8V were observed, except for 1.0V which resulted in an uneven deposit. Testing of the

pure silver coating deposited at 0.5V and 0.8V using the linear tribometer showed improved CoF of 0.3 over an uncoated substrate of 0.6. Analysis of PTFE incorporation was carried out through EDS analysis of fluorine. This showed that only 4wt% fluorine was incorporated even with a substantial amount of 100mL/L PTFE in the electroplating bath which suggested the investigation of other factors affecting particle incorporation, with a marginal CoF improvement of 0.29. The subsequent investigation of substrate roughness effects on PTFE incorporation found that the reduction of substrate surface roughness resulted in decreased PTFE incorporation and higher CoF results. Two level full factorial experiments were subsequently carried out to study the interactions of variables such as voltage, time, agitation speed, KNO3, PTFE concentration on the coating properties. The summary of findings are that tarnished and bright samples were able to be created by varying bath conditions. In addition, the variation of bath conditions resulted in the visual observation of varying deposit roughness, which ultimately affects the tribological performance of the coating. It was also noted that PTFE incorporation in the MMC is not just dependent on its concentrations in the bath and that good adhesion of the coating onto the substrate does not result in good tribological performance. The conditions of 0.8V, 200 RPM agitation speed, 300s plating time, no potassium nitrate included and 100mL/L of PTFE in the bath will form the basis for further development as it managed to result in a rough deposit with improved CoF properties of 0.23.

Chapter 5 Coating Refinement

5.1 Introduction

The full factorial experiments highlighted several key areas requiring further investigation. One of which was the adhesion of the Ag-PTFE coating to the substrate. It has been found that the adhesion of coatings to a substrate is closely interrelated with its wear resistance [160]. The developed coating should exhibit a low CoF and ideally be able to resist wear to prolong the lifespan of the coating.

The coating formulation selected from the full factorial experiments for further development as discussed in the previous chapter was used. To improve its adhesion, the use of strikes, as well as pulse plating, were be considered. Strikes based on three materials were considered, namely silver, copper, and nickel. These metals were chosen for its compatibility with both the stainless steel substrate as well as the silver plating. The strike material would firstly be deposited directly onto the substrate and after a thorough rinsing process, the Ag-PTFE would be deposited. Deposition of the main Ag-PTFE coating would be carried out using PCP. This can be carried out using a variety of different parameters. Trial and error to obtain suitable PCP frequency parameters were carried out through the study of its surface morphology. The frequencies

considered were PCP F=2Hz, F=5Hz, F=10Hz and F=100Hz. Chen et al. reported that the microstructure of MMC coatings largely dictating its wear resistance [161]. Shanthi et al. on the other hand reported the observation that high current efficiencies were obtained for F=10Hz while hard deposits were obtained for F=100Hz [144]. High current efficiencies or hardened deposits coupled with the other PCP benefits would be beneficial to the tribological properties of a coating. On the other hand, neither authors justified their choice in starting their investigations at a minimum of F=10Hz and thus PCP frequencies of F=2Hz and F=5Hz were also considered in this research.

Fractals and electrodeposition defects

Fractals are defined as patterns which are repetitive on all levels in a deposit structure which can be dendritic and possess no practical value apart from the study of metal microstructures in the field of material sciences [162]. In the context of this project, the dendritic surface morphology of the deposit which is of detriment towards its tribological properties is considered to be defects. The formation of these electrodeposition defects are due to pulse current electroplating parameters. It has been found to occur through nanowire self-assembly, where initial nanowire formation forms the base for its continued growth when electroplating is continued [163]. Figure 5-1 shows fractals exhibiting a dendritic, tree-like structure extending from the surface of the substrate. This structure exhibited low performance in supporting external stresses from the tribometer and wore out rapidly. Frequencies resulting in fractals, namely F=2Hz and F=5Hz were subseqeuntly excluded from further investigation.
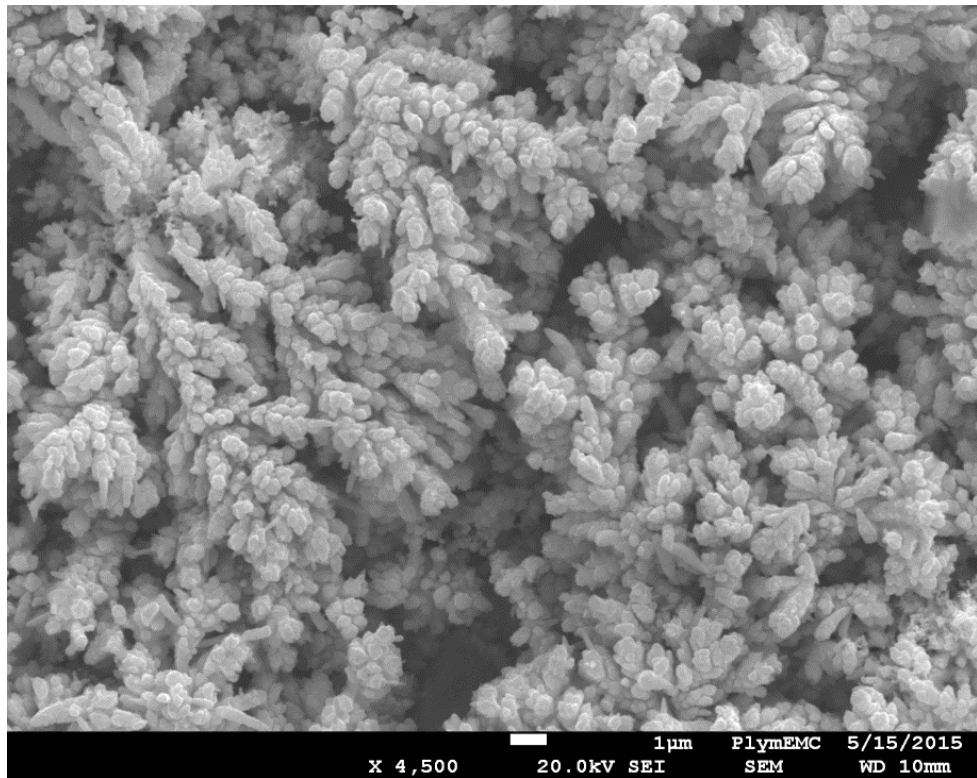
Figure 5-1 Dendritic deposits observed using PCP F=5Hz

Results

The PCP frequencies of F=5Hz and F=10Hz were excluded from further investigation after visual inspection of its surface morphology showed fractal deposit structures which were detrimental to the tribological performance of the coating. The study of strikes and pulse plating effects were focused on rectangular pulse plating frequencies of F=10Hz and F=100Hz with a duty cycle of 50% as deemed suitable from the trial and error method. The exponential increase in frequency tested will highlight notable differences between the deposited MMC.

Table 5-1 Summary of results obtained from the PED tests

Reference	Ag-PTFE Plating Frequency	Base strike	Measured CoF	Adhesion (MPa)
1	F=100Hz	Ag	0.5	1.09
2	F=10Hz		0.5	1.02
3	F=100Hz	Cu	0.45	0.87
4	F=10Hz		0.38	0.84
5	F=100Hz	Ni	0.45	0.81
6	F=10Hz		0.60	0.83
7	F=100Hz	None	0.80	0.72
8	F=10Hz		0.20	0.75

The summary of results obtained from the experiments is seen in

Table 5-1 Summary of results obtained from the PED tests. The metals used for the strikes in ascending order of hardness are silver, copper, and nickel. As a benchmark, the dry sliding of uncoated stainless steel plates registered a CoF of 0.6.

Based on the overall results, the use of strikes and pulse plating helped to increase the adhesion strength between the substrate and the coating with varying degrees of success. The Ag-PTFE deposited on a silver strike exhibited the best adhesion performance, however as previously observed in the full

factorial experiments, this comes at the expense of the CoF performance. The adhesion performance for copper and nickel on the other hand, only marginally exceed that of the coating deposited using pulse plating. Although the Ag-PTFE coating was deposited using the same parameters, the CoF performance varied significantly between frequency and strike pairs.

The reason for the variation in CoF performance can firstly be explained through pulse plating parameters. Pulse plating enables the deposition of smoother; finer grained deposits observed through surface morphology of the coating. As Chen et. al. pointed out, the microstructure of pulse plated composite coatings will largely dictate its wear resistance [161]. Wear resistance is also aided with thicker coatings and harder deposits. Shanthi et al. found that high current efficiencies and hard deposits were possible for silver pulse plated at F=10Hz and F=100Hz respectively [144].

As the Ag-PTFE coating exists as a thin soft film, this wears out relatively quickly, and formation of a transfer film on the counter surface occurs along with exposure of the strike layer. The CoF results for F=100Hz have shown that the strikes prevent the direct adhesive contact between the wear pin and substrate; however, once the Ag-PTFE layer has been worn out, the CoF shows gradual increases due to coating failure. Ag-PTFE coating failure results in the wear pin contacting the strike surface and the strike material forms a composite transfer layer with transfer layer remnants from the Ag-PTFE coating; however, it does not result in prolonged direct strike material to steel contact as this will result in higher CoF.

To understand the high CoF value of the Ag-PTFE coating with no strike, current efficiencies for PCP are typically around 60% whereas DCP current efficiencies

are in excess of 90%. This results in reduced deposit thickness. Once the coating breaks down, the sliding of the wear pin will be in the form of sticking and slipping, therefore exhibiting a higher overall CoF. This phenomenon of sticking and slipping can also be used to explain the higher overall CoF observed for the Ag-PTFE coating within these experiments.

Lower CoF values were observed for F=10Hz coatings in general. The lowest CoF value of 0.2 was achieved without a strike. It is believed that the F=10Hz with no strike has managed to achieve a lower CoF value due to the structure of the deposit itself, where small globules merge to form a large "super-particle." The formation of the spherical Ag-PTFE super-particle has benefits in terms of CoF. As the wear pin slides across the super-particle, a small amount of coating is removed on the top, forming a transfer layer on the counter surface but the coating remains intact. In essence, it achieves better frictional performance by mimicking a thicker coating and acts as a lubrication reservoir. The use of PCP also ensures that these particles are dense in nature, and this also reduces wear. On the other hand, super-particle formation did not occur with the samples where a strike layer had been deposited as seen in Figure 5-2 for both a copper and nickel strike base. Instead, it has been observed that the Ag-PTFE would prefer to adhere directly to the strike material rather than form a super-particle, causing uneven, agglomerated areas of coating. Because of this, the lubricating PTFE is not replenished in an area once it has been worn off.

(a)

(b)
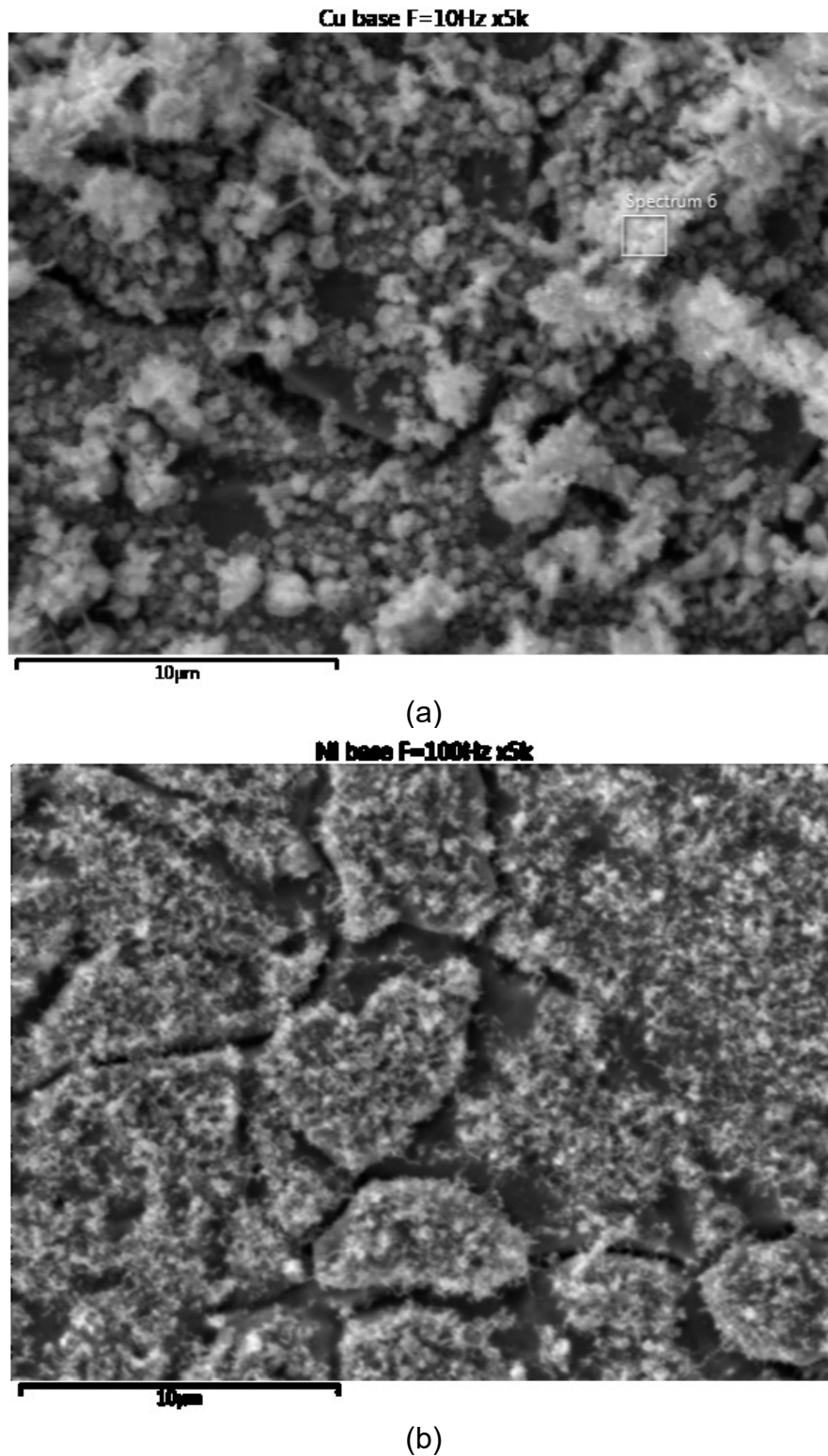
Figure 5-2 Surface morphology of the Ag-PTFE deposit using PCP with (a)

F=10Hz on a copper strike base and (b) F=100Hz on a nickel strike base

observed at x5,000 magnification

In summary, the experiments have shown that different deposit structures such as fractals, particle agglomeration on base strike metals and even super particles can be created through PCP and strikes. PCP at F=100Hz with a 50% duty cycle had resulted in small deposit grains which were unable to facilitate improved tribological performance while the surface morphology of PCP at F=10Hz with a 50% duty cycle had resulted in the formation of agglomerated smaller particles into a larger spherical particle that aids in improving tribological properties. Furthermore, consistent with the findings from the full factorial experiment, the increased adhesion strength of the coating to the substrate does not directly translate into better CoF performance.

5.2 Effects of surfactant addition and pulse plating

The previous section had identified the use of PCP at F=10Hz without the use of a strike for further development in achieving the project objectives. The next step of the process is to study the effects of FC-4 surfactant addition in the dispersion of PTFE particles in conjunction with the use of pulse plating. The use of a cationic FC-4 surfactant is to ensure better dispersion of the PTFE particles while its cationic properties will increase the migration of the dispersed particles to the cathode due to the charge given.

5.2.1 Surface morphology

An initial study was carried out to understand the suitability of using the FC-4 surfactant in the electroplating bath. The surface morphology inspection using SEM in Figure 5-3 showed that a uniform Ag-PTFE deposit was possible with varying particle sizes which covered the surface of the substrate. Large particles in the order greater than 1.5 micrometres were observed; however, an inspection

carried out at high magnification as seen in Figure 5-4 showed that these large particles were in fact comprised of agglomerated nanoparticles (<100nm). Figure 5-5, on the other hand, highlights the drawback in the use of surfactants, where the surfactant is deposited as part of the coating as well.
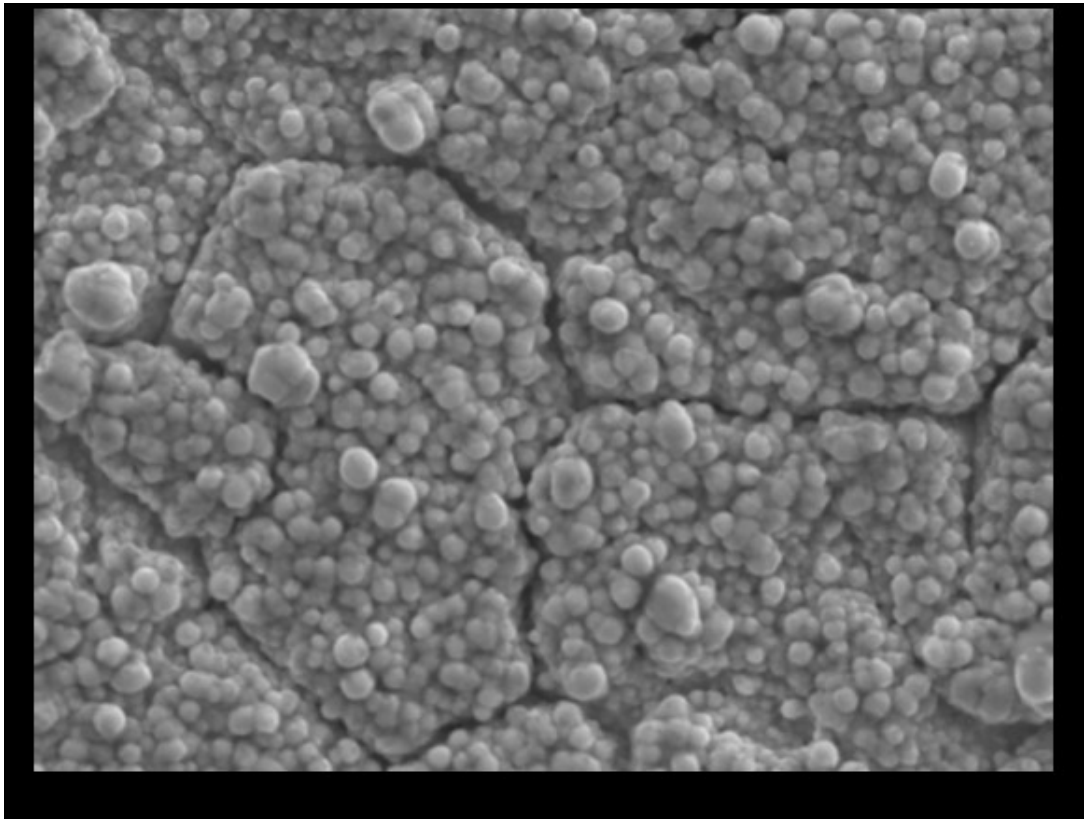
Figure 5-3 Initial surface morphology inspection of the deposit obtained through FC-4 addition in the electroplating bath taken at x5,000 magnification
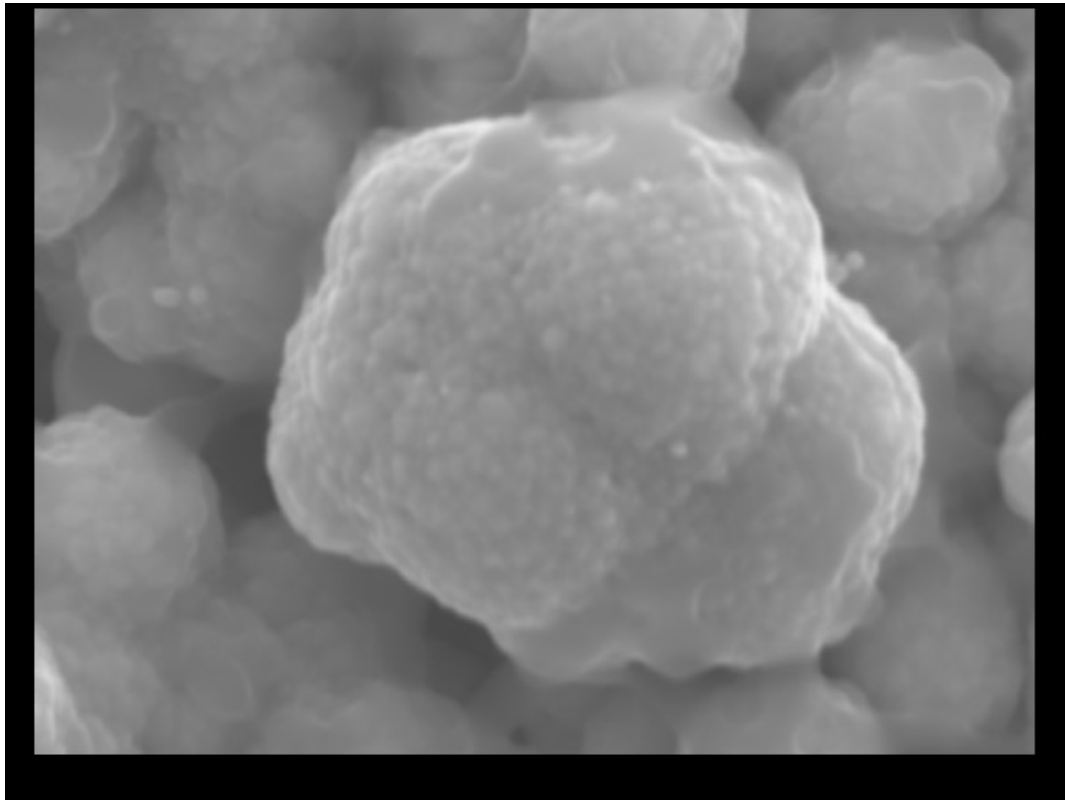
Figure 5-4 Nanoparticles (<100nm) observed from the MMC through the use of

the FC-4 anionic surfactant
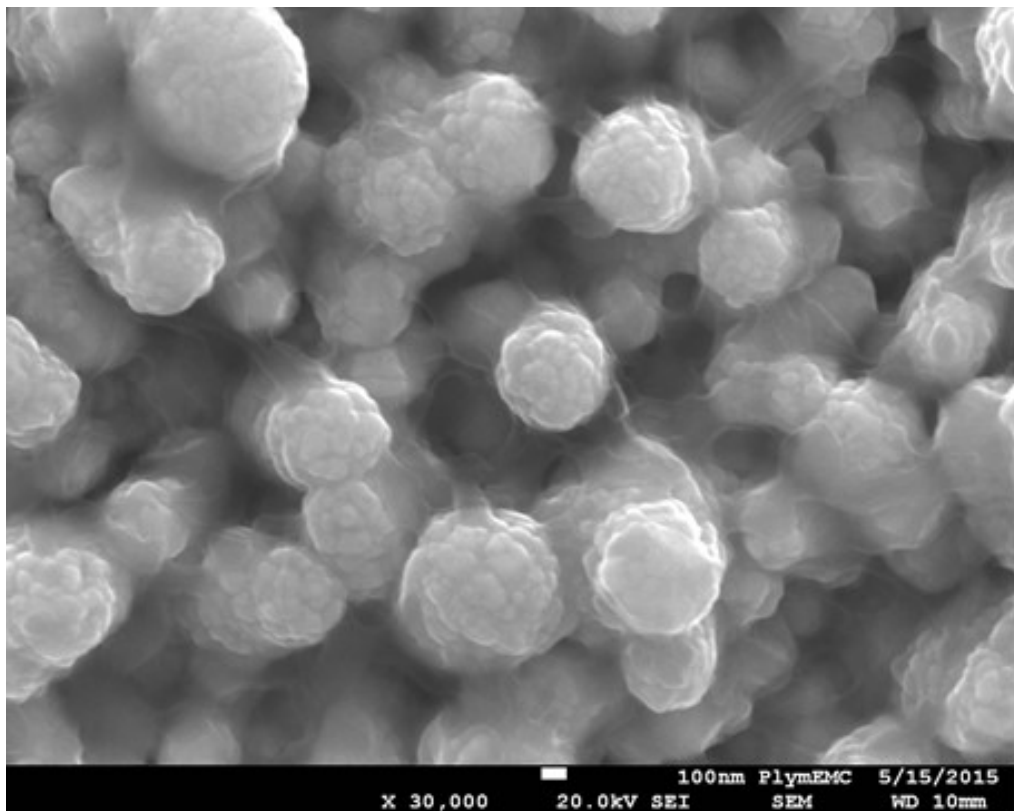
Figure 5-5 Surface morphology of sample where FC-4 is deposited alongside

the main deposit

The next step is to identify an optimal surfactant to PTFE ratio for use in the electroplating bath. This was carried out using a systematic process of studying the differences in surfactant to PTFE ratio as well as its impact on deposits obtained through the use of either DCP or PCP. The three ratios of FC-4 to PTFE considered were 1:1, 1.5:1 and 2:1.

SEM analysis of the DCP samples with FC-4: PTFE ratios of 1:1, 1.5:1 and 2:1 at x1,000 magnification have notably different overall surface morphologies. For the 1:1 ratio sample, the plated layer primarily covers the surface of grains while having the grain boundaries clearly exposed. This is quite similar to the 2:1 ratio sample; however, with the 2:1 ratio sample, the plated layer is much more densely packed. The 1.5:1 ratio plating on the other hand visually resembles spluttering, with the coating not clearly conforming to the grains of the substrate.

On the other hand, visual comparison of the PCP samples at x1,000 magnification show similarities between the surface morphology of the plated samples at FC-4:PTFE ratios of 1:1 and 1.5:1; the major visual differences between these two samples however, lie in the coating density, where the plating at 1.5:1 being more densely packed. Meanwhile, the 2:1 ratio PCP sample is coated primarily on the surface of the grains, with the grain boundaries experiencing limited coverage and being clearly visible. The SEM images for both DCP and PCP samples are shown in Figure 5-6.
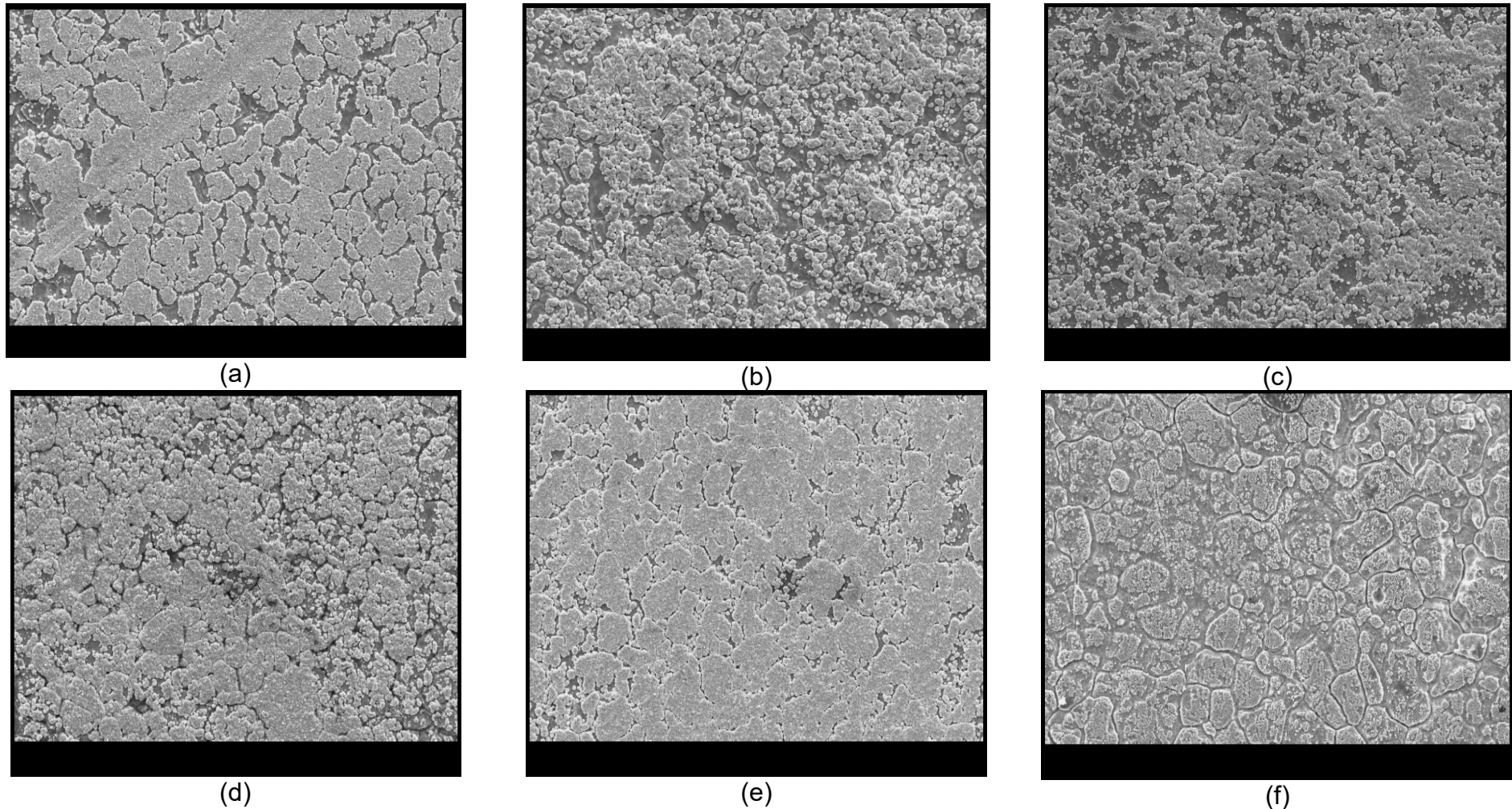
Figure 5-6 SEM micrography at x1,000 magnification (a) DCP with FC-4: PTFE ratio 1:1 (b) PCP with FC-4: PTFE ratio 1:1 (c) DCP with

FC-4: PTFE ratio 1.5:1 (d) PCP with FC-4: PTFE ratio 1.5:1 (e) DCP with FC-4: PTFE ratio 2:1 (f) PCP with FC-4: PTFE ratio 2:1

To better understand the differences between DCP and PCP at the different FC-4 to PTFE ratios, the deposited particles were also analysed at x30,000 magnification as shown in Figure 5-7, with Figure 5-7(b) highlighting the PTFE and pure Ag particles. For all of the DCP samples, average plated particle sizes were approximately 100nm, with bright particles visible of <50nm. The 1:1 ratio DCP sample had noticeably lower amounts of the bright (white) particles. With the 1.5:1 and 2:1 ratio DCP samples, the nanoparticles were fused together to create a larger spherical particle of approximately 1μm in size. On the other hand, although the fusion of nanoparticles occurred on the 1:1 ratio DCP sample, they did not form the larger spherical cauliflower like particles as observed with the other samples.

Observation of the PCP samples at x30,000 magnification noted average particle sizes of approximately 100nm across all samples which were similar to that of the DCP samples. The bright particles were clearly visible on samples with FC-4: PTFE ratios of 1.5:1 and 2:1, with the 2:1 ratio sample having the highest concentration of these nanoparticles. The formation of fused larger particles was also apparent for the PCP samples. The fused particle size for 1:1 and 1.5:1 PCP samples were not dissimilar to that observed with the DCP ones, with a particle size of approximately 1μm. On the other hand, although the fusion of particles occurred on the 2:1 PCP sample, these were of average sizes of approximately 300nm and the fusion of larger particles created a uniform coating over the grain of the substrate.

EDS was carried out using area analysis mode over three randomly selected sites at x1000 magnification with averaged values used. Weight % and atomic % data obtained from EDS was normalised to provide the appropriate values for

quantitatively identifying the plated deposits of silver (Ag) as well as PTFE through its chemical composition of carbon (C) and fluorine (F) elements. For the EDS analysis, as silver is denser than fluorine, atomic % is favoured for use in this paper to provide a more accurate representation of the elemental composition of the plating. Although both C and F elements are present for PTFE, F will be used for determining PTFE presence as carbon is also present in the substrate layer. The EDS was able to find silver, carbon and fluorine elements on all the samples, suggesting successful incorporation of PTFE into the MMC during its deposition on the substrate.
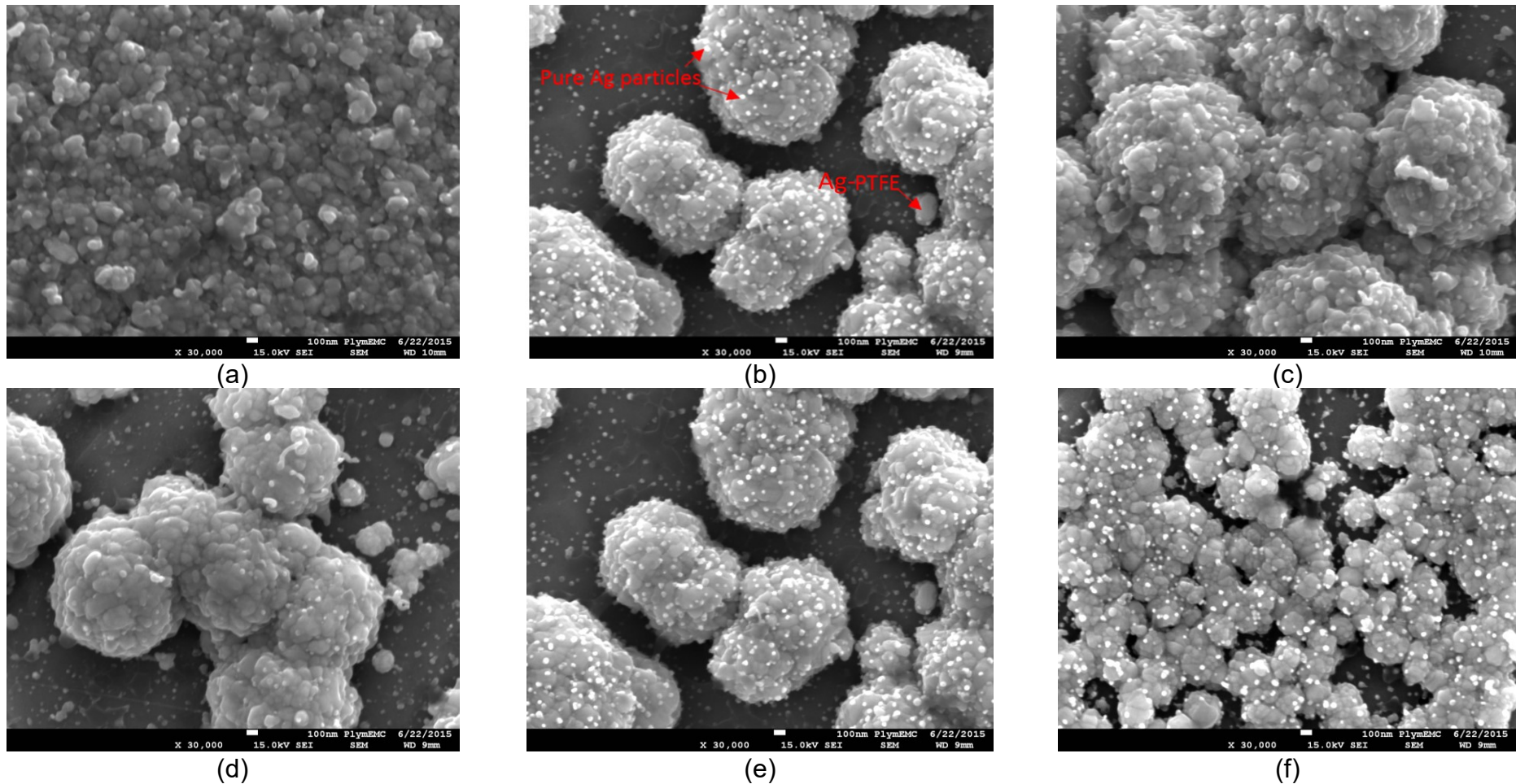
Figure 5-7 SEM micrograph of deposited particles at x30,000 magnification. The brighter tiny particles are identified as pure silver nanoparticles with the globules being Ag-PTFE (a) DCP with FC-4: PTFE ratio 1:1 (b) PCP with FC-4: PTFE ratio 1:1 (c) DCP with FC-4: PTFE ratio 1.5:1 (d) PCP with FC-4: PTFE ratio 1.5:1 (e) DCP with FC-4: PTFE ratio 2:1 (f) PCP with FC-4: PTFE ratio 2:1

5.2.2 Tribology

Tribological data in the form of friction coefficients (CoF) from each of the DCP and PCP samples was obtained over 30 cycles from 3 randomly selected sites (10 cycles per site). The CoF shown in Figure 5-8 was obtained by averaging the mean CoF values across the three sites. Based on this, there is a downward trend for the CoF values with increasing FC-4: PTFE ratio, with a range of between 0.07 and 0.12. For PCP samples, there is an upward trend for the CoF values, with a range of between 0.06 and 0.09. In comparing both DCP and PCP samples, the DCP 1:1 ratio sample has the highest CoF value at 0.12 while the PCP 1:1 ratio sample has the lowest CoF value at 0.06.
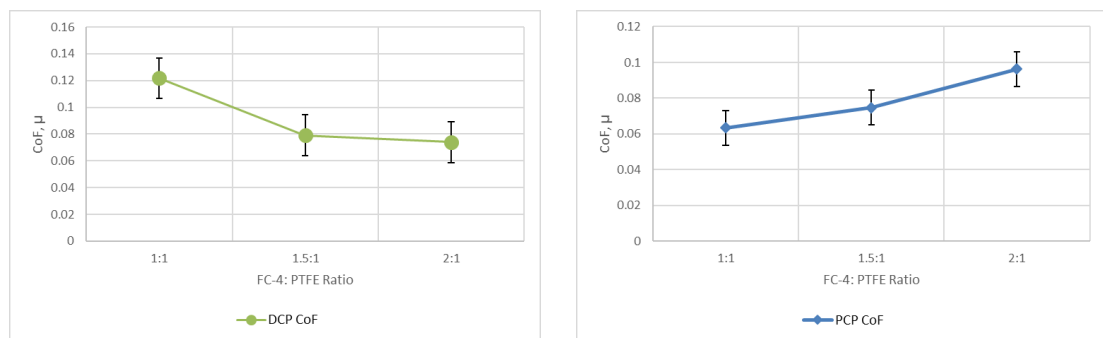
Figure 5-8 Mean coefficient of friction (CoF) for the DCP and PCP samples by FC-4:PTFE ratio

SEM was used to overcome the physical limitations of optical microscopy when it came to better understanding the tribological behaviour of the samples. The wear track observed can be categorised into three main zones as indicated in Figure 5-9. Zone 1 is where contact pressures are at its highest. This zone is where the thin coating is expected to completely wear out and fail. Adhesive wear between substrate and wear pin will also occur here through the failure of the coating to provide an adequate layer between the wear pin surface and the

substrate. Furthermore, adhesion of these surfaces results in sticking and slipping between sliding surfaces, and once the coating has been worn off, the pin would slide against the hard substrate, giving rise to surface fatigue wear of the wear pin. Hard particles liberated from the surface fatigue of the wear pin that are trapped between the sliding surfaces would then result in abrasive wear patterns. The occurrence of stick and slip conditions will register as increases in CoF while abrasive wear can be visually observed on the substrate. Figure 5-9 for the PCP FC-4: PTFE ratio of 2:1 sample shows Zone 1 to be completely devoid of coating, with a breakthrough of the substrate surface layer. The uneven surface because of the change in plastic behaviour of the substrate material is evidence of galling due to poor lubrication. This phenomenon was also observed on the DCP FC-4: PTFE ratio of 1:1 sample. In contrast, the other 4 samples had retained their coating in Zone 1, with the Zone 1 wear track for PCP with FC-4: PTFE ratio 1:1 shown in Figure 5-10.

Zone 2, on the other hand, is the wear track "border" between the highest contact stresses and the untested coating in Zone 3. This zone is where relatively lower contact stresses were imparted onto the coating during testing and can be subsequently subjected to visual analysis using the SEM to better understand the performance of each coating.
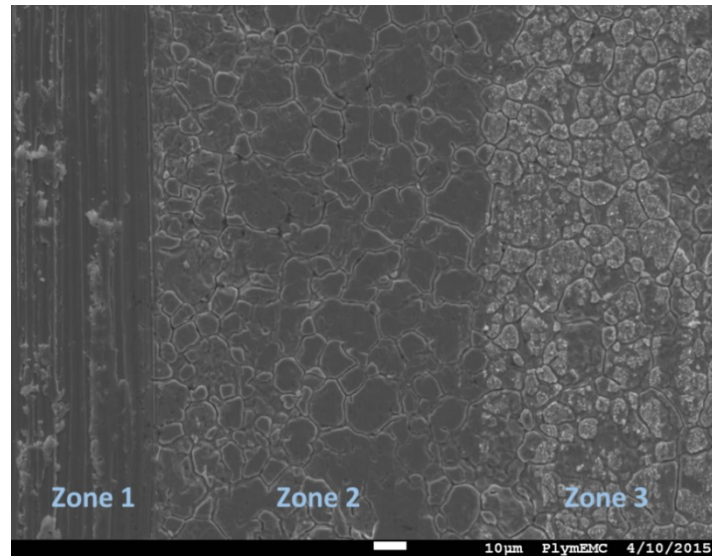
Figure 5-9 Wear track showing the three distinct zones of wear due to contact pressure differences for PCP with FC-4: PTFE ratio 2:1
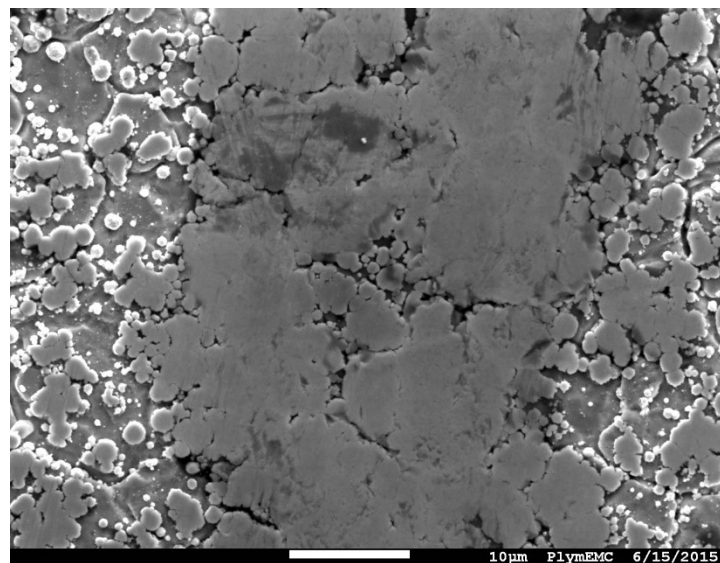
Figure 5-10 Zone 1 wear track for PCP with FC-4: PTFE ratio 1:1 showing retained coating

The different zones can be better illustrated using contact mechanics in Figure 5-11. Assuming a force, F is imparted on the pin in the z-axis direction, the maximum contact pressure will occur in the centre of the pin in the x-y axis,

denoted as Zone 1. The force exerted by the pin will subsequently cause a deformation, d on both the coating and the substrate, with the magnitude of deformation depending on factors such as relative hardness of the materials as well as magnitude of force imparted. The deformation also causes a greater surface area to be in contact with the spherical pin denoted as Zone 2, but the contact pressure in these areas are lower in magnitude.
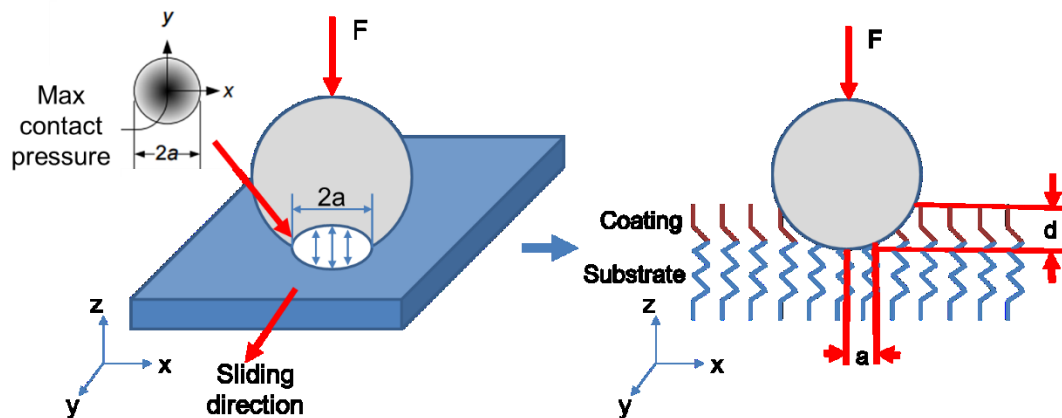
Figure 5-11 Illustration of contact mechanics for the tribometer experiment

Figure 5-12 shows SEM micrography of Zone 2, the wear track borders of both DCP and PCP samples at x4,500 magnification. It appears that most of the coating from the DCP 1:1 sample was removed from the substrate with evidence of galling occurring, which also coincides with it having the worst CoF among the samples considered. Galling has occurred due to the combination of adhesive and frictional forces between the sliding stainless steel surfaces with insufficient lubrication. The tearing of substrate crystal structure resulted in material transfer from the sample to the pin and increase in the CoF value.

Consideration for the hardness of the coating has to be taken as it plays a pivotal role in the friction and wear mechanism. Lower wear is typically associated with harder coatings, and it should be noted that both silver and PTFE fall into the category of soft coatings, where low friction applications are required. With this in consideration, PTFE has a hardness of between 5.9 – 6.5 HV, whereas the Hv of pure silver is around 5 to 6 times that of PTFE. Data obtained from EDS analysis shows a trend of higher silver amounts (and thus harder coatings) being more resistant to wear when comparing across the same electrodeposition method used. It is also important to note that as the wear increases, so does the contact area. Although all of the deposited coatings exhibit desirable CoF performances, the combination of Ag-PTFE shown in Figure 6-10(b) deposited using PCP possesses the best combination of being sufficiently hard in resisting wear while the incorporated PTFE particles provide added lubricity. The wear resistance had resulted in a relatively consistent contact area throughout the experiment. On the other hand, the coatings which have contained the largest amount of embedded PTFE particles had shown the worst wear resistance. Even though relatively large amounts of PTFE were contained in the layer, the PTFE would have been drawn from the bulk by the counter-surface in equally large amounts, resulting in its rapid depletion through wear. This is evident in Figure 6-10(f) for PCP and Figure 6-10(a) for DCP, which had exhibited the worst CoF performance among deposition methods.
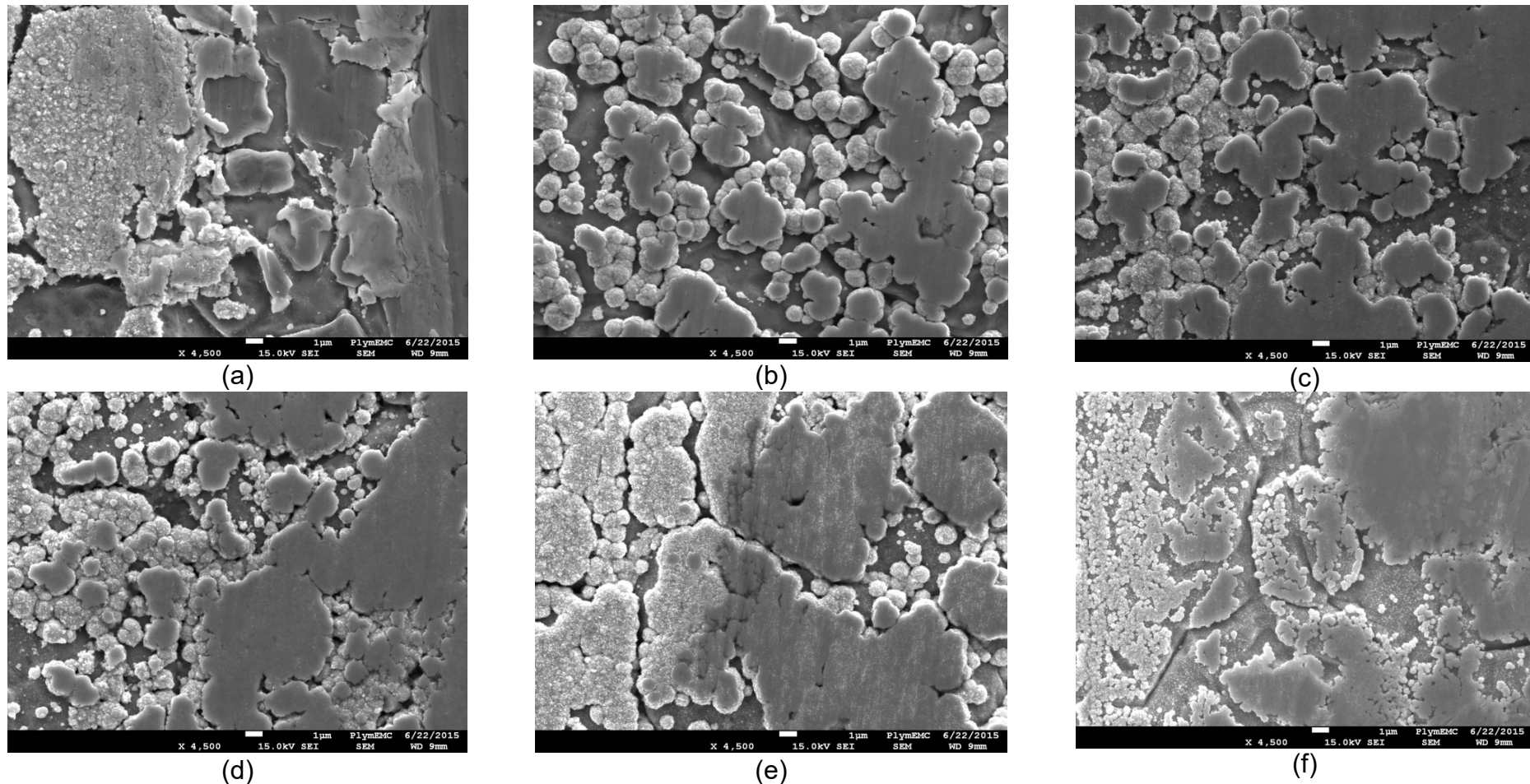
Figure 5-12 SEM micrography Wear track borders taken at x4,500 magnification (a) DCP with FC-4: PTFE ratio 1:1 (b) PCP with FC-4: PTFE ratio 1:1 (c) DCP with FC-4: PTFE ratio 1.5:1 (d) PCP with FC-4: PTFE ratio 1.5:1 (e) DCP with FC-4: PTFE ratio 2:1 (f) PCP with FC-4: PTFE ratio 2:1

5.3 Summary of the chapter

Methods detailed in Chapter 4 were subsequently used to carry out experiments reported in this chapter. The initial trial and error methods were used to determine rough bath parameters capable of depositing a silver coating of acceptable quality. This was then followed by further development of the coating through attempts at incorporating PTFE to create a Ag-PTFE MMC. Low particle incorporation within the MMC triggered studies into the effects of substrate surface roughness in particle incorporation which was important and relevant as it would be used to inform subsequent experiments and investigations. After initial parameters had been narrowed down, a systematic full factorial experiment was used to identify the effects of 5 variables (agitation speed, voltage, potassium nitrate presence, PTFE content and plating time) towards the deposited coating as well as its characteristics in particle incorporation, adhesion, friction, and wear. A weighted decision matrix was then used to identify electroplating bath parameters which would be used for subsequent development. Following the full factorial experiment, experiments were carried out to study the effects of strikes and pulse plating on particle incorporation, adhesion and tribological properties. This saw benefits in providing a gradual improvement to the CoF performance of the coating, but not particle incorporation. As a measure to improve PTFE particle incorporation, a study was carried out to understand the outcomes through use of a cationic FC-4 surfactant. A systematic approach was also taken to identify the appropriate FC-4 to PTFE ratios through the use of both DCP and PCP.

The main aim of this project is to develop a self-lubricating coating which is quantifiable not just through the significant presence of lubrication particles, but also its CoF performance on a linear tribometer. The experimental findings in this

chapter can therefore conclude that the quantity of incorporated PTFE particles with the Ag-PTFE MMC does not directly influence its tribological performance. Furthermore, although wear resistance of the coating was beneficial in keeping the coating intact over the wear cycles imposed, it did not result in significant tribological benefits observed through experiments carried out. This suggests that a compromise has to be made between coating wear and CoF performance depending on the intended coating application. The coating formulation exhibiting the best CoF will be used for testing in the next chapter to assess its viability in being used for threaded compression fitting nuts.

The key findings from this chapter are firstly, out of the frequencies trialled, PCP frequencies of F=2Hz and F=5Hz resulted in dendritic coating defects being deposited. PCP frequencies of F=10Hz and F=100Hz were subsequently trialled alongside the use of silver, nickel and copper strikes. The experiments found that there was no tribological benefit to the use of strikes in combination with PCP due to the adhesion preference of the Ag-PTFE deposit towards the strike metal as opposed to the substrate. In contrast, the best CoF performance of 0.2 was obtained for PCP without a strike at F=10Hz. Further refinement of the coating using varying ratios of the FC-4 surfactant to PTFE were investigated, alongside the use of DCP and PCP. A high FC-4 to PTFE ratio of 2:1 improved the CoF to 0.12 using DCP while the inverse was observed for PCP, where an FC-4 to PTFE ratio of 1:1 resulted in a CoF of 0.06. The low CoF coincided with observations made on the SEM of the Ag-PTFE coating still being intact within areas of highest contact stresses.

Chapter 6 Coating assessment for threaded compression fittings

6.1 Introduction

A suitable coating was selected to be plated onto nuts based on performance results from previous developmental processes. The nuts which were to be used in the make-up experiment of the threaded compression fittings were subjected to thorough cleaning and degreasing based on the procedures detailed in Chapter 3. The outer surfaces of the nut were masked using a non-conductive paint, and the same electroplating process was followed based on surface area data obtained from a CAD drawing of the nut. Three different nut sets were tested. The Ag-PTFE coating would be tested alongside a pure Ag coating deposited using the non-cyanide bath and DCP. Although the main aim of this study is focused on non-cyanide silver plating, it is beneficial also to include a commercial silver cyanide plated coating to put the results obtained into context.

6.2 Torque-angle curve

Torque experiments were carried out based on the setup discussed in the previous section in an attempt to understand the performance of each coating

during the make-up process. The tightening of the nut required is 1.25 turns as recommended by the manufacturer and data was continually recorded across the 1.25 turns (450°) rotation range to be used for further analysis based on the torque-angle signature method.

This method is commonly used to characterise the fastener installation process and is proposed to characterise the compression fitting installation process. There are several notable key differences between the fastener and compression fitting installation process as recommended by manufacturers. Firstly, threaded fasteners require a rundown zone which is also called the prevailing torque zone. On the other hand, the assembly process of threaded compression fittings has already achieved this through "finger tightening" of the nut as recommended by manufacturers. Secondly, although the make-up of compression fittings also experience snugging alignment where the components and contact surfaces are either drawn into alignment or a stable situation similar to threaded fasteners, the magnitude of forces required is likely to be relatively low and would have occurred during finger tightening. This means that both the prevailing torque as well as the nonlinear snugging area of the curve which is a complex function of the drawing together the mating parts and ensuring a snug fit of the system will not show on the torque angle curve for threaded compression fitting make up. The third zone is where elastic clamping occurs for fasteners and where swaging occurs for compression fittings. The is where the torque angle curve for threaded compression fittings start. Finally, the components in the compression fitting system will not "yield" under normal circumstances and as such the fourth zone will be primarily applicable to threaded fasteners where the yield point of the joint, gasket, threads or clamped components has been exceeded. The torque angle

curve for attempt 1 of the commercial cyanide silver nut is illustrated in Figure 6-1 below.
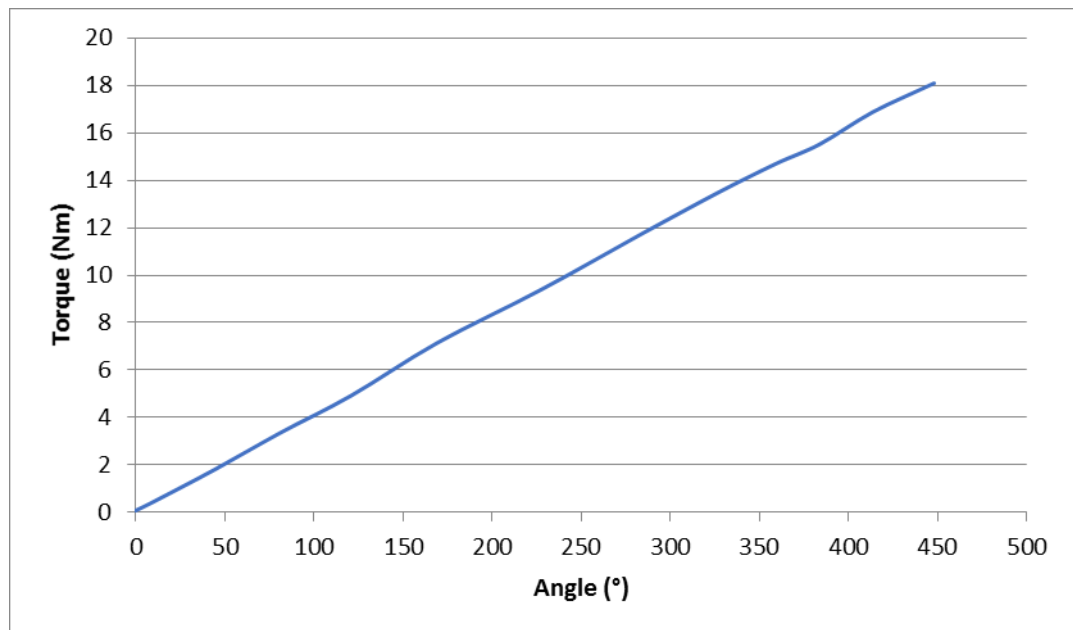
Figure 6-1 Torque angle curve for nut 1 attempt 1 of the commercial cyanide silver nut

The maximum magnitude of torque for each coating has been presented in a graphical format in Figure 6-2. Manufacturers of threaded compression fittings do not stipulate a torque target or specification to be achieved during make-up and thus the commercial cyanide silver coating serves to provide a comparison. Comparing the coatings based on each attempt, the commercial cyanide silver plated coating exhibited consistently lower maximum tightening torque values when compared to the non-cyanide Ag and Ag-PTFE coatings. Although being useful in providing the maximum torque achieved during make-up for fasteners, the torque-angle technique does not provide adequate information about each

coating performed for an informed comparison and analysis to be made.

Considering this, the torque-angle slope was subjected to detailed analysis.
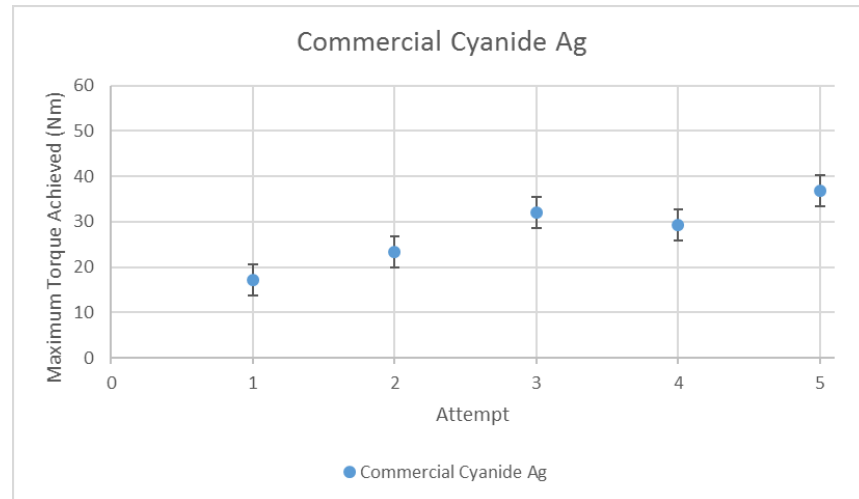
(a)
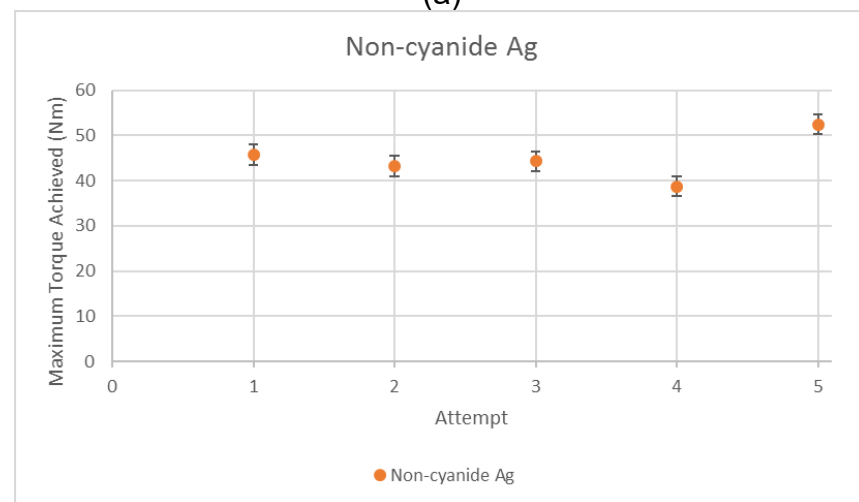
(b)
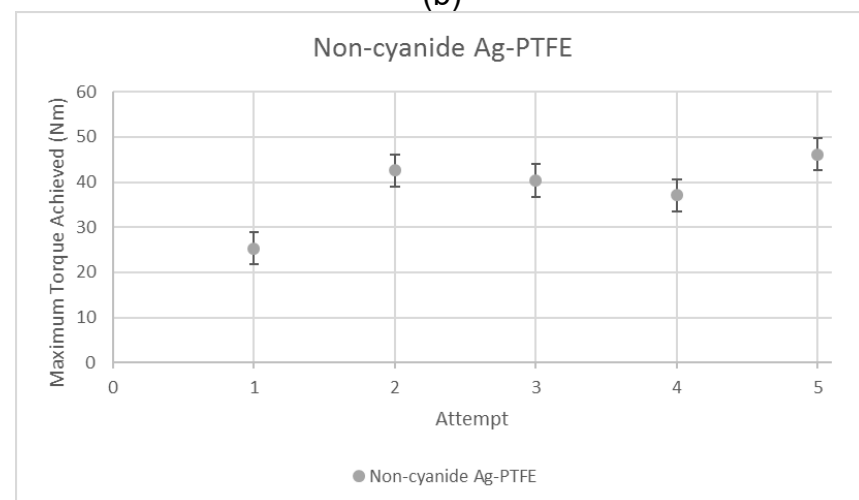
(c)

Figure 6-2 Maximum magnitudes of torque in Nm recorded during the make-up process for each coating (a) Commercial cyanide Ag (b) Non-cyanide Ag coating (c) Non-cyanide Ag-PTFE coating

Torque-angle slope

The torque-angle slope from the make-up process was considered to better understand the performance characteristics of the coatings. This slope is calculated using the torque over angle and is broken down into ten rotation ranges from the continuous torque and angle measurements. Each range covers 45 degrees of rotation for the slope to be calculated. This in turn provides the average force in Nm per angle for each rotation range. The coating torque-angle slopes are grouped by attempts for the coatings considered in Figure 6-3. The performance characteristics of each coating will be discussed in greater detail in the following sections.
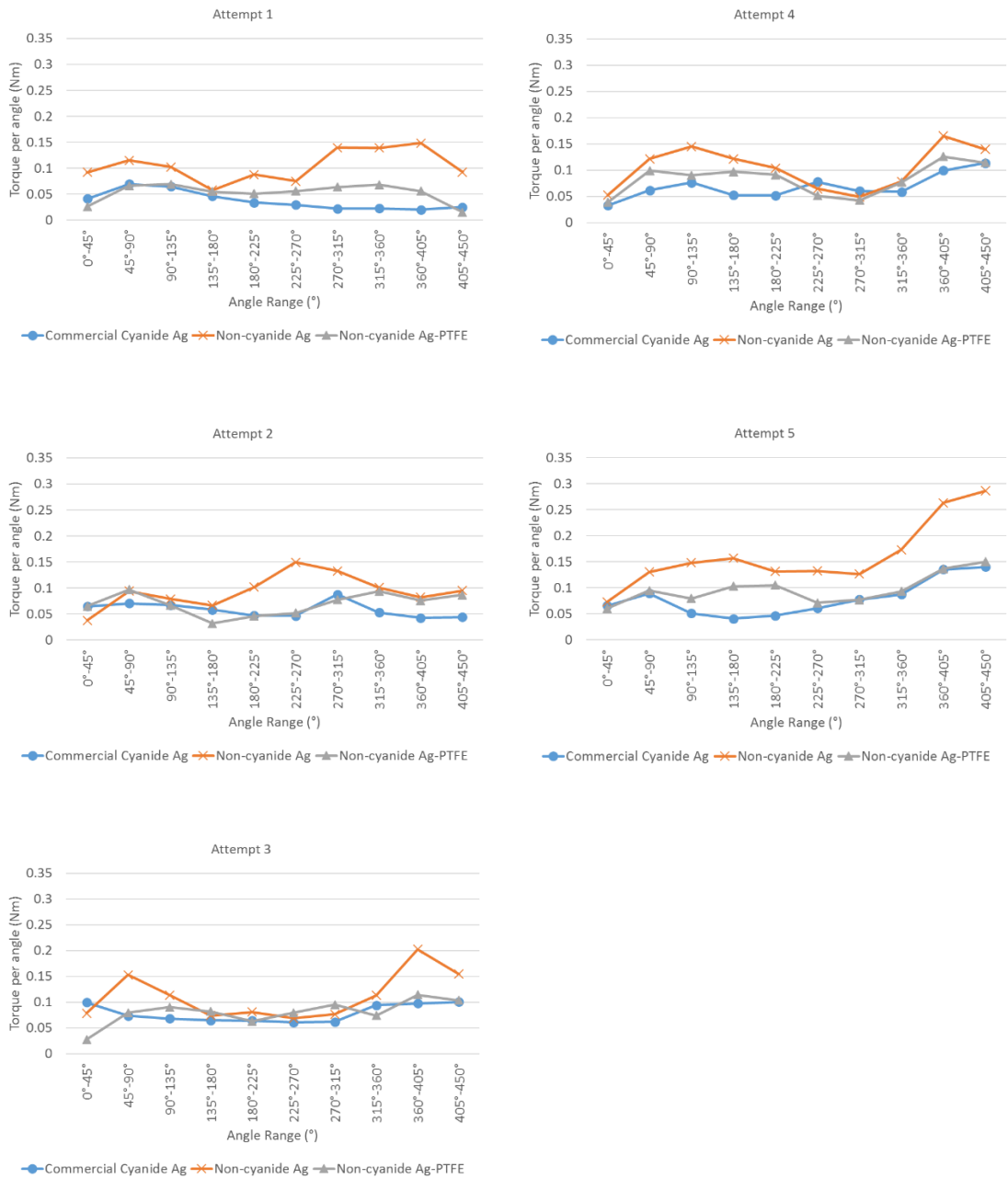
Figure 6-3 Torque-angle slope by grouped by attempts for the commercial cyanide silver, non-cyanide silver and non-cyanide Ag-PTFE coatings

6.3 Commercial cyanide Ag coating performance

The performance exhibited during the first make-up attempt showed that the average torque peaked between 45-90 degrees of rotation before exhibiting a downward trend in torque per angle. This downward trend was present on the first and second make-up attempts, but the magnitude of the downward trend gradually decreased. The following three make-up attempts then exhibited an upward trend that is increasing in magnitude shown in Figure 6-4.
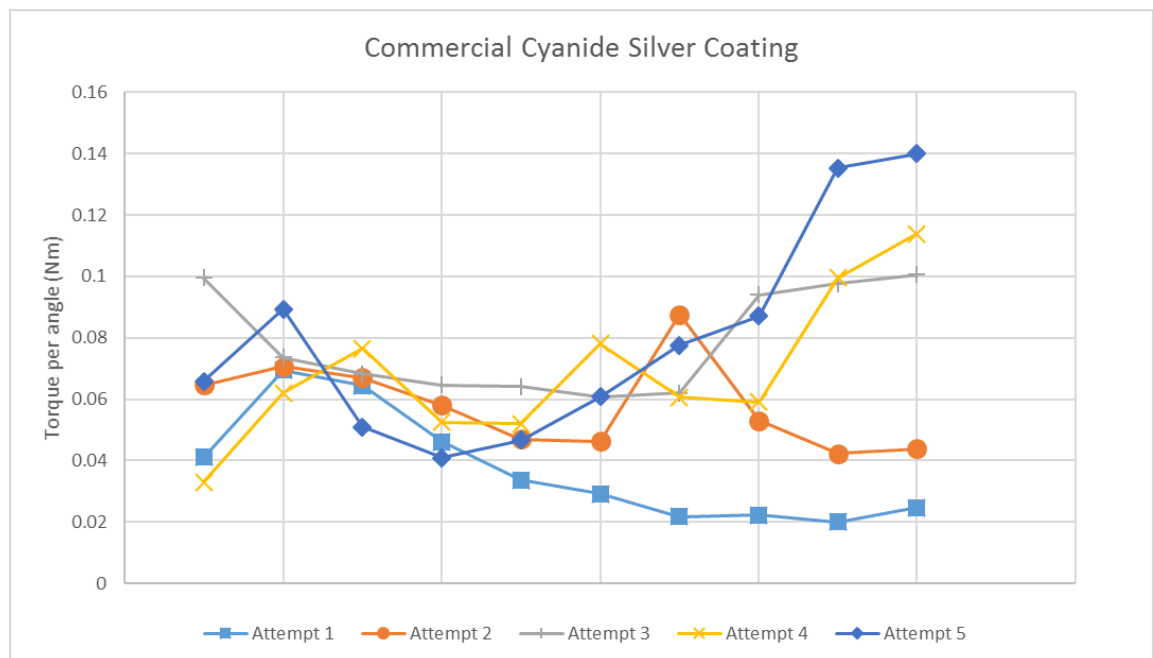
Figure 6-4 Torque-angle curve for the cyanide silver coated nut

The post testing inspection revealed traces of a transfer film between thread contact areas which would have aided in the lubrication during the make-up process. Visual inspection of the coating also indicated that the first few threads of the coated nut experienced heavy wear which is typical of threaded parts. The underside of the nut which is in contact with the back ferrule also experienced

heavy wear. Wear induced during the first make-up attempt had resulted in coating performance reduction for the following make-up attempts. This is evident from the sudden peak in torque required during attempt 2, where the coating started to experience failure through sticking and slipping. Peaks were also observed in later attempts which suggest the gradual onset of wear towards the coating. The ability of the coating to create a transfer film which was providing lubrication between the contact surfaces would have also been impaired. Spread and distribution analysis of the torque measurements suggest the increase in wear of the coating under the high operational stresses which have resulted in its impairment in providing adequate solid lubrication after consequent make-up processes; however, as seen in Figure 6-3 it had still managed to maintain a relatively stable performance when compared with attempts against the other coatings considered.

6.4 Non-cyanide pure Ag coating performance

For the non-cyanide pure Ag coating, the consistent higher overall slope average relative to the other coatings in Figure 6-3 suggests that higher friction is inherent in the system. Although post testing visual inspection revealed traces of transfer film on the contact surfaces, it was less apparent as opposed to the commercial cyanide Ag coating. Examination of the maximum torque values achieved during each make-up process reveals that the coating had consistently achieved the highest torque among the other coatings. This is further supported by the torque-angle slope analysis, where the non-cyanide Ag coating required the highest average torque per angle to make-up. Furthermore, the coating had behaved erratically and relatively unpredictably as seen in Figure 6-5 comparing the results

of make-up attempts. This is a relatively clear indication of coating failure through repeated sticking and slipping of the contact surfaces during the make-up process.
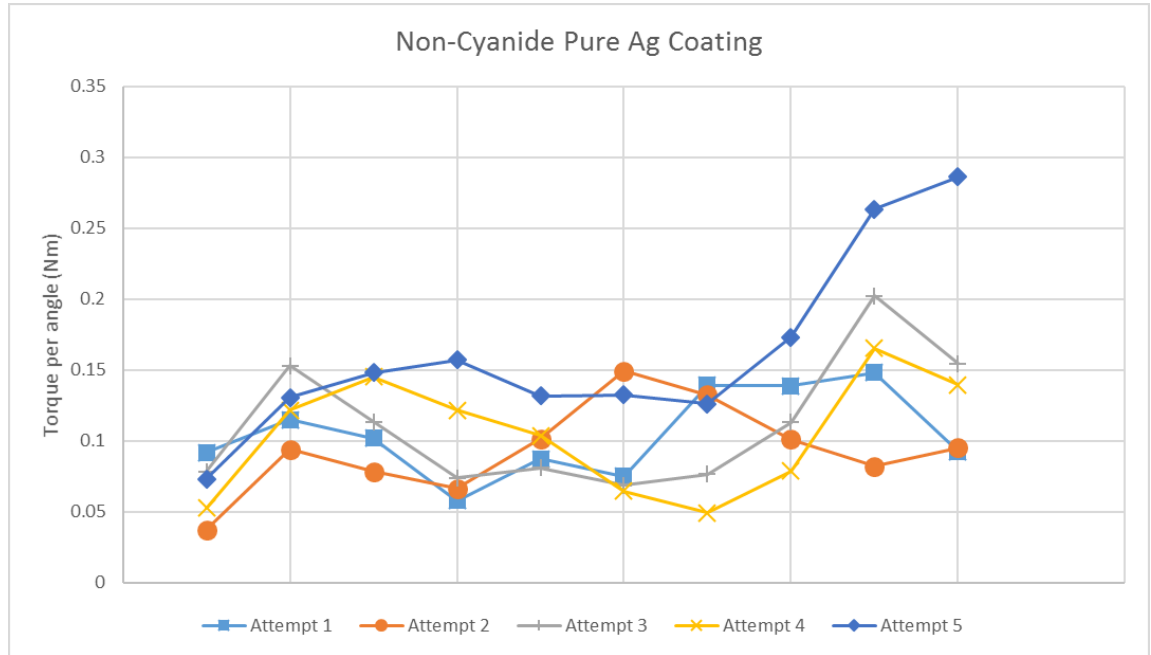
Figure 6-5 Torque-angle curve for the non-cyanide pure silver coated nut

6.5 Non-cyanide Ag-PTFE coating performance

The non-cyanide Ag-PTFE coating managed to exhibit a more consistent performance over its non-cyanide Ag counterpart; however, its performance was still generally below that of the commercial cyanide Ag coating seen in Figure 6-3. Based on the maximum torque observed during the make-up process, the non-cyanide Ag-PTFE coating required on average approximately 8Nm more input torque. Post make-up visual inspection showed small trace amounts of transfer film in relation to the other coatings considered. This is a common phenomenon with PTFE due to its low surface tension. When compared across attempts as shown in Figure 6-6, the fluctuating torque values registered are an indication of

coating wear through repeated stick and slip occurrences. In the context of comparing this with the pure silver non-cyanide coating, the average torque values for the Ag-PTFE coating are consistently lower, signifying that the PTFE embedded in electroplated silver contributes to providing superior tribological properties.
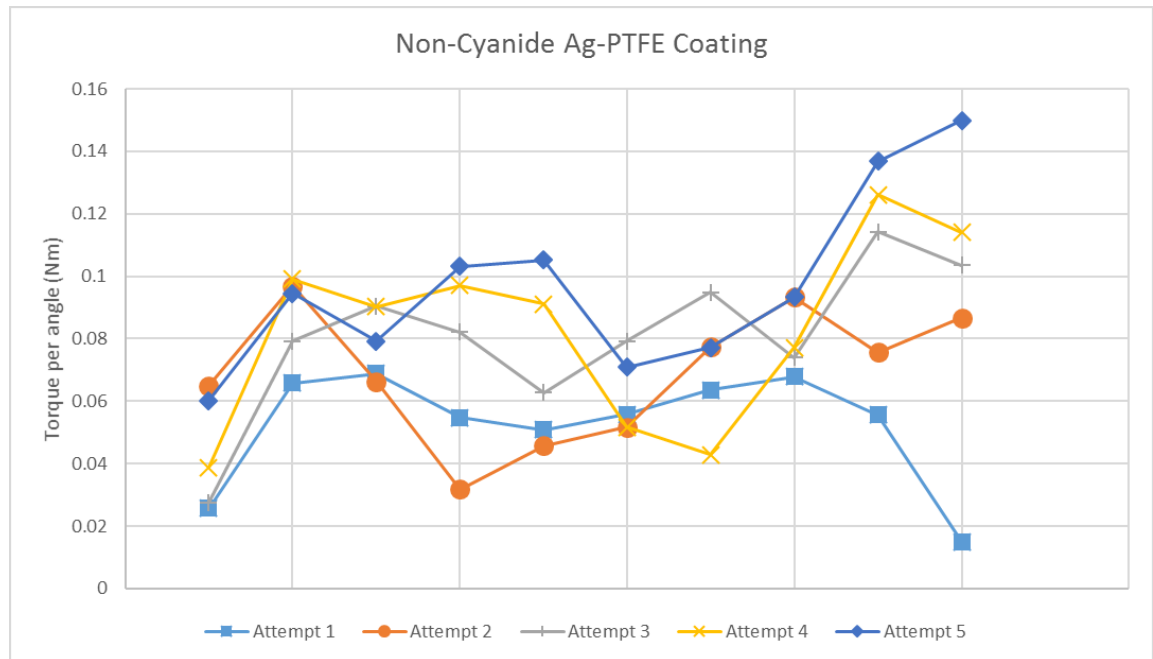
Figure 6-6 Torque-angle curve for the non-cyanide Ag-PTFE coated nut

6.6 Discussion

Gansheimer noted that it is difficult to lubricate threads due to badly machined surfaces and high pressures with low sliding speed [68]. This is where solid lubricants are able to perform where liquid lubrication fails, and it is thus of great importance that the electroplated coatings are able to carry out its intended function. The discussion will thus be focused on both the issues faced by the electroplated coatings as well as the performance of coatings tested.

Current distribution – Threaded sections

The first aspect when considering the tribological performance of a complex geometry is current distribution. This can be obtained by dividing the current with the apparent area. The behaviour of current is that it has a tendency to concentrate at edges and points, with a preference to flow readily to parts closer to the opposing electrode than to distant parts. Because of this phenomenon, the current density across a complex geometry is not uniform and thus the thickness of an electroplated deposit will not be uniform over complex surfaces as it is based on current density. This variation in coating thickness is illustrated in Figure 6-7, observed from a cutaway nut section.
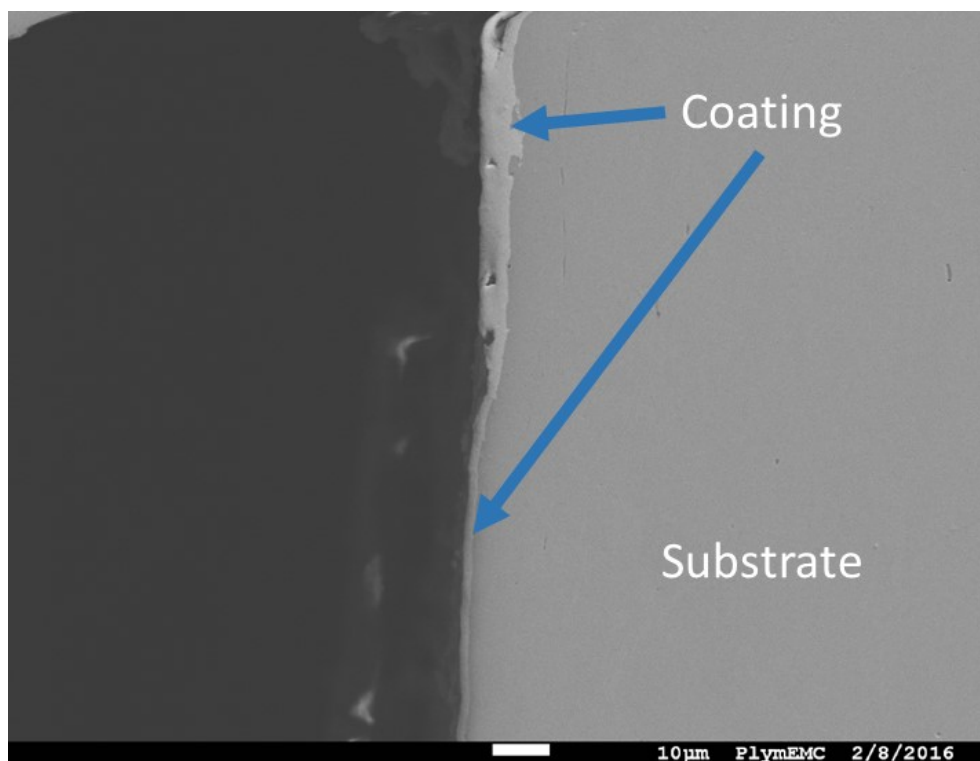
Figure 6-7 Variation in coating thicknesses observed from the nut under-head as a result of current distribution

Coating thicknesses

Variation in coating thickness that exists as a result of plating design can ultimately lead to differences in make-up torque values, especially when a soft coating is considered. This can be used to explain the overall differences in average torque values for the commercial cyanide and the non-cyanide silver and Ag-PTFE coatings.

Coating thickness measurements were carried out through SEM after cutting and polishing a section of the nut which was mounted in resin. As expected, variations were observed in coating thicknesses not only on the threads but also on the nut under-head for all the nuts. This has the potential to affect commercial application of the nut through reduced wear resistance, especially in areas where the coating is thinner. The measured coating thickness for the commercial cyanide silver is 15 microns. This is as opposed to the design thickness for the non-cyanide silver and Ag-PTFE coatings tested. For the non-cyanide silver coating, a theoretical coating thickness of 3.83 microns was set. A theoretical coating thickness of 2.3 microns for the Ag-PTFE was set based on the assumption of 60% current efficiency. The measured coating thicknesses for the non-cyanide silver and Ag-PTFE were approximately 3.3 microns and 2.1 microns respectively.

This can be used to explain why the commercial cyanide silver coating has managed to perform consistently better as it is approximately five to seven times as thick as its non-cyanide counterparts tested during the experiment. When viewed from a different perspective, it can be said that the non-cyanide Ag-PTFE coating managed to keep up with the performance of a coating which was substantially thicker.

Linear tribometer vs. torque test

There are key differences in the experiments for obtaining CoF from the linear tribometer and the tribological performance observed of the same coating in a nut. Firstly, there is a difference in temperature of the coating as a result of the sliding process. On the linear tribometer, the sliding process occurs in an open environment. The pin is only in contact with one area for a short period. As the pin slides across the surface of the coating, heat generated on the coating is dissipated after the pin passes. Furthermore, the heat generated on the pin surface is transferred through conduction when it comes into contact with a new surface area. On the other hand, when the compression fitting is assembled, the coating on the nut under head will experience constant sliding contact throughout the whole range of rotation, without any opportunity to dissipate any heat generated. Secondly, on considering specific material properties, PTFE is not good at dissipating heat, and its tribological performance is affected by temperature. This is a material trait which puts it at a disadvantage when compared to silver which is a very good thermal conductor.

Torque-Angle Spikes

The spikes in the torque noted during the repeated attempts are attributed to the sticking and slipping between contact surfaces. One way of looking at this is to consider it an early indication of coating failure. On the other hand, this does not explain how the coating is still able to perform within a relatively constant average torque range after the coating has "failed". Instead, consider that the counter surface is an uncoated one which is badly machined. As the sliding occurs, migration of the coating material occurs through the formation of a transfer film

on the counter surface. A coated material with a high wear rate will also result in the transfer film being able to resist erosion due to wear. This can then be used to explain the constant fluctuations occurring on the coatings. An example of this is where the Ag-PTFE coating had encountered more fluctuations in torque but was still able to outperform the non-cyanide silver coating by requiring less overall average torque during the make-up process.

Excess torque

An assumption can be made that approximately 17Nm of tightening torque is sufficient for successful make-up of the system based on ideal conditions. This value represents the lowest torque value from the cyanide silver coating after a 450 degree cycle of rotation. However, significantly higher readings of maximum torque in the torque-angle curve were registered for all the coatings tested during the make-up attempts which require an adequate explanation as to where this excess torque has gone in the system.

During the compression fitting make-up process, there are several unlubricated contact surfaces, namely the interfaces between the front ferrule with the body as well as the interface between the back and front ferrule. If the CoF between these unlubricated contact surfaces are greater than the CoF between the back ferrule and the coated (lubricated) nut, the torque application will cause the lubricated surfaces to slip and rotate. Upon continuous make-up using new ferrules with no previous transfer film residue to aid in lubrication, the CoF of the worn nut coating will exceed the CoF between the unlubricated surfaces. This will result in the front ferrule rotating against the body during make-up. As these surfaces are unlubricated, adhesive wear which can ultimately lead to galling of

the surfaces will occur between the unlubricated contact surfaces as seen in both

Figure 6-8 and Figure 6-9.

Figure 6-8 Galling damage on front ferrule observed from the fifth attempt of

non-cyanide Ag coating
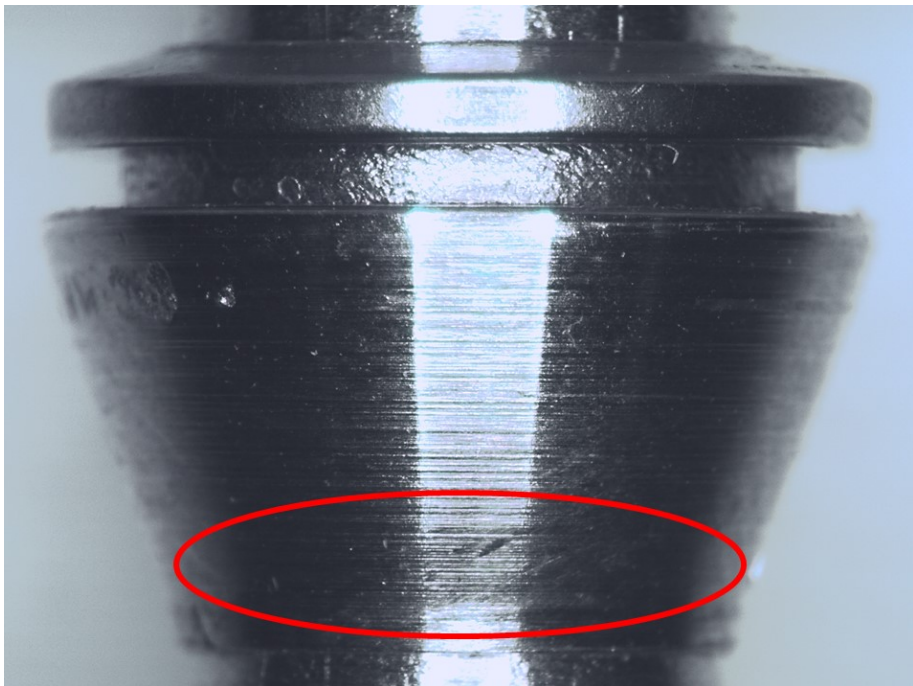
Figure 6-9 Galling damage on front ferrule observed from the fifth attempt of commercial cyanide Ag coating

As the opposing forces within the system increase, the application of a higher input torque is required to overcome this resulting in the front ferrule pushing downwards and outwards. This then creates extra resistance in the system when the front ferrule expands and comes into contact with the nut to create an extra contact surface. This very phenomenon was observed as shown in Figure 6-10 and can be used to explain significantly high peaks observed on the torque-angle slope for the coatings tested.
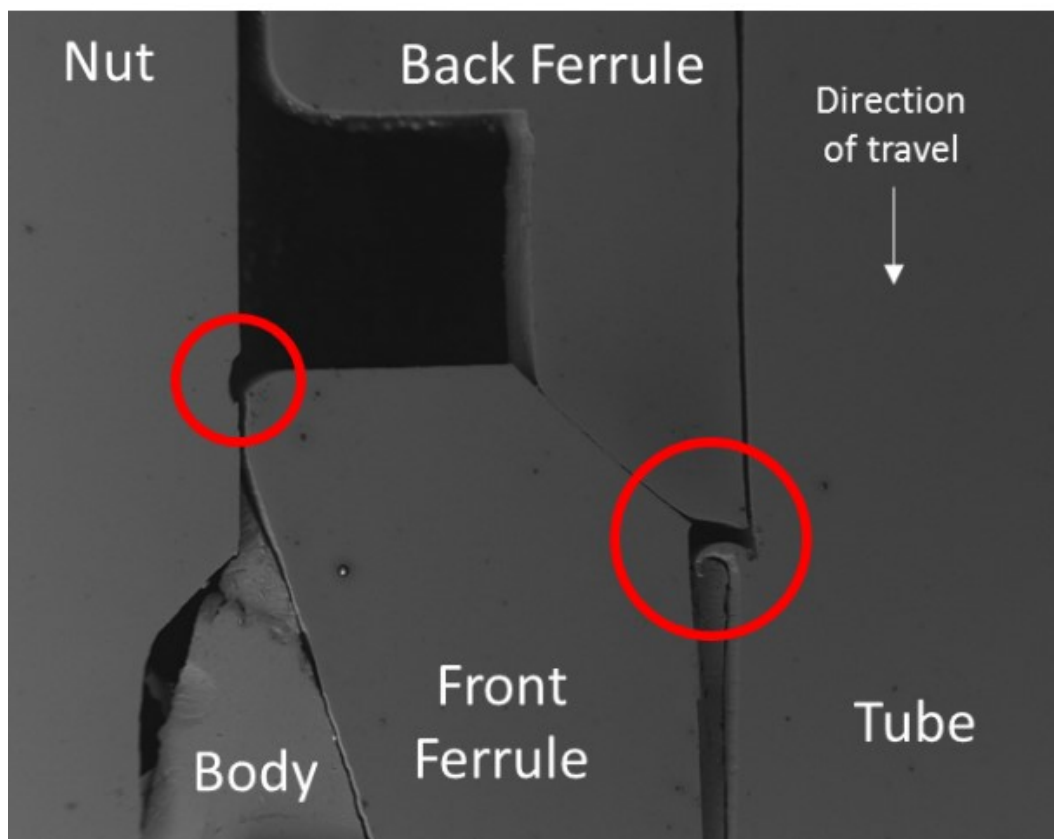
Figure 6-10 Observed damages from the fifth attempt of non-cyanide Ag coating to the tube and nut as circled in red

6.7 Summary of the chapter

The summary of key findings for this chapter are that firstly, the non-cyanide silver coating exhibited consistently poor performance of the coatings considered when defined by both total assembly input torque required as well as from the torque-angle slope. The investigation into the poor performance of the non-cyanide silver coating found that it was as a result of inadequate lubrication between the back ferrule and nut underhead during make-up. The inadequate lubrication caused the contact between the front ferrule and body to slip and the rotation of these unlubricated stainless steel surfaces caused galling, which greatly increased the input torque required.

It was also found that when using maximum torque values recorded during make-up to quantify performance, all coatings experienced deterioration in coating performance across the make-up attempts. The commercial cyanide silver coating required approximately 2.1 times more input torque on the final make-up attempt than its initial attempt. In contrast, the Ag-PTFE coating only required 1.8 times more torque, suggesting that the Ag-PTFE coating is more robust due to less performance loss, even though the Ag-PTFE coating was 7 times thinner.

Chapter 7 Summary and conclusions

7.1 Summary

This research was focused on the development of a self-lubricating non-cyanide Ag-PTFE composite coating. Chapter 2 comprised of the literature review which highlighted key gaps in current knowledge. Chapter 3 detailed the methodology in which the research in developing the coating would be carried out, which comprised of 3 stages, namely initial development, coating refinement and finally coating assessment for use in threaded compression fittings. The key development stages along with CoF outcomes are visually summarised in Figure 7-1, which were reported in Chapters 4 to 6.

From a tribological perspective, vast CoF improvements have been made throughout the course of this research. The initial uncoated substrate had a CoF of 0.6 which was improved to 0.3 using a pure, non-cyanide succinimide silver coating. Initial attempts at depositing an Ag-PTFE MMC resulted in a marginal CoF improvement to 0.29, while subsequent investigation of electroplating parameters through the two-level full factorial experiments improved PTFE incorporation while also reducing the CoF to 0.23 as found in Chapter 4.
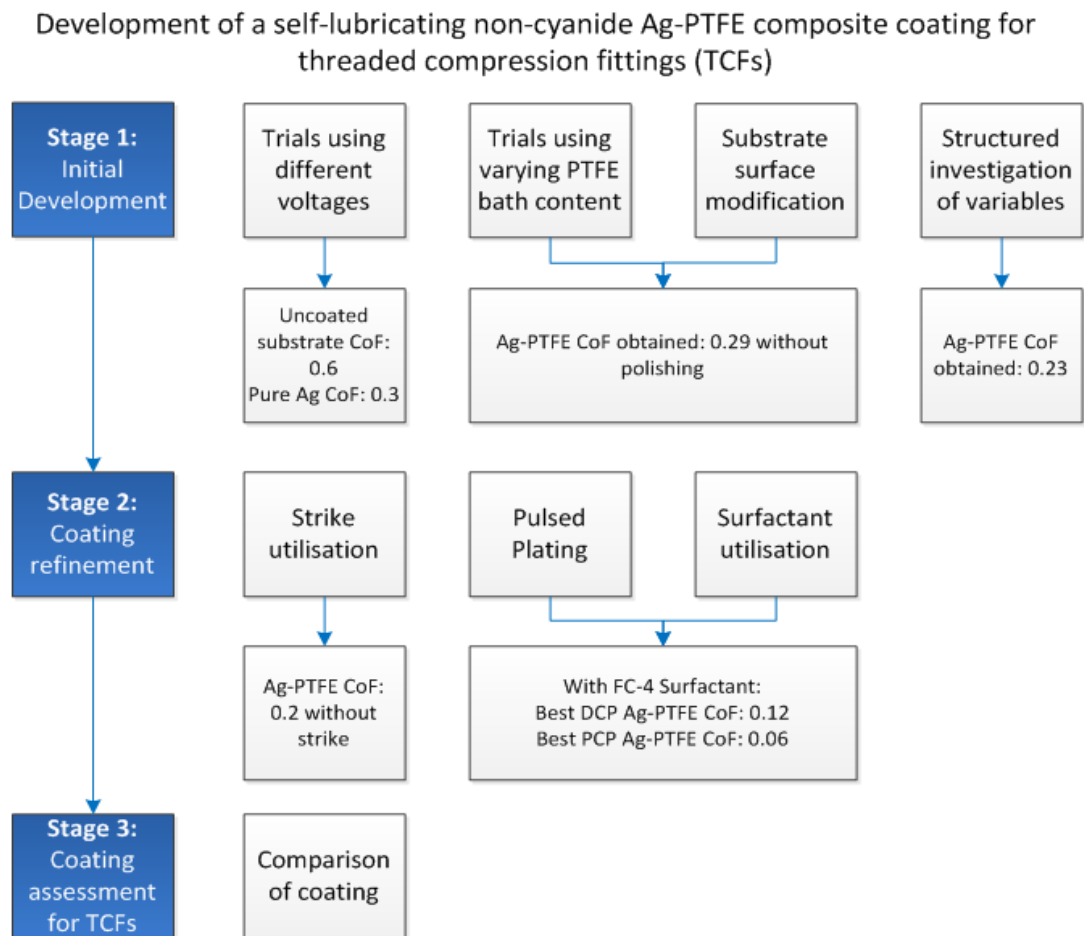
Figure 7-1 Self-lubricating non-cyanide Ag-PTFE development framework with

CoF outcomes

Chapter 5 refined the coating through investigating PCP usage and strikes which found a CoF reduction to 0.2 without the need for a strike. The CoF of 0.06 was ultimately achieved by using PCP at F=10Hz in combination with the FC-4 surfactant in a FC-4:PTFE ratio of 1:1. In comparison, the best CoF performance achieved through DCP was a CoF of 0.12 with the FC-4:PTFE ratio of 2:1. On the other hand, the PTFE particle incorporation was also >8wt %, meeting the incorporation requirements for the coating to be deemed self-lubricating.

Chapter 6 was where non-cyanide Ag and non-cyanide Ag-PTFE coatings were deposited onto the inner surfaces of stainless steel nuts and subsequent make-up attempts were carried out to compare their performance, with commercial cyanide Ag coated nuts used as a benchmark. The commercial cyanide silver coating required approximately 2.1 times more input torque on the final make-up attempt than its initial attempt. In contrast, the Ag-PTFE coating only required 1.8 times more torque, suggesting that the Ag-PTFE coating is more robust due to less performance loss, even though the Ag-PTFE coating was 7 times thinner.

7.2 Conclusions

The aim of this project was to develop a self-lubricating non-cyanide Ag-PTFE composite coating suitable for use in threaded compression fittings of the ferruled type with several distinct objectives. The first objective was to develop a non-cyanide silver electroplating bath capable of depositing a coating on a stainless-steel substrate. The second objective was to develop a self-lubricating coating that possesses superior tribological properties over a pure silver coating. The third objective was to investigate the performance of the non-cyanide silver and silver PTFE coating when used on threaded compression fittings. The project aim and objectives have been met, resulting in several unique contributions to knowledge because of this study. First is the successful development and characterisation of a self-lubricating non-cynanide Ag-PTFE coating on stainless steel without a strike resulting in improved CoF of 0.06 from the CoF of 0.6 based on an unlubricated surface. Second is the application of a non-cyanide Ag-PTFE MMC for threaded compression fittings. Third is the characterisation of the make-up process of threaded compression fittings through the proposed use of the

torque-angle slope in assessing coating performance for threaded compression fittings during make-up.

As a concluding note, it should be noted that this study is limited to laboratory testing and deployment on an industrial level has yet to be thoroughly investigated. One key assumption for the work that was carried out is based on PTFE being in abundant supply within the bath. Furthermore, the impact of the coating on corrosion and its survivability under the wide range of operating temperatures were not within the scope of this research. As such, these points could warrant further areas of scholarship will be discussed in greater detail in the next chapter.

Chapter 8 Future Work

The development of a self-lubricating non-cyanide Ag-PTFE composite coating that is suitable for threaded compression fittings requires core understanding of tribology as part of its intended use and chemistry used during its fabrication process. The work carried out in this study has highlighted several opportunities for further areas of scholarship. These are summarised into their specific headings.

Manufacture

Based on the assumption that electroplating is the chosen method for depositing the silver coating, opportunities for future work arise in the area of transferring the knowledge obtained from this study to a manufacturing environment, where issues such as cost will come into consideration. Furthermore, the electroplating baths used in industry are typically open and exposed. Issues such as surface evaporation rate of the bath have to be considered alongside issues such as hydrolysis and bath maintenance (steady bath temperature control, pH, etc.). There is also the scope for studying particle incorporation within an industrial scale electroplating bath which could also provide valuable information into the

replenishment requirements of PTFE based on its exhaustion rate from the electroplating process. This potential study of particle incorporation could also include the ideal hydrodynamic conditions for optimal particle incorporation rates.

Installation (make-up process) and use

The transportation of solids and gases where compression fittings are core instruments of can be considered relatively low-tech but the failure of components could have a devastating impact. Furthermore, some of these fittings are used in the harshest possible environments of high temperatures and corrosion. There are opportunities to further advance this industry through the application of current knowledge and technology during the installation of these components as well as over its service life. A prominent example is through the make-up process, where instead of providing an angle target to achieve, specifications for torque and angle could be provided to ensure that adequate force is applied. In addition to that, the silver coating is coupled with stainless steel to prevent galling. Issues such as the role of the coating in preventing thread corrosion could warrant further study. Furthermore, an assumption that component tolerances were representative was made during the experiment involving threaded compression fittings. In reality, a range of manufacturing tolerances exist, and the impact of the screw thread and ferrule manufacturing tolerances on the impact of the make-up process could be studied in further detail. These have the impact to directly impact the performance of the coating.

Coating tribology

The study has highlighted clear tribological benefits in incorporating PTFE into the silver MMC with the detriment of wear properties due to PTFE being a

relatively soft material. It is possible to potentially reduce wear of the composite coating through increasing the coating hardness. Wear performance of the coating can potentially be increased by incorporating inorganic particles such as SiC, SiO2 or boron nitride while potentially preserving the self-lubrication of PTFE by providing additional support to the PTFE structure. Furthermore, there are opportunities to expand the study of the coating through encompassing other factors. For instance, this study was limited to a single size of nut tested and further work could expand on coating tribology for various sizes of nut and even different thread types. A focused study on the effects of high temperature towards the coating performance could also be mounted.

Predictive model

Advances in computing technology mean that various processes can be simulated and studied in more detail. These could include the effects of trapped debris or lubrication on the installation stresses and quality of the installation. Simulation could also be applied to optimisation electroplating bath conditions for particle incorporation.

Appendix 1 Tribometer Data Collection Steps

The data collection process steps are as follows:

1. Check that all cables and connections are connected, power supplied to equipment

2. Ensure that the signal filter amplification is set to x500 for Strain Gauge (SG) input and x1 for Fibre Optic (F/O) Sensor input

3. Check that the system is at a steady state

4. F/O Sensor calibrated to Vmax = 5.28 and force/deflection linear equation calculated

5. SG force/deflection linear equation calculated

6. Check friction pin for excess wear

7. Mount sample on the 5 degree incline

8. Without the pin touching the test sample, adjust the SG resistor to read Vout = -0.025V (+/-0.025)

9. Applying the least amount of downwards force onto the pin, carefully tighten the friction pin until Vout = 0.025V (+/-0.025)

10. Using the motor controller software, set the required run distance

11. Start LABVIEW and run the data acquisition/collection application

12. Start data acquisition and start the motor cycle immediately (+2s/-0S)

Consumables Parts List

Component/Part	Supplier	Reference
Strain gauge	RS Components	RS Stock No 632-146
Potentiometer	RS Components	RS Stock No 692-8519P

Appendix 2 ISO Screw thread profile measurements
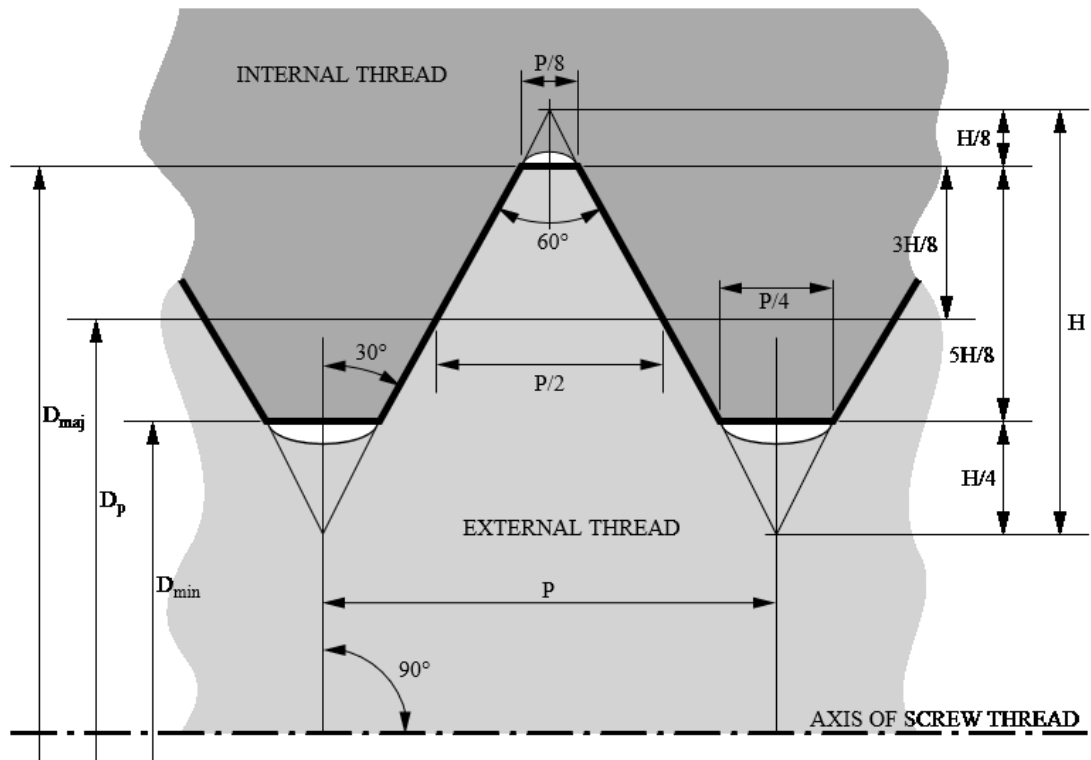
The ISO screw thread profile measurements are defined by the following criteria:

P = 0.05" (1.27mm)

H = 0.0433" (1.0998mm)

D_{maj} = 0.4375" (11.1125mm)

Appendix 3 Norbar Equipment Specification

Rotary Torque Transducer

These transducers are designed to measure the torque output from rotating shafts, particularly torque controlled power tools including impulse wrenches.

- Classified to BS7882:2008, typically better than Class 1 for the primary classification range (±0.5% of reading from 20% to 100% of full scale).
- "SMART" – TST and TTT instruments will automatically recognise calibration details.
- Supplied with a UKAS accredited calibration certificate.
- Designed to give excellent performance with impulse tools.
- Optional angle measurement – contact Norbar for details.
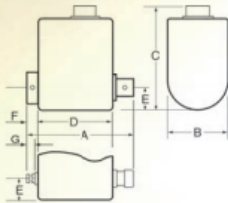
Rotary Torque Transducers – S.I. Calibration

Capacity	Part No.	Sq. Drive	Maximum RPM*		Dimensions (mm)						
		in	Continuous	Intermittent	A	B	C	D	E	F	G
5 N.m	50708.xxx	¼" m/f Hex	5000	11000	116	30	68	56	13	39	25.5
20 N.m	50709.xxx	¼" m/f Hex	5000	11000	116	30	68	56	13	39	25.5
20 N.m	50710.xxx	¼" m/f	5000	11000	71.5	30	71.5	56	13	6	-
75 N.m	50711.xxx	⅜" m/f	5000	11000	77	30	74	56	15	8	-
200 N.m	50712.xxx	½" m/f	2500	7600	87	42	82.5	58	21	12	-
250 N.m	50713.xxx	¾" m/f	2000	5000	106	52	93.5	60	26	21	-
500 N.m	50714.xxx	¾" m/f	2000	5000	106	52	93.5	60	26	21	-
1500 N.m	50715.xxx	1" m/f	1000	4400	125	63	104	64.5	31.5	29	-

Rotary Torque Transducers – Imperial Calibration

Capacity	Part No.	Sq. Drive	Maximum RPM*		Dimensions (mm)						
		in	Continuous	Intermittent	A	B	C	D	E	F	G
50 lbf.in	50717.xxx	¼" m/f Hex	5000	11000	116	30	68	56	13	39	25.5
15 lbf.ft	50718.xxx	¼" m/f Hex	5000	11000	116	30	68	56	13	39	25.5
15 lbf.ft	50719.xxx	¼" m/f	5000	11000	71.5	30	71.5	56	13	6	-
50 lbf.ft	50720.xxx	⅜" m/f	5000	11000	77	30	74	56	15	8	-
150 lbf.ft	50721.xxx	½" m/f	2500	7600	87	42	82.5	58	21	12	-
200 lbf.ft	50722.xxx	¾" m/f	2000	5000	106	52	93.5	60	26	21	-
300 lbf.ft	50723.xxx	¾" m/f	2000	5000	106	52	93.5	60	26	21	-
1000 lbf.ft	50724.xxx	1" m/f	1000	4400	125	63	104	64.5	31.5	29	-

* Continuous is defined as 100% usage at the given speed in either direction and intermittent as usage 10% of the total time at the given speed.

T-Box XL and TDMS (Torque Data Management System)

The T-Box XL together with Norbar's Torque Data Management System (TDMS) software provides the complete solution for torque tool calibration, data logging and data management and archiving on your PC.

- T-Box XL features a colour 7" (178 mm) touch screen LCD display with graphic on screen icons for simple tool selection. Feature modes include Click Hydraulic, Pulse and Stall tools that enable the most common torque products to be tested by a simple touch of the screen.
- T-Box XL also features a "Pulse Tool Mode" which uses a mathematical algorithm to accurately determine the output torque from Impulse tools.
- T-Box XL comes pre-loaded with Tool Templates for the entire Norbar product range of Torque Wrenches, Pneutorques and EvoTorques enabling the user to simply assign individual tools to perform calibrations to the relevant ISO standard. Other tool templates can be created by the operator.
- Graphical analysis and display of joint profiles are available using the Graph Mode.
- T-Box XL can connect up to 4 Smart Transducers including transducers with angle capabilities for instant connectivity. Alternatively, non Norbar transducers with a mV/V output can be programmed into the T-Box XL memory.
- T-Box XL has 2 USB ports, one RS232 serial port and an ancillary connection (USB cable supplied as standard).
- T-Box XL can log data at a rate of 5 readings per second or can be set to log torque data at the required angle increment, for example, take a torque reading at every degree.

T-Box XL shown with Neck Strap and Mounting Bracket.

197

T-Box XL and TDMS

- T-Box XL is supplied with Norbar's new Torque Data Management System software (TDMS) for complete tool data management and archiving on your PC.
- TDMS enables data to be viewed graphically, in an SPC format, or as a Calibration Certificate (available in English, French, German, Italian, Spanish, Russian, Hungarian and Norwegian).
- T-Box XL contains a large capacity memory that will enable a user to collect data and store in excess of 100,000 individual test results directly to the instrument and then synchronise to the TDMS software.

T-Box XL kit includes: -
- T-Box XL instrument complete with UKAS accredited bi-directional calibration certificate
- Carry Case
- Quick Reference Guide
- Mounting foot and bolts
- Neck strap and mounting kit
- Power supply with appropriate local mains supply cable (100 - 240 v)
- USB cable
- USB memory stick pre-loaded with TDMS software
- T-Box XL Operator's Manual
- TDMS Operator's Manual.

T-Box XL & TDMS

Part No.	Description
43258	T-Box XL Instrument with TDMS Software
61132	TDMS Software (supplied on USB Flash Drive)

T-Box XL Accessories

Part No.	Description
60216.200	T-Box XL to 10 way lead, for Norbar Rotary Transducers
60217.200	T-Box XL to 6 way lead, for Norbar Static and Annular Transducers
60223.200	T-Box XL to no connector (for non-Norbar Transducers)
60248	Serial Data Lead Kit

Torque vs Angle graph produced using TDMS software

Accuracy:

Input Voltage	Equivalent torque	Accuracy	Calibration uncertainty*
@0.5 mV	5% of capacity	±0.1% of reading	±0.13%
@1.0 mV	10% of capacity	±0.05% of reading	±0.08%
@2.0 to 18.9 mV	20% to 120% of capacity	±0.05% of reading	±0.06%

*Using a coverage factor of k=2, to give a confidence level of approximately 95%.

Resolution: 5 active digits for all Norbar transducers.
Weight (T-Box XL only): 1.9 Kg (4.2 lb).
Dimensions: 162 mm high x 205 mm wide x 60 mm deep.

Torque and Angle vs Time graph produced using TDMS software

Appendix 4 Weighted decision matrix scoring for each key criteria by output range

Criteria	Output Range(s)	Score
CoF Performance	<0.25	9
	0.25 - 0.3	3
	0.3 - 0.4	1
	>0.4	0
Particle incorporation	>10%	9
	5 - 10%	3
	2 - 5%	1
	<2%	0
Adhesion	>1.5	9
	1 - 1.5	3
	0.5 – 1	1
	<0.5	0
Galling and Wear	No galling observed; Moderate wear	9
	Some galling observed; moderate wear	3
	Serious galling/high wear	1
	N/A	0

References

[1]   W. Knoll and R. C. Advincula, Functional Polymer Films. Wiley, 2011.

[2]   K. Seshan, Handbook of Thin Film Deposition. Elsevier Science, 2012.

[3]   D. Smith, Thin-Film Deposition: Principles and Practice. McGraw-Hill Education, 1995.

[4]   A. Korkin and D. J. Lockwood, Nanoscale Applications for Information and Energy Systems. Springer New York, 2012.

[5]   D. Q. Zhao and E. Abel, "Novel Non-Leaching Antimicrobial Silver PTFE Surfactant Coatings for Preventing Catheter Related Infections." Engineering and Physical Sciences Research Council, University of Dundee, 2001.

[6]   R. Barrett, "Nasa Reference Publication 1228: Fastener Design Material," 1990.

[7]   S. de Souza, "Smart coating based on polyaniline acrylic blend for corrosion protection of different metals," Surf. Coatings Technol., vol. 201, no. 16–17, pp. 7574–7581, 2007.

[8]   Y. Fu, M. Hou, H. Xu, Z. Hou, P. Ming, Z. Shao, and B. Yi, "Ag–polytetrafluoroethylene composite coating on stainless steel as bipolar plate of proton exchange membrane fuel cell," J. Power Sources, vol. 182, no. 2, pp. 580–584, 2008.

[9]   V. I. Rigou, G. Marginean, D. Frunzăverde, and C. V. Câmpian, "Silver based composite coatings with improved sliding wear behaviour," Wear, vol. 290–291, pp. 61–65, Jun. 2012.

[10]   ASTM International, "Standard Test Method for Galling Resistance of Materials G98-02." West Conshohocken, PA, USA, p. 4, 2009.

[11]   Y. Xie and M. X. Yao, "Measurement of the threshold galling stress of hardfacing alloys," Wear, vol. 255, no. 1–6, pp. 509–516, Aug. 2003.

[12]   Parker Hannifin, Function of Fittings, 4100–8/UK ed. Cleveland, Ohio: Parker Hannifin, 2015.

[13]   R. D. Arnell, P. Davies, J. Halling, and T. Whomes, Tribology: Principles and Design Applications. Macmillan Education UK, 1991.

[14]   P. J. Boden, "Disposal of toxic wastes—1. Electroplating and electrochemical machining wastes," Conserv. Recycl., vol. 1, no. 1, pp. 111–118, 1976.

[15]   A. Blair, "Silver plating," Met. Finish., vol. 99, Supple, no. 1, Supplement 1, pp. 303–308, 2002.

[16]   J. V Powers and K. R. Grebe, "Non-Cyanide Silver Plating Bath." United States, 1968.

[17]   R. Morrissey, "Gold and Silver Plating Basics," 2011. [Online]. Available: http://www.pfonline.com/articles/gold-and-silver-plating-basics. [Accessed: 15-Sep-2014].

[18]   D. Thiemig, R. Lange, and A. Bund, "Influence of pulse plating parameters on the electrocodeposition of matrix metal nanocomposites," Electrochim. Acta, vol. 52, no. 25, pp. 7362–7371, 2007.

[19]   A. F. Zimmerman, D. G. Clark, K. T. Aust, and U. Erb, "Pulse electrodeposition of Ni–SiC nanocomposite," Mater. Lett., vol. 52, no. 1–2, pp. 85–90, Jan. 2002.

[20]   P. Berçot, E. Peña-Muñoz, and J. Pagetti, "Electrolytic composite Ni–PTFE coatings: an adaptation of Guglielmi's model for the phenomena of incorporation," Surf. Coatings Technol., vol. 157, no. 2–3, pp. 282–289, 2002.

[21]   Y. L. Wang, Y. Z. Wan, S. M. Zhao, H. M. Tao, and X. H. Dong, "Electrodeposition and characterization of Al2O3–Cu(Sn), CaF2–Cu(Sn) and talc–Cu(Sn) electrocomposite coatings," Surf. Coatings Technol., vol. 106, no. 2–3, pp. 162–166, 1998.

[22]   E. Pena-Munoz, P. Berçot, A. Grosjean, M. Rezrazi, and J. Pagetti, "Electrolytic and electroless coatings of Ni–PTFE composites: Study of some characteristics," Surf. Coatings Technol., vol. 107, no. 2–3, pp. 85–93, 1998.

[23]   A. Grosjean, M. Rezrazi, and P. Berçot, "Some morphological characteristics of the incorporation of silicon carbide (SiC) particles into electroless nickel deposits," Surf. Coatings Technol., vol. 130, no. 2–3, pp. 252–256, 2000.

[24]   A. Hovestad and L. J. J. Janssen, "Electrochemical codeposition of inert particles in a metallic matrix," J. Appl. Electrochem., vol. 25, no. 6, pp. 519–527, 1995.

[25]   A. Hovestad and L. J. Janssen, "Electroplating of Metal Matrix Composites by Codeposition of Suspended Particles," in Modern Aspects of

Electrochemistry, vol. 38, B. E. Conway, C. G. Vayenas, R. White, and M. Gamboa-Adelco, Eds. Springer US, pp. 475–532, 2005.

[26]   A. Hovestad, R. Heesen, and L. Janssen, "Electrochemical deposition of zinc–polystyrene composites in the presence of surfactants," J. Appl. Electrochem., vol. 29, no. 3, pp. 331–338, 1999.

[27]   S. H. Yeh and C. C. Wan, "Codeposition of SiC powders with nickel in a Watts bath," J. Appl. Electrochem., vol. 24, no. 10, pp. 993–1000, 1994.

[28]   S. H. Yeh and C. C. Wan, "A Study of SiC/Ni Composite Plating in the Watts Bath," Plat. Surf. Finish., vol. 84, p. 54, 1997.

[29]   B. J. Hwang and C. S. Hwang, "Mechanism of Codeposition of Silicon Carbide with Electrolytic Cobalt," J. Electrochem. Soc., vol. 140, no. 4, pp. 979–984, 1993.

[30]   D. Guo, M. Zhang, Z. Jin, and R. Kang, "Pulse Plating of Copper-ZrB2 Composite Coatings," J. Master. Sci. Technol., vol. 22, no. 4, pp. 514–518, 2005.

[31]   J. R. Roos, J. P. Celis, J. Fransaer, and C. Buelens, "The development of composite plating for advanced materials," JOM, vol. 42, no. 11, pp. 60–63, 1990.

[32]   Q. Zhao, Y. Liu, and C. Wang, "Development and evaluation of electroless Ag-PTFE composite coatings with anti-microbial and anti-corrosion properties," Appl. Surf. Sci., vol. 252, no. 5, pp. 1620–1627, 2005.

[33]   J. L. Stojak, J. Fransaer, and J. B. Talbot, "Review of Electrocodeposition," in Advances in Electrochemical Science and Engineering, Volume 7, Wiley-VCH Verlag GmbH, pp. 193–223, 2001.

[34]   A. Bund and D. Thiemig, "Influence of bath composition and pH on the electrocodeposition of alumina nanoparticles and copper," J. Appl. Electrochem., vol. 37, no. 3, pp. 345–351, 2007.

[35]   I. Garcia, J. Fransaer, and J.-P. Celis, "Electrodeposition and sliding wear resistance of nickel composite coatings containing micron and submicron SiC particles," Surf. Coatings Technol., vol. 148, no. 2–3, pp. 171–178, Dec. 2001.

[36]   S.-C. Wang and W.-C. J. Wei, "Kinetics of electroplating process of nano-sized ceramic particle/Ni composite," Mater. Chem. Phys., vol. 78, no. 3, pp. 574–580, Feb. 2003.

[37]   M. Kaisheva and J. Fransaer, "Influence of the Surface Properties of SiC Particles on Their Codeposition with Nickel," J. Electrochem. Soc. , vol. 151, no. 1, pp. C89–C96, Jan. 2004.

[38]   E. A. Pavlatou, M. Stroumbouli, P. Gyftou, and N. Spyrellis, "Hardening effect induced by incorporation of SiC particles in nickel electrodeposits," J. Appl. Electrochem., vol. 36, no. 4, pp. 385–394, 2006.

[39]   F. C. Walsh and C. Ponce de Leon, "A review of the electrodeposition of metal matrix composite coatings by inclusion of particles in a metal layer: an established and diversifying technology," Trans. IMF, vol. 92, no. 2, pp. 83–98, 2014.

[40]   J. Yang, "On The Use of Statistical Analysis for Tribological Evaluation of a Solid Lubricant," Ecole Centrale de Lyon, 2013.

[41]   H. P. Jost, "Lubrication (Tribology) Education and Research - A report on the present position and industry's needs," London, 1966.

[42]   J. A. Tichy and D. M. Meyer, "Review of solid mechanics in tribology," Int. J. Solids Struct., vol. 37, no. 1–2, pp. 391–400, Jan. 2000.

[43]   F. J. Clauss, Solid Lubricants and Self-Lubricating Solids. Elsevier Science, 2012.

[44]   S. Bahadur, "Friction and Wear of Polymers and Composites," in Tribology of Mechanical Systems: A Guide to Present and Future Technologies, J. Vižintin, Ed. New York: ASME Press, pp. 239–266, 2004.

[45]   E. Rabinowicz, Friction and Wear of Materials. Wiley, 1995.

[46]   J. F. Archard, "Wear theory and mechanisms," in Wear Control Handbook, New York: American Society of Mechanical Engineers, pp. 39–79, 1980.

[47]   I. V Kragel'skiĭ, V. V Alisin, N. K. Myshkin, and M. I. Petrokovets, Tribology--lubrication, friction, and wear. Professional Engineering Publishing Ltd., 2001.

[48]   K. Kato, "Wear in relation to friction - A review," in Wear, vol. 241, no. 2, pp. 151–157, 2001.

[49]   K. Holmberg, A. Matthews, and H. Ronkainen, "Coatings tribology— contact mechanisms and surface design," Tribol. Int., vol. 31, no. 1–3, pp. 107– 120, Jan. 1998.

[50]   F. P. Bowden and D. Tabor, The Friction and Lubrication of Solids, no. v. 1. Clarendon Press, 2001.

[51]   K. C. Ludema, Friction, Lubrication, Wear: Textbook in Tribology. Florida: CRC Press, 1996.

[52]   K. Miyoshi, "Solid Lubricants and Coatings for Extreme Environments: State-of-the-Art Survey," Cleveland, Ohio, 2007–214668, 2007.

[53]   K. Holmberg, H. Ronkainen, and A. Matthews, "Tribology of thin coatings," Ceram. Int., vol. 26, no. 7, pp. 787–795, Aug. 2000.

[54]   H. Jiang, R. Browning, J. Whitcomb, M. Ito, M. Shimouse, T. Chang, and H. Sue, "Mechanical Modeling of Scratch Behavior of Polymeric Coatings on Hard and Soft Substrates," Tribol. Lett., vol. 37, no. 2, pp. 159–167, 2010.

[55]   J. Leslie, An experimental inquiry into the nature and propagation of heat. London, 1804.

[56]   J. A. Greenwood and J. B. P. Williamson, "Contact of Nominally Flat Surfaces," Proc. R. Soc., vol. 295, 1966.

[57]   M. Sedlaček, B. Podgornik, and J. Vižintin, "Influence of surface preparation on roughness parameters, friction and wear," Wear, vol. 266, no. 3, pp. 482–487, 2009.

[58]   The American Society of Mechanical Engineers, "ASME B1.1-2003: Unified Inch Screw Threads." The American Soicety of Mechanical Engineers, 2003.

[59]   J. Bickford, Handbook of Bolts and Bolted Joints. Taylor & Francis, 1998.

[60]   BSEN ISO, "ISO 16047: 2005(E)," Fasteners – torque/clamp force testing. International Organization for Standardization, Geneva, Switzerland, 2005.

[61]   Parker Hannifin, "Comression Instrumentation Tube Fittings," 2015. [Online]. Available: http://ph.parker.com/us/en/compression-instrumentation-tube-fittings. [Accessed: 02-Apr-2016].

[62]   Brennan Industries, "Double and Single-Ferrule Instrumentation Tube Fittings," Instrumentation Fittings Catalogue, 2013. [Online]. Available: https://brennaninc.com/documents/InstrumentationFittingsCat.pdf. [Accessed: 02-Jan-2015].

[63]   W. Eccles, "Tribological Aspects of the Self-Loosening of Threaded Fasteners," University of Lancashire, 2010.

[64]   T. Yokoyama, M. Olsson, S. Izumi, and S. Sakai, "Investigation into the self-loosening behavior of bolted joint subjected to rotational loading," Eng. Fail. Anal., vol. 23, pp. 35–43, Jul. 2012.

[65]   CETR, "Tribology Testing of Fasteners: Optimization of Materials." [Online]. Available: http://www.cetr.com/Brochures/tribology_testing_of_fasteners.htm. [Accessed: 16-Dec-2015].

[66]   Q. Zou, T. Sun, S. Nassar, G. Barber, and A. Gumul, "Effect of Lubrication on Friction and Torque-Tension Relationship in Threaded Fasteners," Tribol. Trans., vol. 50, no. 1, pp. 127–136, Apr. 2007.

[67]   W. Eccles, I. Sherrington, and R. D. Arnell, "Frictional changes during repeated tightening of zinc plated threaded fasteners," Tribol. Int., vol. 43, no. 4, pp. 700–707, Apr. 2010.

[68]   J. Gansheimer and J. Wessely, "Lubrication of threads," Wear, vol. 65, no. 2, pp. 201–206, Dec. 1980.

[69]   R. Shoberg, "Engineering Fundamentals of Threaded Fastener Design and Analysis," 2014. [Online]. Available: http://www.hexagon.de/rs/engineering fundamentals.pdf. [Accessed: 05-Apr-2014].

[70]   W. Eccles, "Torque to Yield Tests," 2016. [Online]. Available: http://www.boltscience.com/pages/torque-angle-graph.htm. [Accessed: 04-Apr-2016].

[71]   J. W. Dini, Electrodeposition - The Materials Science of Coatings and Substrates. New Jersey, 1993.

[72]   ASTM International, "Standard Terminology Relating to Electroplating." West Conshohocken, PA, p. 9, 2006.

[73]   F. C. Walsh and C. Ponce de León, "Versatile electrochemical coatings and surface layers from aqueous methanesulfonic acid," Surf. Coatings Technol., vol. 259, pp. 676–697, 2014.

[74]   V. S. Bagotsky, Fundamentals of Electrochemistry. Wiley, 2005.

[75]   H. H. Lou and Y. Huang, "Encyclopedia of chemical processing," Taylor & Francis, 2005.

[76]   K.-M. Yin, S.-L. Jan, and C.-C. Lee, "Current pulse with reverse plating of nickel-iron alloys in a sulphate bath," Surf. Coatings Technol., vol. 88, no. 1–3, pp. 219–225, Jan. 1997.

[77]   A. Marlot, P. Kern, and D. Landolt, "Pulse plating of Ni–Mo alloys from Ni-rich electrolytes," Electrochim. Acta, vol. 48, no. 1, pp. 29–36, Nov. 2002.

[78]   M. Ghaemi, "Effects of direct and pulse current on electrodeposition of manganese dioxide," J. Power Sources, vol. 111, no. 2, pp. 248–254, Sep. 2002.

[79]   T. PEARSON and J. K. DENNIS, "Facts and fiction about pulse plating," Trans. Inst. Met. Finish., vol. 69, pp. 75–79, 1991.

[80]   P. F. Mentone, "Pulse vs. DC plating," Met. Finish., vol. 103, no. 6, pp. 14–18, Jun. 2005.

[81]   J. J. Kelly, P. E. Bradley, and D. Landolt, "Additive Effects during Pulsed Deposition of Cu-Co Nanostructures," J. Electrochem. Soc. , vol. 147, no. 8, pp. 2975–2980, Aug. 2000.

[82]   V. S. Saji and R. M. Cook, Corrosion Protection and Control Using Nanomaterials. Elsevier Science, 2012.

[83]   E. Budevski, G. Staikov, and W. J. Lorenz, Electrochemical phase formation and growth: an introduction to the initial stages of metal deposition. VCH, 1996.

[84]   C. Kollia, Z. Loizos, and N. Spyrellis, "Influence of pulse reversed current technique on the crystalline orientation and surface morphology of nickel electrodeposits," Surf. Coatings Technol., vol. 45, no. 1–3, pp. 155–160, May 1991.

[85]   P. T. Tang, T. Watanabet, J. E. T. Andersen, and G. Bech-Nielsen, "Improved corrosion resistance of pulse plated nickel through crystallisation control," J. Appl. Electrochem., vol. 25, no. 4, pp. 347–352, 1995.

[86]   R. Mishra and R. Balasubramaniam, "Effect of nanocrystalline grain size on the electrochemical and corrosion behavior of nickel," Corros. Sci., vol. 46, no. 12, pp. 3019–3029, Dec. 2004.

[87]   C. Y. Dai, Y. Pan, S. Jiang, and Y. C. Zhou, "The effect of prepared parameters on the microstructure of electrodeposited nanocrystalline nickel coating," Surf. Rev. Lett., vol. 11, no. 04n05, pp. 433–442, Aug. 2004.

[88]   S. T. and D. Y. Li, "Tribological, mechanical and electrochemical properties of nanocrystalline copper deposits produced by pulse electrodeposition," Nanotechnology, vol. 17, no. 1, p. 65, 2006.

[89]   S. Brankovic, Electrodeposition for Energy Applications, no. 10. Electrochemical Society, 2008.

[90]   W. E. G. Hansal, S. Roy, P. Leisner, T. Green, and A. Reichenbach, Pulse Plating. Leuze, 2012.

[91]   Alexi Antipov, "Tribology Investigation of Silver and Gold Electroplated in Presence of Nano-diamonds and Nano-Alumina," 2009.

[92]   S. Burling, "Silver Keeps Pace," Prod. Finish., vol. 71, no. 14, pp. 24–28, 2007.

[93]   M. Schlesinger and M. Paunovic, Modern Electroplating. Wiley, 2011.

[94]   I. Belov, C. Zanella, C. Edström, and P. Leisner, "Finite element modeling of silver electrodeposition for evaluation of thickness distribution on complex geometries," Mater. Des., vol. 90, pp. 693–703, Jan. 2016.

[95]   The Chicago Metal Finishers Institute, "Non-Cyanide Silver as a Substitution for Cyanide Processes," The Illinios Waste Management and Research Centre, Illinios, 2002.

[96]   S. Jayakrishnan, S. R. Natarajan, and K. I. Vasu, "Alkaline noncyanide bath for electrodeposition of silver," Met. Finish., vol. 94, no. 5, pp. 12–15, 1996.

[97]   E. P. Leahy and G. A. Karustis, "Non-cyanide acidic silver electroplating bath and additive therefore," U.S. Patent 4 067 784, Jan 10, 1978.

[98]   F. I. Nobel, W. R. Brasch, and A. J. Drago, "Cyanide-free plating solutions for monovalent metals." U.S. Patent 5 302 278, Apr 12, 1994.

[99]   T. Asakawa, "Silver plating baths and silver plating method using the same." U.S. Patent 5 601 696, Feb 11, 1997.

[100]   R. Morrissey, "Non-cyanide silver plating bath composition." U.S. Patent 2007 0151 863, Jul 05, 2007.

[101]   M. Clauss and W. Zhang-Berlinger, "Cyanide-free silver electroplating solutions." U.S. Patent 2012 0067 735, Mar 22, 2012.

[102]   B. G. Xie, J. J. Sun, Z. B. Lin, and G. N. Chen, "Electrodeposition of Mirror-Bright Silver in Cyanide-Free Bath Containing Uracil as Complexing Agent Without a Separate Strike Plating Process," J. Electrochem. Soc., vol. 156, pp. D79–D83, 2009.

[103]   E. Hradil, H. Hradil, and A. M. Weisberg, "Silver complex, method of making said complex and method and electrolyte containing said complex for electroplating silver and silver alloys," U.S. Patent 412 6524, Nov 21,1978.

[104]   E. Hradil, H. Hradil, and A. M. Weisberg, "Non-cyanide bright silver electroplating bath therefor, silver compounds and method of making silver compounds." U.S. Patent 424 6077, Jan 20, 1981

[105]   A. Valiūnienė, G. Baltrūnas, R. Valiūnas, and G. Popkirov, "Investigation of the electroreduction of silver sulfite complexes by means of electrochemical FFT impedance spectroscopy," J. Hazard. Mater., vol. 180, no. 1–3, pp. 259–263, Aug. 2010.

[106]   M. Miranda-Hernández and I. González, "Effect of Potential on the Early Stages of Nucleation and Growth during Silver Electrocrystallization in Ammonium Medium on Vitreous Carbon," J. Electrochem. Soc. , vol. 151, no. 3, pp. C220–C228, Mar. 2004.

[107]   B. J. Polk, M. Bernard, J. J. Kasianowicz, M. Misakian, and M. Gaitan, "Microelectroplating Silver on Sharp Edges toward the Fabrication of Solid-State Nanopores," J. Electrochem. Soc. , vol. 151, no. 9, pp. C559–C566, Sep. 2004.

[108]   M. Palomar-Pardave, M. T. Ramirez, I. Gonzalez, A. Serruya, and B. R. Scharifker, "Silver Electrocrystallization on Vitreous Carbon from Ammonium

Hydroxide Solutions," J. Electrochem. Soc. , vol. 143, no. 5, pp. 1551-1558, May 1996.

[109] B. Reents, W. Plieth, V. A. Macagno, and G. I. Lacconi, "Influence of thiourea on silver deposition: Spectroscopic investigation," J. Electroanal. Chem., vol. 453, no. 1–2, pp. 121–127, Aug. 1998.

[110] O. Azzaroni, P. L. Schilardi, R. C. Salvarezza, and A. J. Arvia, "Smoothening Mechanism of Thiourea on Silver Electrodeposition. Real Time Imaging of the Growth Front Evolution," Langmuir, vol. 15, no. 4, pp. 1508–1514, Feb. 1999.

[111] G. M. de Oliveira, M. R. Silva, and I. A. Carlos, "Voltammetric and chronoamperometric studies of silver electrodeposition from a bath containing HEDTA," J. Mater. Sci., vol. 42, no. 24, pp. 10164–10172, 2007.

[112] Z.-B. Lin, B.-G. Xie, J.-S. Chen, J.-J. Sun, and G.-N. Chen, "Nucleation mechanism of silver during electrodeposition on a glassy carbon electrode from a cyanide-free bath with 2-hydroxypyridine as a complexing agent," J. Electroanal. Chem., vol. 633, no. 1, pp. 207–211, Aug. 2009.

[113] Z.-B. Lin, J.-H. Tian, B.-G. Xie, Y.-A. Tang, J.-J. Sun, G.-N. Chen, B. Ren, B.-W. Mao, and Z.-Q. Tian, "Electrochemical and in Situ SERS Studies on the Adsorption of 2-Hydroxypyridine and Polyethyleneimine during Silver Electroplating," J. Phys. Chem. C, vol. 113, no. 21, pp. 9224–9229, May 2009.

[114] A. Basile, A. I. Bhatt, A. P. O'Mullane, and S. K. Bhargava, "An investigation of silver electrodeposition from ionic liquids: Influence of

atmospheric water uptake on the silver electrodeposition mechanism and film morphology," Electrochim. Acta, vol. 56, no. 7, pp. 2895–2905, Feb. 2011.

[115] F.-H. Yeh, C.-C. Tai, J.-F. Huang, and I.-W. Sun, "Formation of Porous Silver by Electrochemical Alloying/Dealloying in a Water-Insensitive Zinc Chloride-1-ethyl-3-methyl Imidazolium Chloride Ionic Liquid," J. Phys. Chem. B, vol. 110, no. 11, pp. 5215–5222, Mar. 2006.

[116] M.-C. Tsai, D.-X. Zhuang, and P.-Y. Chen, "Electrodeposition of macroporous silver films from ionic liquids and assessment of these films in the electrocatalytic reduction of nitrate," Electrochim. Acta, vol. 55, no. 3, pp. 1019–1027, Jan. 2010.

[117] R. Bomparola, S. Caporali, A. Lavacchi, and U. Bardi, "Silver electrodeposition from air and water-stable ionic liquid: An environmentally friendly alternative to cyanide baths," Surf. Coatings Technol., vol. 201, no. 24, pp. 9485–9490, Oct. 2007.

[118] R. Morrissey, "Noncyanide Silver Plating," 2014. [Online]. Available: http://www.technic.com/apac/sites/default/files/assets/pdfs/literature/Noncyanide Silver Plating.pdf. [Accessed: 15-Aug-2014].

[119] J. W. Dini, R. J. Morrissey, and D. R. Pacheco, "Materials Characterization of a Non-Cyanide Silver Electrodeposit," Plat. Surf. Finish., vol. 84, pp. 62–67, 1997.

[120] C. Shanthi, S. Barathan, R. Jaiswal, R. M. Arunachalam, and S. Mohan, "The effect of pulse parameters in electro deposition of silver alloy," Mater. Lett., vol. 62, no. 30, pp. 4519–4521, Dec. 2008.

[121]   H. Takele, H. Greve, C. Pochstein, V. Zaporojtchenko, and F. Faupel, "Plasmonic properties of Ag nanoclusters in various polymer matrices," Nanotechnology, vol. 17, no. 14, p. 3499, 2006.

[122]   K. Holmberg and A. Matthews, Coatings Tribology: Properties, Mechanisms, Techniques and Applications in Surface Engineering. Elsevier Science, 2009.

[123]   J. Drobny, Fluoroplastics. iSmithers Rapra Publishing, 2006.

[124]   J. K. Lancaster, "Accelerated wear testing of PTFE composite bearing materials," Tribol. Int., vol. 12, no. 2, pp. 65–75, 1979.

[125]   X. Lu, K. C. Wong, P. C. Wong, K. A. R. Mitchell, J. Cotter, and D. T. Eadie, "Surface characterization of polytetrafluoroethylene (PTFE) transfer films during rolling–sliding tribology tests using X-ray photoelectron spectroscopy," Wear, vol. 261, no. 10, pp. 1155–1162, 2006.

[126]   S. Beckford, Y. A. Wang, and M. Zou, "Wear-Resistant PTFE/SiO2 Nanoparticle Composite Films," Tribol. Trans., vol. 54, pp. 849–858, 2011.

[127]   C. G. Fink and J. D. Prince, "The codeposition of copper and graphite," Trans. Am. Electrochem. Soc., vol. 54, pp. 315–321, 1928.

[128]   P. Karl-Heinz, "Dispersion Coatings with PTFE," Prod. Finish., vol. 63, no. 2, pp. 34–39, 1999.

[129]   J. S. Hadley and L. E. Harland, "Electroless nickel/PTFE composite coatings," Met. Finish., vol. 85, no. 12, pp. 51–53, 1987.

[130]   S. S. Tulsi, "Composite PTFE-Nickel coatings for low friction applications," Mater. Des., vol. 4, no. 6, pp. 919–923, 1983.

[131]   M. Kumar Dubey, J. Bijwe, and S. S. V Ramakumar, "PTFE based nano-lubricants," Wear, vol. 306, no. 1–2, pp. 80–88, 2013.

[132]   H. Wei and H. Eilers, "Electrical conductivity of thin-film composites containing silver nanoparticles embedded in a dielectric fluoropolymer matrix," Thin Solid Films, vol. 517, no. 2, pp. 575–581, 2008.

[133]   K. Helle and R. C. Groot, "Stable dispersion of positively charged polyfluorocarbon resin particles." Google Patents, 1981.

[134]   R. Sieh, H. R. Le, and A. M. Cree, "Process optimisation of non-cyanide Ag–PTFE metal matrix composite electroplating for threaded connections," Trans. IMF, vol. 93, no. 5, pp. 232–240, Sep. 2015.

[135]   J. . Celis and J. R. Roos, "Electrolytic and Electroless Composite Coatings," in Reviews in Coatings and Corrosion, no. 5, Scientific Publications Division, Freund Publishing House., 1982.

[136]   P.K.N. Bartlett, "Industrial training report AKZO," Arnhem, 1980.

[137]   R. V. Williams and P. W. Martin, "Electrodeposited Composite Coatings," Trans. Inst. Met. Finish., vol. 182, no. 42, 1964.

[138]   N. Guglielmi, "Kinetics of the Deposition of Inert Particles from Electrolytic Baths," J. Electrochem. Soc., vol. 119, no. 8, pp. 1009–1012, 1972.

[139] J. P. Celis, J. R. Roos, and C. Buelens, "A Mathematical Model for the Electrolytic Codeposition of Particles with a Metallic Matrix," J. Electrochem. Soc., vol. 134, no. 6, pp. 1402–1408, 1987.

[140] C. T. J. Low, R. G. A. Wills, and F. C. Walsh, "Electrodeposition of composite coatings containing nanoparticles in a metal deposit," Surf. Coatings Technol., vol. 201, no. 1–2, pp. 371–383, 2006.

[141] M. Mahmoudi and V. Serpooshan, "Silver-Coated Engineered Magnetic Nanoparticles Are Promising for the Success in the Fight against Antibacterial Resistance Threat," ACS Nano, vol. 6, no. 3, pp. 2656–2664, Mar. 2012.

[142] W. Liu, T. Yang, C. Li, P. Che, and Y. Han, "Regulating silver morphology via electrochemical reaction," CrystEngComm, vol. 17, no. 31, pp. 6014–6022, 2015.

[143] Z. Dong, X. Le, Y. Liu, C. Dong, and J. Ma, "Metal organic framework derived magnetic porous carbon composite supported gold and palladium nanoparticles as highly efficient and recyclable catalysts for reduction of 4-nitrophenol and hydrodechlorination of 4-chlorophenol," J. Mater. Chem. A, vol. 2, no. 44, pp. 18775–18785, 2014.

[144] C. Shanthi, S. Barathan, R. Jaiswal, and R. M. Arunachalam, "Study of surface morphology in DC and pulse plating of silver alloy," Indian J. Eng. Mater. Sci., vol. 16, pp. 128–132, 2009.

[145] F. Ren, L. Yin, S. Wang, A. A. Volinsky, and B. Tian, "Cyanide-free silver electroplating process in thiosulfate bath and microstructure analysis of Ag

coatings," Trans. Nonferrous Met. Soc. China, vol. 23, no. 12, pp. 3822–3828, 2013.

[146] D.-S. Jang and D. E. Kim, "Optimum film thickness of thin metallic coatings on silicon substrates for low load sliding applications," Tribol. Int., vol. 29, no. 4, pp. 345–356, 1996.

[147] G. Tronci and M. B. Marshall, "Understanding the behaviour of silver as a low friction coating in aerospace fasteners," Tribol. Int., vol. 100, pp. 162–170, 2016.

[148] J. Valli, "A review of adhesion test methods for thin hard coatings," J. Vac. Sci. Technol. A Vacuum, Surfaces, Film., vol. 4, p. 3007, 1986.

[149] J. Tomastik and R. Ctvrtlik, "Nanoscratch test — A tool for evaluation of cohesive and adhesive properties of thin films and coatings," EPJ Web Conf., vol. 48, 2013.

[150] H. Ronkainen, A. Laukkanen, and K. Holmberg, "Friction in a coated surface deformed by a sliding sphere," Wear, vol. 263, no. 7, pp. 1315–1323, 2007.

[151] Health and Safety Executive, Safety Requirements for Pressure Testing. United Kingdom: Health and Safety Executive, 2012.

[152] Metal Finishing, Universal Metal Finishing Guidebook, 81st Editi. New York: Metal Finishing, 2013.

[153] H. Guo and A. Mettas, "Design of Experiments and Data Analysis," in Reliability and Maintainability Symposium, p. 27, 2010.

[154]   H. R. Le, A. Howson, M. Ramanauskas, and J. A. Williams, "Tribological Characterisation of Air-Sprayed Epoxy-CNT Nanocomposite Coatings," Tribol. Lett., vol. 45, no. 2, pp. 301–308, 2012.

[155]   J. Williams, Engineering Tribology: Cambridge: Cambridge University Press, 2005.

[156]   V. P. Greco and W. Baldauf, "Electrodeposition of Ni-Al2O3 and Cr-TiO2 dispersion hardened alloys," Plating, vol. 55, pp. 250–257, 1968.

[157]   Y. Suzuki and O. Asai, "Adsorption-Codeposition Process of Al2 O 3 Particles onto Ag ‐ Al2 O 3 Dispersion Films," J. Electrochem. Soc. , vol. 134, no. 8, pp. 1905–1910, Aug. 1987.

[158]   C. C. Lee and C. C. Wan, "A Study of the Composite Electrodeposition of Copper with Alumina Powder," J. Electrochem. Soc. , vol. 135, no. 8, pp. 1930–1933, Aug. 1988.

[159]   S. Wang, L. Pan, and Q. Li, "Tribological behaviors of polytetrafluoroethylene composites under dry sliding and seawater lubrication," J. Appl. Polym. Sci., vol. 130, no. 4, pp. 2523–2531, Nov. 2013.

[160]   D. H. Buckley, "Adhesion and Wear Resistance of Materials," Cleveland, Ohio, 1986.

[161]   L. Chen, L. Wang, Z. Zeng, and T. Xu, "Influence of pulse frequency on the microstructure and wear resistance of electrodeposited Ni–Al2O3 composite coatings," Surf. Coatings Technol., vol. 201, no. 3–4, pp. 599–605, Oct. 2006.

[162]   M. Schlesinger and M. Paunovic, "Electroless and Electrodeposition of Silver," Mod. Electroplat., pp. 131–138, 2011.

[163] G. K. Strukova, G. V. Strukov, E. Y. Postnova, A. Y. Rusanov, and I. S. Veshchunov, "Mesoscopic Models of Plants Composed of Metallic Nanowires," J. Bionic Eng., vol. 10, no. 3, 2013.